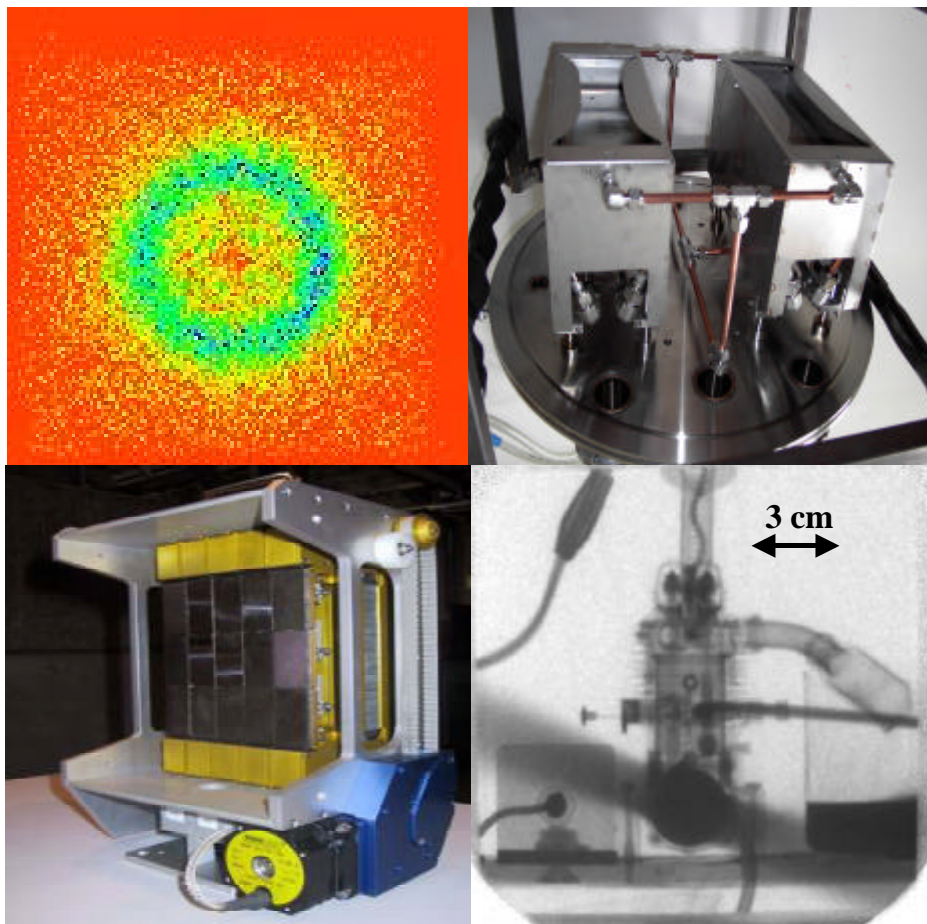


Institute for
Experimental Physics E21

Annual Report 2002
Annual Report 2002



Annual Report 2002
of the Institute for Experimental Physics E21
Prof. Dr. P. Böni
Technische Universität München

Annual Report 2002
of the Institute for Experimental Physics E21
published: 12.3.2003
Edited by Florian Grünauer, E21
<http://www.physik.tu-muenchen.de/lehrstuehle/E21>

Physik-Department E21
Technische Universität München
James-Franck-Strasse
D-85747 Garching, Germany

Phone: +49 89-289-14711
Fax: +49 89-289-14713

Copyright:
Inquiries about copyright and reproduction etc.
should be addressed to the authors.

INDEX

Preface	4
1 Neutron Scattering and Magnetism	6
1.1 Focusing parabolic guide for very small samples.....	7
1.2 Horizontally focusing Heusler analyzer for TASP without depolarising zero field region.....	9
1.3 Observation of soliton chirality in the Ising-chain system CsCoBr ₃	11
1.4 Phonon density-of-states in intermediate valence Ce ₂ Ni ₃ Si ₅	13
1.5 Crystal field effects on Er ³⁺ and Nd ³⁺ ions in intermediate valence Ce ₂ Ni ₃ Si ₅	15
1.6 Search for the crystal field splitting in TmB ₁₂	17
1.7 Mapping of magnetic excitations in single-Q chromium.....	19
1.8 Specific heat study of the spin-chain compounds Ca _{2+x} Y _{2-x} Cu ₅ O ₁₀	21
1.9 Frustrated phase separation in the overdoped regime of '123' high-T _c superconductors	23
1.10 X-ray and magnetization studies on FeCoV/Ti multilayers.....	25
1.11 Preparation and Characterization of FeCoV/Ti Multilayers: a Comparison.....	27
1.12 Critical spin dynamics in CsMnBr ₃	29
1.13 Polarized SANS studies from the weak itinerant helimagnet MnSi.....	31
1.14 Design of an inelastic neutron spectrometer for catalytic applications at FRM-II	32
1.15 MIRA -- Very cold neutrons for new methods	34
1.16 Testing the shielding of the monochromator of Mira by Monte Carlo Method	37
1.17 RESEDA Spectrometer: Jahresbericht 1.1.-31.12.02.....	39
1.18 MUPAD Spectrometer: Annual Report 1.1.-31.12.02	42
1.19 Multiple Small Angle Neutron Scattering.....	44
2 Neutron Radiography and Tomography	46
2.1 The design and construction of the neutron tomography facility ANTARES	47
2.2 Steps toward a dynamic neutron radiography of a combustion engine	51
2.3 Phase contrast radiography using thermal neutrons	53
2.4 Neutron Topography at TOPSL.....	55
2.5 Influence of gaps in shieldings against neutron radiation.....	57
2.6 Estimation of the imaging quality of Munich's new neutron radiography station	59
3 Sample environments	61
3.1 Minimization of the background radiation of a sample environment	62
4 Positron Physics	64
4.1 Experimental facilities at the intense positron source at FRM II	65
4.2 Investigation of the Annealed Copper Surface by Positron Annihilation Induced Auger Electron Spectroscopy	67
4.3 High Resolution Gamma Spectrometer for Doppler Broadening Measurements of the 511 keV Positron Annihilation Line.....	70
4.4 Investigation of Laser Treated AlN and Silica by Positron Lifetime Measurements.....	72
5 Reactor Physics	75
5.1 Nuclear Licensing of the FRM-II.....	76
5.2 Fuel Element with Reduced Enrichment for the FRM-II.....	77
6 Activities 2002	78
6.1 Publications	79
6.2 Conference, Workshop and Seminar Contributions	82
6.3 Lectures, Courses and Seminars	85
6.4 Committee Memberships.....	86
6.5 E21 Members	87
6.6 Associated Members at FRM-II	88
6.7 Guests	88

PREFACE

After the retirement of Prof. Gläser on September 30, 2001, the joining of the different subgroups of E21 proceeded in a rather smooth way and we managed to create some sort of "corporate identity". This endeavour was successful despite various difficult boundary conditions. One of them was caused by a serious illness of our secretary since August 2002, one of the key persons in E21. Thanks to the generous help of B. Russ and the support of the faculty administration we managed to overcome this difficult situation. In addition, we had difficulties with budgeting due to problems we experienced with SAP (a new accounting system at TUM). Last but not least, our scientific work was seriously hampered by the ongoing delay by the Ministry of Environmental Protection (BMU) to provide the final permission to run the FRM-II. We are very grateful that other facilities, mostly in France and Switzerland, helped us to compensate for the loss of beam time.

Let us now come to some of the highlights of E21 in 2002. The installation of the beam lines of E21 at the FRM-II progressed very well. The design of the shielding for the radiography/tomography (ANTARES) beam line was finalized and the demanding task of designing the shielding blocs in the form of a "three dimensional puzzle" came to an end. The blocs are ordered and will be installed early in spring 2003. The primary components of the beam line MIRA for very cold neutrons are installed. Here we mention in particular the monochromator shielding that was installed within 4 months after the order was placed. The neutron spin-echo spectrometer RESEDA is still in a very advanced state and waiting for neutrons... E21 was strongly engaged in developing new techniques and methods for neutron scattering. Due to the lack of neutrons this work was mostly done at the ILL in Grenoble, France, and at PSI in Switzerland. In collaboration with F. Demmel and R. Gähler we investigated at the ILL methods to improve the coil geometry for neutron spin echo (ZETA) and for mapping of inelastic scattering in reciprocal space in itinerant magnets (IN3), respectively. At PSI we have investigated a new focusing technique using parabolic mirrors. In addition, in collaboration with PSI a new type of mechanics for focusing with Heusler monochromator crystals was developed.

The laboratories of E21 in the Physics Department have improved rather dramatically after we succeeded to obtain most of the promised laboratory space after fighting for

almost two years! We acquired two Bruker X-ray diffractometers, namely a D5000 for reflectivity measurements from multilayers and a D500 for powder diffraction. In addition we upgraded the Physical Property Measurement System PPMS with an option to measure thermoelectric properties of samples. The D500 is presently in its commissioning phase and will be equipped soon with a closed cycle refrigerator to attain temperatures as low as 10 K.

Of course, all the installations are being used for doing science. In this respect, the year 2002 was very successful. Most neutron scattering measurements of E21 were performed at SINQ at PSI due to the lack of neutrons in Garching. One of the highlights was the first observation of single-handed, chiral fluctuations in very low magnetic fields in the helical ferromagnet MnSi using polarized neutrons. The results were published on the cover page of Physical Review Letters. In addition, we investigated the chirality of field-induced solitons in low-dimensional spin systems where we observed rather dramatic effects. In a E21-ILL collaboration we managed to improve the quality of time-resolved radiography by measuring the movement of the pistons in a car motor with very high resolution. These results may lead to detailed investigations of the combustion process in motors. In the field of artificial magnetic structures we investigated the morphology and magnetic properties of multilayers that were fabricated at facilities at PSI and TUM. The goal is the engineering of the hysteretic behaviour of multilayers.

The research group around the technical director of the FRM-II, Prof. K. Schreckenbach that belongs scientifically to E21, continues their investigation in fundamental physics with the set-up TRINE searching for a possible violation of the time reversal symmetry in the system of the free neutron decay. The till best limit for the D-coefficient was obtained, which is an important information for particle physics beyond the standard model. Furthermore, the research with positrons in collaboration with the Universität der Bundeswehr in Munich was pursued. The novel type of a slow positron source was successfully tested at a cold neutron beam at the ILL, Grenoble, and will be placed at the foreseen FRM-II in-pile position before the nuclear start-up. An experiment on Auger-spectroscopy induced by positron annihilation gave first signals with a laboratory positron source. This set-up will be one of the

instruments at the FRM-II intense source of slow positrons.

A major field of work in 2002, in particular for Profs. K. Schreckenbach and K. Böning, was to take the – hopefully – final actions in the nuclear licensing procedure of the FRM-II. In January 2002 the BMU issued its Federal Supervisory Assessment containing some 65 questions or conditions to the Bavarian Licensing Authority, the Ministry of Environment StMLU. The groups at the TUM and its general contractor Framatome-ANP have carefully discussed all these topics until July 2002. At the end of October 2002 the

BMU sent an updated list of questions, which still contained some 10 topics with a focus on “beyond design basis accident scenarios”. After all the documents resulting from that have been submitted by about the end of 2002, we are pretty confident now to receive the green light to start up and operate the FRM-II within a few more months only. – The planning of a new fuel element of the FRM-II with reduced enrichment represented another field of activity that, however, can actually start only once the FRM-II has received its licence to operate.

Garching, in February 2003

Peter Böni

Klaus Böning

Klaus Schreckenbach

1 NEUTRON SCATTERING AND MAGNETISM

1.1 Focusing parabolic guide for very small samples

P. Böni¹ and J. Stahn²

¹Technical University of Munich, Physics Department E21, D-85747 Garching, Germany

²Laboratory for Neutron Scattering, ETHZ & PSI, CH-5232 Villigen PSI.

We show that neutrons can be very efficiently focused by using parabolic neutron guides leading to gains of more than 50 on areas as small as 1 mm². The advantages are i) ease of implementation, ii) improved signal to noise ratio, and iii) largest gain at focal point. (Boni_02_Focusing.doc)

The interest in modern materials like multilayers, superconductors, GMR and CMR materials as well as biological samples has increased significantly. These samples can often only be grown in small quantities and neutron scattering experiments are difficult to perform. Therefore, it is necessary to focus neutron beams to as small areas as possible to increase the flux at the sample position. Of course, due to the theorem of Liouville the divergence of the beam is increased too leading to a coarser q -resolution.

For PGAA it has become common practice to use a Kumakhov lens [1] that consists of thousands of glass capillaries focusing the beam to a spot with a diameter as small as 0.7 mm. Until recently, such a lens was installed at SINQ providing an intensity gain of ≈ 16 . It was also used for CEF-measurements on the triple-axis spectrometer TASP [2]. The major disadvantage is that due to the identical area at the entrance and the exit of the capillaries the whole exit area of an end position of a

neutron guide is wasted leading also to an increased background.

In order to overcome these problems we have investigated the possibility of using a small guide with an entrance area of 16 mm \times 16 mm that focuses the beam on an area < 1 mm². The length of the whole device is 455 mm. The interior surfaces (coated with supermirror $m = 3$) were parabolically shaped to focus the parallel beam onto a single spot at the focal point. The performance was simulated by means of the program package McStas from Risø National Laboratory.

We show in Fig. 1 the beam profiles at the exit and at the focal point of the device. For the incident beam we assumed a flat spectrum $0.5 \text{ \AA} \leq I \leq 11.5 \text{ \AA}$ and a rather large divergence of 0.76° corresponding to the situation at beam line SXD at ISIS. It is seen that gains of a factor of 50 can easily be realized on a spot of less than 1 mm². This is a rather exciting result when compared with a Kumakhov lens.

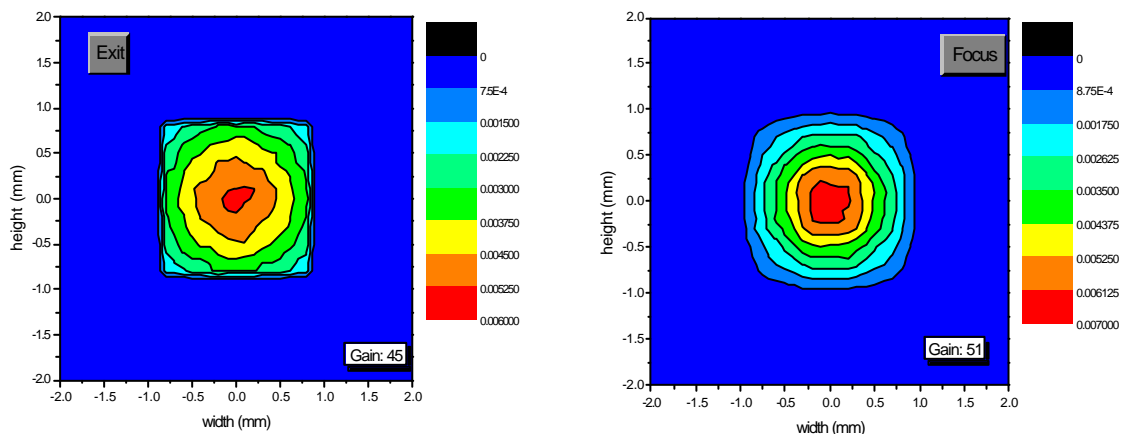


Fig. 1: Intensity distribution of the neutron beam at the exit and the focal point of a 455 mm long parabolic neutron guide. The gain ($G = 51$) at the focal point is higher than at the exit of the guide ($G = 45$).

A prototype of the device was built and characterized on TOPSI at SINQ using neutrons with $I = 4.88 \text{ \AA}$. In a simple setup we mounted the device on a translation table and recorded the neutrons that were focused on an

aperture with a quadratic cross section $2 \text{ mm} \times 2 \text{ mm}$ that was positioned before a ^3He detector. The distance between exit and aperture was varied between $7 \text{ mm} \leq L \leq 80 \text{ mm}$. Fig. 2 shows the measured intensity when

the focusing unit is translated through the neutron beam. The maximum intensity is observed at a translation $u_{ty} = 12$ mm. The two minima in intensity occur when the glass walls intersect the beam. The shoulder around $u_{ty} = 25$ mm corresponds to the intensity of the non-focused direct beam. The measured gain $G \cong 6$ is reduced when compared with the calculation because the measured intensity corresponds to the total number of neutrons that is transmitted through the aperture of 4 mm^2 that is much larger than the spot size at the focal

point of $\cong 0.49 \text{ mm}^2$. Hence, the result is compatible with the McStas simulation. We point out that the intensity does not change for $7 \text{ mm} < L < 40 \text{ mm}$ indicating that the point of the maximum flux is indeed at the focal point and not at the exit of the device.

Because the input area of the focusing device is so small one may consider filling up the full cross section of the beam tube with parabolic focusing units. This way, gains of up to 500 may be realized for PGAA applications.

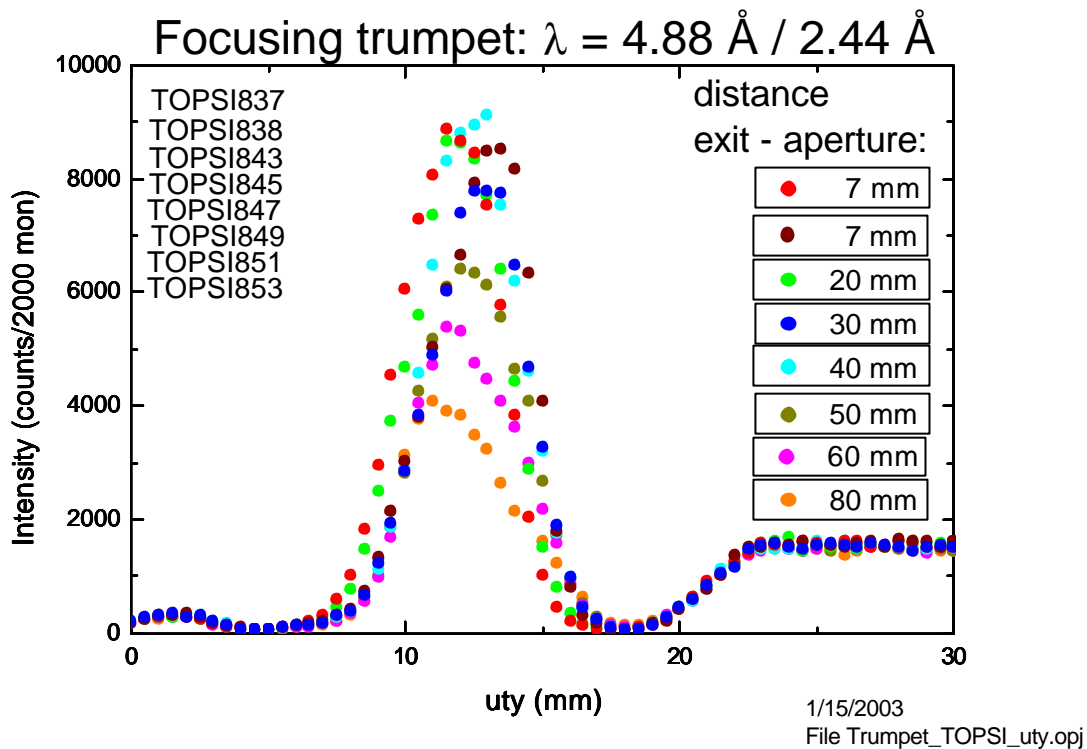


Fig. 2: Intensity of the neutron beam versus position of the beam tube.

References

- [1] M. A. Kumakhov and V. A. Sharov, *Nature* **357**, 390 (1992).
- [2] P. Böni, *Physica B* **276-278**, 6 (2000).

1.2 Horizontally focusing Heusler analyzer for TASP without depolarising zero field region

B. Roessli¹, A.Podlesnyak¹, R. Thut¹, Ch. Kägi¹, T. Mühlebach¹, R. Schneider¹, R. Bürge¹, P. Böni²

¹Laboratory for Neutron Scattering, ETH Zürich & PSI, CH-5232 Villigen PSI, Switzerland

²Physik-Department E21, Technische Universität München, D-85747 Garching, Germany

In the actual full-polarization analysis set-up, the spin-state of the scattered neutron beam is analyzed by a bender installed before the analyzer. With that set-up, however, it is not possible to take advantage of the horizontally focusing PG002 analyzer. For that reason, a new horizontally focusing Heusler has been constructed for TASP. Due to a clever arrangement of the magnetic field there is no zero field region and no correction coils are required.

The triple-axis spectrometer TASP is located at the end of a cold neutron guide at SINQ and has been in operation since 1997. An option with full polarization analysis is available. In the course of the past years the demand for polarized neutrons has steadily increased reaching now an average of 25% of the scheduled beam-time. To polarise the neutron beam, a remanent bender is installed after the monochromator. The advantage of such a device is that no spin-flipper is needed to select the neutron polarization [1]. To analyse the polarisation of the scattered beam, a second bender is usually inserted in the collimator insert before the analyzer. Because the benders have a collimation of about 80°, it is not possible to operate the spectrometer in the focusing mode on the analyzer side. Therefore it was decided to build a new horizontally focusing Heusler analyzer.

The new analyzer consists of 15 Cu₂MnAl Heusler single-crystals (*d* spacing = 3.43) of dimensions 2.5cm x 5cm produced at the Institute Laue-Langevin, Grenoble. The reflectivity and the mosaic of the single crystals have been tested on the 3-axis spectrometer 3AX at the late reactor Saphir at PSI (Fig. 1).

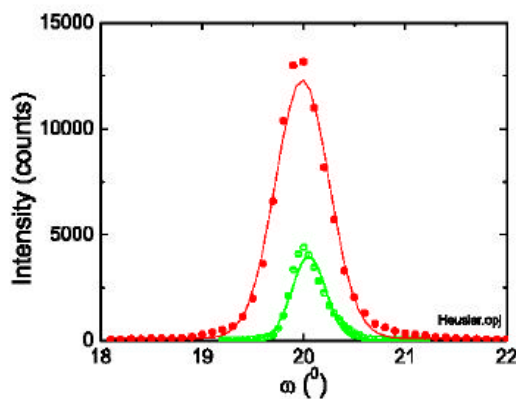


Fig. 1: Rocking curves of on of the best Heusler (open circles) and graphite (filled circles) monochromators. The solid lines are fits to a Gaussian.

The Heusler and graphite monochromators have the same size and we used the same spectrometer configuration for the characterisation ($\lambda = 2.276$, perfect Ge(111) monochromator). The comparison shows that the samples have a similar mosaic while the peak intensity of Heusler is reduced by a factor of $4405/13170 = 0.33$. Taking into account that the measurements were done in zero field and that it was not magnetized the factor will actually go up to about 0.4. Note, that a factor of two in intensity is lost due to the polarization of the beam. The data shows that we can expect a reasonably high performance of the Heusler analyzer.

Each single crystal is mounted on an individual small goniometer, that allows aligning the scattering plane both in the horizontal and vertical directions. Three such pieces are mounted on top of each other to build one of the columns of the analyzer blades (Fig. 2). The top and bottom crystals are inclined by an angle of 3° to focus the beam in the vertical direction onto the detector. To allow for a fully polarized beam, the Heusler crystals have to be magnetized in the vertical direction with respect to the scattering plane. In contrast to previous designs we have built individual yokes for each column of monochromator and optimized the permanent magnets such that no change in sign of the magnetic field occurs before the analyser. This design is not only mechanically very stable it also facilitates the use of guide fields around the analyser. Five analyzer columns form then the complete analyzer. Each of these blades can be mechanically rotated to achieve horizontal focusing. The mechanics are fully motorized and computer controlled, so that the radius of the horizontal curvature can be adjusted as a function of energy.



Fig. 2: Picture of the new Heusler analyzer assembly. As explained in the text the 3 columns of the analyzer are magnetized individually to allow horizontal focusing.

References

- [1] F. Semadeni, B. Roessli, and P. Böni, *Physica B* 297, 152-154 (2001).

1.3 Observation of soliton chirality in the Ising-chain system CsCoBr₃

H.B. Braun^{1,2}, J. Kulda¹, P. Böni², B. Roessli³, K. Krämer⁴, and D. Visser⁵

¹Institut Laue-Langevin, Grenoble, France

²Technical University of Munich, Physics Department E21, D-85747 Garching, Germany

³Laboratory for Neutron Scattering, ETHZ & PSI, CH-5232 Villigen PSI, Switzerland

⁴ISIS, Rutherford Appleton Laboratory, Chilton, Didcot OX11 0QX, United Kingdom

⁵Department of Chemistry, University of Bern, Switzerland

Solitons are the elementary excitations in the quasi 1D Ising compound CsCoBr₃. We have observed a novel chiral asymmetry associated with the quasielastic Villain mode and the 2-soliton continuum in the inelastic neutron scattering cross section. This proves that Ising-type solitons acquire an intrinsic chirality through quantum fluctuations.

The emergence of chiral correlations is one of the central themes in science ranging from the existence of chiral molecules to chiral symmetry breaking in particle physics. In magnetism, static helical structures have been studied with Ho as a prominent example. On the other hand, it is well known that quantum effects play an important role in low-dimensional magnetic systems, which may behave differently depending on their spin quantum number. Spin chains with integer spin exhibit a Haldane gap while half-integer spin chains are gapless, hinting towards a higher symmetry in the latter systems.

Theoretical arguments have shown that chirality emerges as a new degree of freedom of solitons in spin-1/2 systems. This is intimately connected with the decay of a magnon into two solitons, most easily seen in the Ising limit, where a state with two well separated solitons $|\uparrow\downarrow\uparrow\uparrow\downarrow\dots\downarrow\uparrow\uparrow\downarrow\uparrow\downarrow\rangle$ has the same energy as a single spin flip. Such states are exact eigenstates of the Ising Hamiltonian prop. J_z . The transverse exchange $J_t \sum_i [S_i^x S_{i+1}^x + S_i^y S_{i+1}^y]$ induces quantum dynamics of the solitons and gives rise to the one-soliton dispersion [1] as shown in Fig.1

$$\mathbf{e}(k) = (J_z/2) + J_t \cos 2k + g\mathbf{m}_B B_z \cos k \quad (1)$$

Here we have included an external magnetic field B_x in transverse direction. It should be stressed that the $\cos 2k$ dispersion is not a consequence of a unit-cell doubling due to local antiferromagnetic order – the same effect also occurs for ferromagnetic solitons. Rather the two bandminima at $k = \pm\pi/2$ have different chirality as illustrated in Fig. 1. An external field transverse to the Ising direction lifts the chiral degeneracy, and gives rise to a nonvanishing polarization dependent part of the structure factor

$$i\mathbf{P} \cdot \int dt e^{-i\omega t} \langle \mathbf{S}_q(t) \wedge \mathbf{S}_{-q}(0) \rangle \quad (2)$$

where \mathbf{P} is the polarization of the incident neutrons. We have measured the inelastic neutron response at the triple-axis spectrometers IN14, IN20 at ILL in Grenoble working at IN14 with fixed $k_f = 1.5 \text{ \AA}^{-1}$ with an energy resolution of 0.2 meV. Fig. 2 shows the detected asymmetry between different polarization directions with respect to the external field, together with the theoretical predictions with no free parameters, the parameters being determined from the unpolarized measurements.

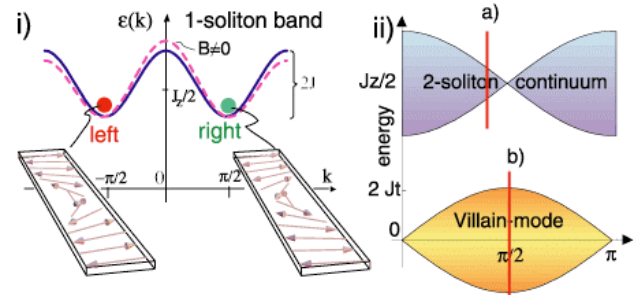


Fig. 1: (i) One soliton dispersion giving rise to a (ii) 2-soliton continuum due to soliton pair creation and a Villain-mode continuum due to transitions between thermally activated states of the one-soliton band.

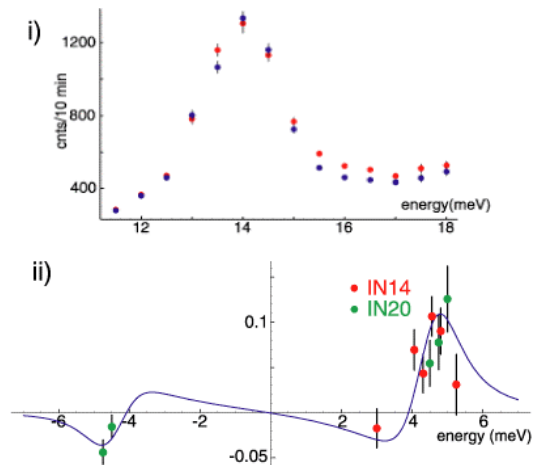


Fig. 2: (i) Total cross section of the 2-soliton continuum at $q_c=0.4$ as a function of energy, cf. cut a) in Fig. 1. Blue dots correspond to spin-flip, red dots to non spin-flip intensities indicating opposite soliton chiralities (ii) Total polarization of the cross-section for the Villain mode at $q_z=0.5$, together with the theoretical prediction at a field of $B=3.3T$.

References

- [1] J. Villain, Physica D 79, 1 (1975); F. Devreux and J.P. Boucher, J. Physique 48, 1663 (1987); S.E. Nagler et al., Phys.Rev.Lett. 49, 590 (1984) Sharov, Nature **357**, 390 (1992).
- [2] H.B. Braun, in "Complementarity between Neutron and Synchrotron X-Ray Scattering" ed. By A. Furrer, World Scientific (1998)

1.4 Phonon density-of-states in intermediate valence $\text{Ce}_2\text{Ni}_3\text{Si}_5$

E.Clementyev¹, I.Sashin², P.A.Alekseev³, V.N.Lazukov³ and L.C.Gupta⁴

¹Technical University of Munich, Physics Department E21, D-85748 Garching, Germany

²FLNP, Joint Institute for Nuclear Research, 141980 Dubna, Russia

³RRC "Kurchatov Institute", 123182 Moscow, Russia

⁴Tata Institute of Fundamental Research, 400005 Bombay, India

Inelastic neutron scattering measurements of the phonon density-of-states in intermediate valence $\text{Ce}_2\text{Ni}_3\text{Si}_5$ and its nonmagnetic isostructural reference compound $\text{Y}_2\text{Ni}_3\text{Si}_5$ have been performed at temperatures 10K to 300K. The phonon density-of-states in $\text{Y}_2\text{Ni}_3\text{Si}_5$ is temperature-independent. The temperature dependence of the phonon spectrum in $\text{Ce}_2\text{Ni}_3\text{Si}_5$ is indicative of a coupling of valence fluctuations and lattice vibrations.

Intermediate valence (IV) rare earth compounds, in which a lanthanide ion can be regarded as fluctuating between two different states, are prone to display anomalies in their vibrational properties because changes in the 4f-shell occupancy are associated with large differences in the ionic radius. But whereas significant phonon anomalies have been found in Sm and Tm-based IV compounds [1] only a few indications have been reported so far in the case of Ce [2].

The intermetallic compound $\text{Ce}_2\text{Ni}_3\text{Si}_5$ exhibits typical IV properties [3]. The characteristic Kondo energy is about 100K. A very special feature of this compound is the strong temperature dependence of the Ce valence [4]. The energies of valence fluctuations and lattice vibrations are close to each other in $\text{Ce}_2\text{Ni}_3\text{Si}_5$ and, therefore, sizable effects of the electronic instability on the lattice dynamics can be anticipated.

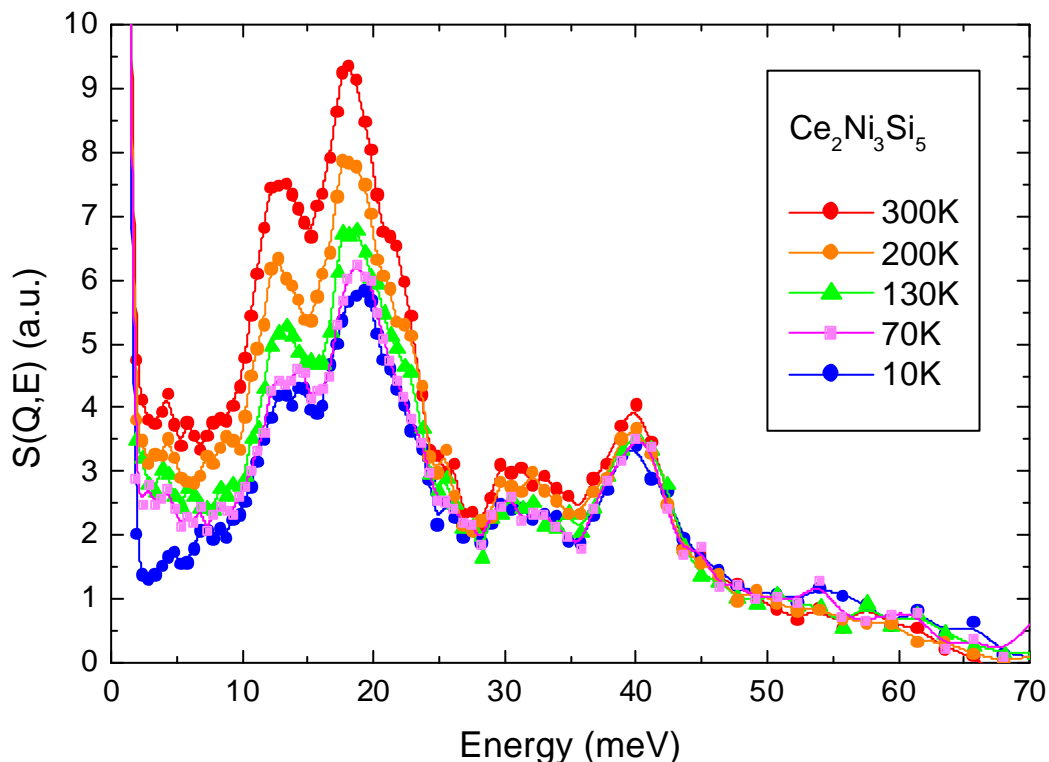


Fig. 1: Background-corrected inelastic neutron scattering spectra of $\text{Ce}_2\text{Ni}_3\text{Si}_5$ measured at temperatures 10K to 300K.

The inelastic neutron scattering (INS) measurements were carried out in the temperature range 10K to 300K on the time-of-flight spectrometer KDSOG-M of inverted geometry located at the IBR-2 pulsed reactor in Dubna. The final energy was fixed at $E_f=4.9$ meV. A pyrolytic graphite analyzer was used in combination with a beryllium filter to suppress higher-order contaminations.

Fig.1. shows the background-corrected INS spectra of $Ce_2Ni_3Si_5$ measured in the temperature range 10K to 300K. The data taken at different scattering angles (80 to 140 degrees) were averaged to get a good approximation of the incoherent neutron scattering function. Several phonon bands show up in the INS spectra. The temperature effects (caused not only by the Bose

temperature factor but also by a shift of the phonon bands) are observed in the low-energy part of the spectra. The heavier rare-earth and nickel ions contributions dominate for this energies.

Fig.2 depicts the generalized phonon density-of-states (GDOS) of $Y_2Ni_3Si_5$. Clearly all the major peaks of the GDOS don't show any sizable temperature dependence as expected for a nonmagnetic reference compound.

The INS spectra of $Ce_2Ni_3Si_5$ combined with those of $Y_2Ni_3Si_5$ will allow a careful estimation of the magnetic contribution to the neutron scattering function to get the phonon GDOS of the former compound. This work is in progress now.

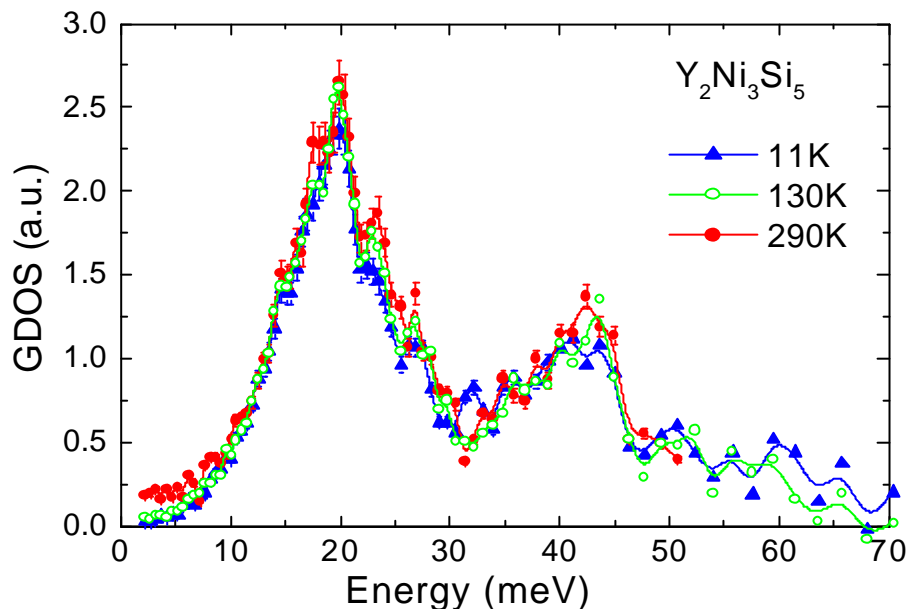


Fig. 2: Generalized phonon density-of-states of $Y_2Ni_3Si_5$ obtained from INS spectra.

References

- [1] H.A.Mook and R.M.Nicklow, Phys. Rev. B **20**, 1656 (1979).
- [2] E.S.Clementyev, P.A.Alekseev, M.Braden, J-M.Mignot, G.Lapertot, V.N.Lazukov and I.P.Sadikov, Phys. Rev. B **57**, R8099 (1998).
- [3] C.Mazumdar, R.Nagarajan, S.K.Dhar, L.C.Gupta, R.Vijayaraghavan and B.D.Padalia, Phys. Rev. B **46**, 9009 (1992).
- [4] C.Mazumdar, R.Nagarajan, C.Godart, L.C.Gupta, B.D.Padalia and R.Vijayaraghavan, J. Appl. Phys. **79**, 6347 (1996).

1.5 Crystal field effects on Er^{3+} and Nd^{3+} ions in intermediate valence $\text{Ce}_2\text{Ni}_3\text{Si}_5$

E.Clementyev¹, I.Sashin² and L.C.Gupta³

¹Technical University of Munich, Physics Department E21, D-85748 Garching, Germany

²FLNP, Joint Institute for Nuclear Research, 141980 Dubna, Russia

³Tata Institute of Fundamental Research, 400005 Bombay, India

Magnetic spectral response of Er^{3+} and Nd^{3+} ions in intermediate valence host matrix $\text{Ce}_2\text{Ni}_3\text{Si}_5$ has been measured by inelastic neutron scattering. A full crystal field splitting scheme was established for Nd^{3+} . Experimental information allows unambiguous determination of the crystal field potential for Er^{3+} .

The hybridization of the 4f shell with conduction electrons is believed to give rise to anomalous properties in rare-earth based compounds. A study of cerium-based compounds is of particular interest as in this case the 4f shell contains just one electron, which may help us to explain this system with relative ease.

$\text{Ce}_2\text{Ni}_3\text{Si}_5$ has been reported to demonstrate properties typical for intermediate valence (IV) systems [1]. Prior to measurements of the dynamic spectral response in pure $\text{Ce}_2\text{Ni}_3\text{Si}_5$ compound it's important to get an estimation of a strength of the crystal field (CF) interaction vs the Kondo energy. The ratio of these two basic interactions plays a crucial role in the formation of the ground state and magnetic properties in cerium-based systems. Unfortunately, cerium ions do not provide us such an opportunity due to a substantial degree of delocalization of the cerium 4f shell, expected in $\text{Ce}_2\text{Ni}_3\text{Si}_5$. That is why using a paramagnetic impurity ions with a stable valence is the only possible way to learn something on the CF interaction.

The first measurements of the CF effects in $\text{Ce}_2\text{Ni}_3\text{Si}_5$ were performed using the Er^{3+} and Nd^{3+} ions as paramagnetic impurities. Many CF transitions show up in the inelastic neutron scattering (INS) spectra measured on the triple axis spectrometer Drüchhal (SINQ neutron source, Villigen PSI). However the energy transfer range was limited by 10 to 12 meV so not all the CF transitions were visible [2].

The main aim of the present experiments was to enlarge the energy transfer range to get a full CF splitting scheme for Er^{3+} and Nd^{3+} ions in $\text{Ce}_2\text{Ni}_3\text{Si}_5$. INS measurements have been performed on the time-of-flight spectrometer KDSOG-M of inverted geometry located at the IBR-2 pulsed reactor (Dubna). The final neutron energy was fixed $E_f=4.9$ meV. Such a geometry allows getting the INS spectra in the energy transfer range up to about 200 meV.

Fig.1. shows the INS spectra of $\text{Ce}_2\text{Ni}_3\text{Si}_5$ sample with Er^{3+} paramagnetic impurity. The magnetic contribution dominates in the energy transfer range $E<10$ meV.

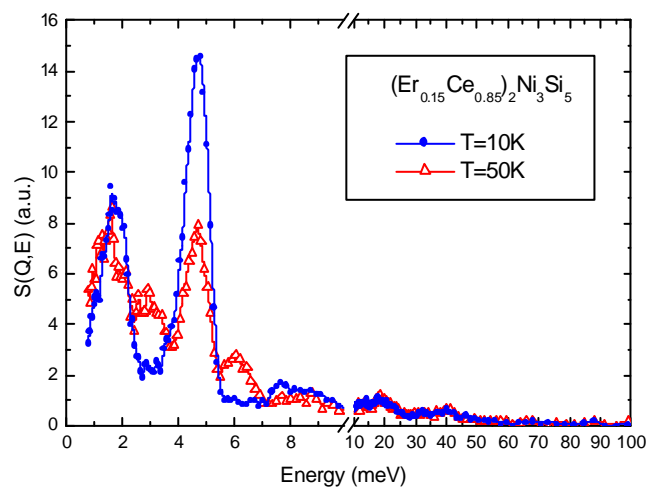


Fig. 1: Background-corrected inelastic neutron scattering spectra of $(\text{Er}_{0.15}\text{Ce}_{0.85})_2\text{Ni}_3\text{Si}_5$.

Its temperature dependence is indicative of the CF transitions out of the ground state. No sizable magnetic scattering was detected at higher energies. In the case of Nd^{3+} (see Fig.2) two CF transitions from the ground state were detected at $10\text{meV} < E < 20\text{ meV}$. At higher energies only the phonon contribution to the neutron scattering function is visible. Thus a

full CF splitting scheme is established for Nd^{3+} , namely $E=0, 6.2, 9.2, 14.8$ and 17.4 meV .

As to Er^{3+} ions in $\text{Ce}_2\text{Ni}_3\text{Si}_5$, a few CF states are invisible but the INS experiment provides enough data to calculate the CF parameters and to restore a full CF splitting scheme.

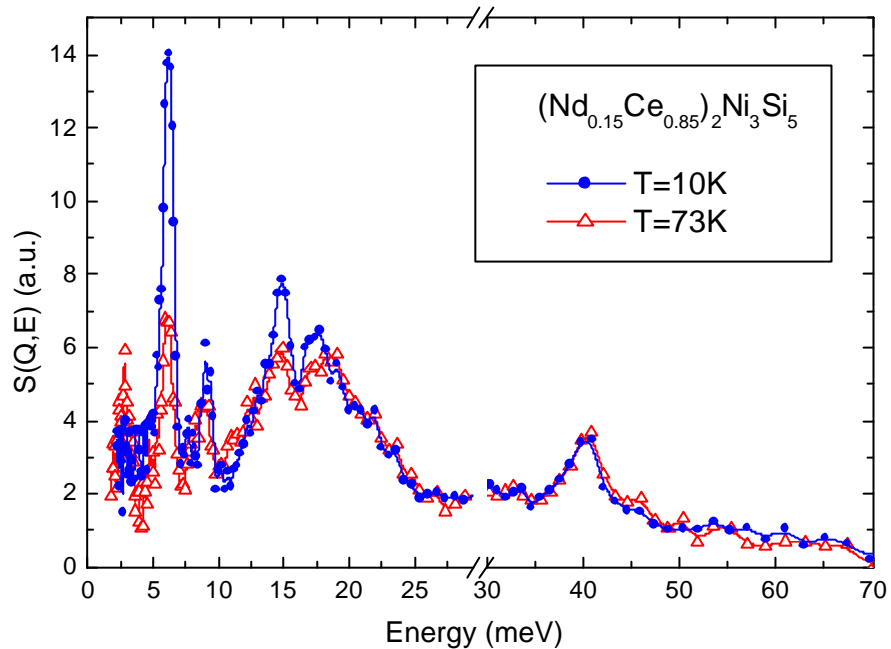


Fig. 2: Background-corrected inelastic neutron scattering spectra of $(\text{Nd}_{0.15}\text{Ce}_{0.85})_2\text{Ni}_3\text{Si}_5$.

References

- [1] C.Mazumdar, R.Nagarajan, S.K.Dhar, L.C.Gupta, R.Vijayaraghavan and B.D.Padalia, Phys. Rev. B **46**, 9009 (1992).
- [2] E.Clementyev and L.C.Gupta, unpublished.

1.6 Search for the crystal field splitting in TmB_{12}

A.Murasik¹, A.Szopnik², E.Clementyev³, S.Janssen⁴ and N.Shitsevalova⁵

¹Institute of Atomic Energy, Swierk, Poland

²Institute for Low Temperature Wrocław, Poland

³Technical University of Munich, Physics Department E21, D-85748 Garching, Germany

⁴Paul Scherrer Institute Villigen, Switzerland

⁵Institute for Problems of Material Science Kiev, Ukraine

Neutron inelastic scattering experiments performed on the time of flight spectrometer FOCUS using a powder sample TmB_{12} enriched with ^{11}B isotope show at low temperatures two clearly visible CF transitions at 7.5 and 14 meV, which basing on the temperature behaviour of the spectrum, allowed us to determine the crystal field splitting scheme in this compound with the CF parameters: $W = 0.104$ meV and $x = -0.071$.

We have shown in the previous work [1] that TmB_{12} orders antiferromagnetically at low temperatures. Its magnetic structure has been described as a modulation of magnetic moments, propagating along three crystallographic direction. The heat capacity measurements allowed us to determine the Schottky contribution to the specific heat from which two crystal-field parameters $x \cong -0.15$ and $W \cong 1.1$ K yielding the $\Gamma_5^{(1)}$ triplet as a lowest level was found. This result agrees well with neutron data but the crystal field splitting scheme needed further confirmation. However, there were some doubts concerning the possibility of performing successful neutron inelastic experiments. First of all, (as proved by the diffraction experiment) the enrichment of the sample with low absorbing ^{11}B isotope was not 100% yielding in effect poor signal-to-background ratio. Secondly, due to a large amount of nonmagnetic ions in the sample, one could expect also the significant phonon scattering. In these circumstances we have decided to perform a testing measurement on the time of flight instrument "FOCUS" (PSI, Villigen, Switzerland). To optimise the experimental conditions a flat geometry was used, *i.e.* the sample was contained in two sheets of aluminum foil of 50 x 30 mm size covering 60 x 30 mm beam aperture. The sample was placed at an angle of $\cong 30$ degrees with respect to the incoming beam to favour reflection geometry applicable for a highly absorbing material.

Several neutron spectra have been collected including the variation of incoming energy E_i , energy transfers DE and temperature. Fig. 1 displays the main feature of the INS experiment. It shows two principal maxima (cf: spectrum (b) and (c)) taken at different geometry and different incoming energies.

The spectrum (b) displays the intensity variation with temperature characteristic for

the ground state CF transition. On (c), the de-excitation of two levels at about 7.5 meV and 14 meV is visualized by two sizable peaks. The crystal field splitting scheme displayed on (a) is based on performed experiments as well as a simulation of calculated intensities from which one can conclude that the main contribution to the scattering, results from transitions between three lowest levels.

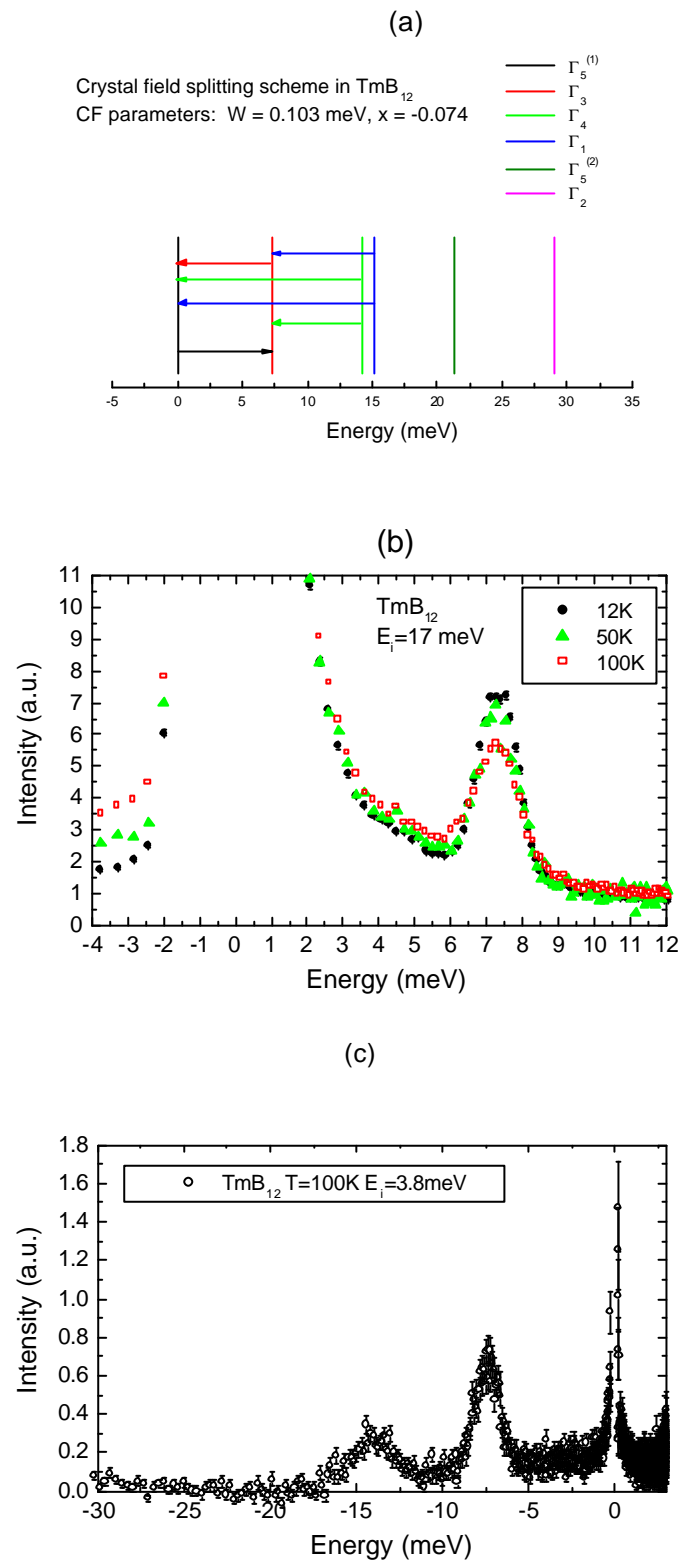


Fig. 1 Crystal field splitting scheme and observed CF transitions in TmB_{12} .

References

[1] A.Czopnik, A.Murasik, L.Keller, N.Shitstevalova and Y.Paderno, Phys. Stat. Sol. (b) **221**, R7 (2000)

1.7 Mapping of magnetic excitations in single-Q chromium

P. Böni¹, E. Clementyev¹, F. Demmel², and G. Shirane³

¹Technical University of Munich, Physics Department E21, D-85748 Garching, Germany

²Institute Laue Langevin, F-38042 Grenoble Cedex 9, France

³Physics Department, Brookhaven National Laboratory, Upton, New York 11973

The low-energy excitations of antiferromagnetic Cr have been measured by means of inelastic neutron scattering using a novel multi detector setup of the triple-axis spectrometer IN3. A huge area in the [100]/[010] scattering plane was investigated around a few reciprocal lattice positions. The observed intensity maps indicate that the low-energy excitations for $E = 6$ meV are arranged on a ring in the Q_h - Q_k scattering plane around the commensurate positions. The multi detector system on the IN3 spectrometer has proved to be a very powerful "excitation scanner".

Cr is one of the most thoroughly studied itinerant antiferromagnets. The richness of the phenomena observed in Cr derives from its spin-density-waves (see [1] and references therein). Recently interest has been focused on the unusual spectral features of chromium, namely the low-energy Fincher-Burke (FB) excitations around the commensurate positions [2]. The origin of these modes and their relevance with regard to incommensurate order is unclear. A series of high-resolution measurements was performed recently to characterize the behavior of the FB modes [3,4]. However experimental information is rather scarce since contour maps of intensity were collected only along two directions in \mathbf{Q} -space around the commensurate wavevector $\mathbf{Q} = (1,0,0)$.

The primary goal of the measurements was to explore a large region in the Q_h - Q_k scattering plane around the commensurate positions and produce contour maps of excitation spectra at different neutron energy transfers. A conventional triple-axis spectrometer (TAS) is not well suited for such a study due to the enormous number of points in \mathbf{Q} -space to be measured. That is why a novel multi detector TAS was used to map out the magnetic excitation spectrum of Cr. The TAS IN3 (ILL) was equipped with a set of 32 analyser crystals positioned on an arc around the sample (see [5] for details). Constant- E scans were performed in the [100]/[010] scattering plane at $T = 230$ K and fixed final energy $E_f = 31$ meV. Fig. 1 depicts the points in the Q_h - Q_k plane covered by a single constant- E scan.

The (radial) \mathbf{Q} -resolution along the h -direction is rather coarse due to the size of the individual analyser crystals, while the (tangential) \mathbf{Q} -resolution along the k -direction can be made significantly smaller because it is mostly given by the step size of the orientation of the single crystal on the sample table and the sample mosaic.

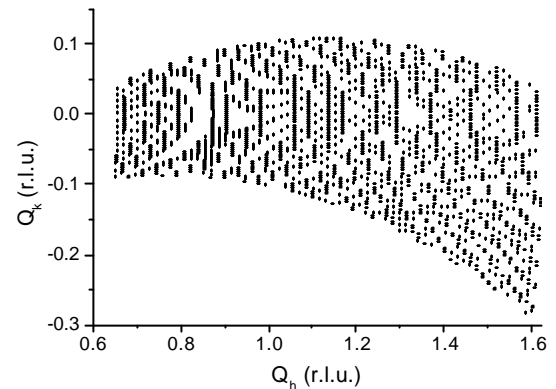


Fig. 1: Points in the Q_h - Q_k plane covered by a typical constant- E scan.

The scans were performed around the reciprocal lattice positions $\mathbf{Q} = (1,0,0)$, $(0,1,0)$ and $(1,1,0)$ at several energy transfers $0 \text{ meV} < E < 20 \text{ meV}$. The scattering intensity measured around $\mathbf{Q} = (1,0,0)$ at $E = 6$ meV is shown in Fig. 2.

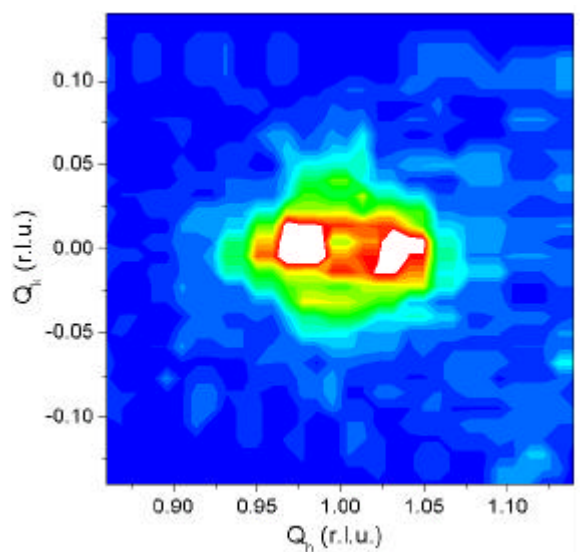


Fig.2: Contour map of the excitation spectra of Cr as measured at $E = 6$ meV around $\mathbf{Q} = (1,0,0)$.

The strong incommensurate scattering is clearly seen at $\mathbf{Q} = (1+\delta,0,0)$ as white spots. These modes emerge from the magnetic satellites. A striking feature is a ring of intensity between the incommensurate peaks with a hole at $\mathbf{Q} = (1,0,0)$ at $E = 6$ meV. This feature represents the FB excitations. In addition, we also see an increase of the intensity at the silent positions $(1,\pm\delta,0)$.

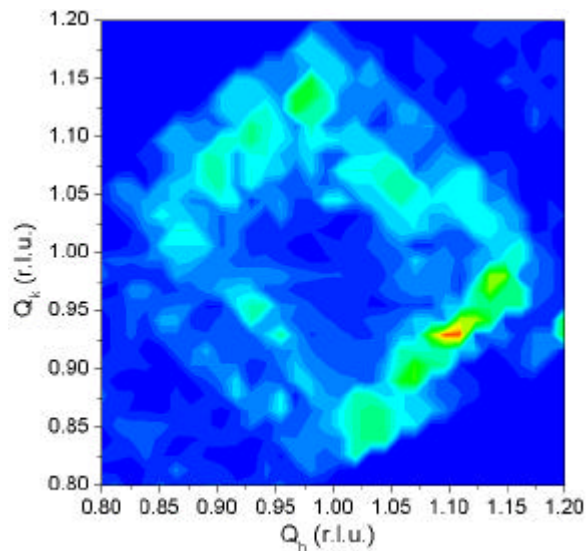


Fig. 3: Contour map of the excitation spectra of Cr at $E = 8$ meV measured around $\mathbf{Q} = (1, 1, 0)$.

It is worth to note that no magnetic intensity was observed at the reciprocal lattice position $\mathbf{Q} = (1,1,0)$, which is not accompanied by magnetic satellites. Only the phonon contribution is present in the spectrum as a rectangle (see Fig. 3). It is directly seen that the longitudinal phonons along have a larger velocity of sound than the transverse phonons.

The most salient feature of the present study is the ring of intensity around $\mathbf{Q} = (1,0,0)$ that confirms the results on the new excitations in Cr [4]. We point out that the present experiments have been performed on a different Cr crystal and very different experimental conditions than in reference [4]. Similar scans have been performed around the $(0,1,0)$ Bragg peak, where the \mathbf{Q} -resolution along the h -direction is excellent, while along the k -direction it is coarse.

The TAS IN3 with a novel multi detector setup proves to be a useful inelastic spectrometer to investigate large areas in reciprocal space. The experiment was carried out in a view to encourage such experimental methods in the TAS spectroscopy. In principle, it would be rather trivial to increase the performance of the multi-detector setup by a factor of 10 by moving the multidetector from the thermal ^{58}Ni guide position to a thermal beam port at the ILL.

References:

- [1] E. Fawcett, Rev. Mod. Phys. **60**, 209 (1988).
- [2] S. K. Burke, W. G. Stirling, K. R. A. Ziebeck, and J. G. Booth, Phys. Rev. Lett. **51**, 494 (1983).
- [3] P. Böni, B. Roessli, E. Clementyev, Ch. Stadler, G. Shirane, and S. A. Werner, Applied Physics A **74** (suppl.), S716 (2002).
- [4] H. Hiraka, Y. Endoh, P. Böni, M. Fujita, K. Yamada, and G. Shirane, Phys. Rev. E **67**, 064423 (2003).
- [5] F. Demmel, The ILL Millenium Symposium & European Users Meeting, Grenoble, 305 (2001).

1.8 Specific heat study of the spin-chain compounds $\text{Ca}_{2+x}\text{Y}_{2-x}\text{Cu}_5\text{O}_{10}$

A. Mirmelstein^{1,2}, V. Kargl¹, A. Amato³, J. Karpinski⁴, S. Kazakov⁴, P. Böni¹, A. Erb⁵

¹Technical University of Munich, Physics Department E21, D-85748 Garching, Germany

²Institute for Metal Physics, Russian Academy of Sciences, 620219 Ekaterinburg GSP-170, Russia

³Laboratory for Muon Spin Spectroscopy, Paul Scherrer Institute, CH-5232 Villigen PSI, Switzerland

⁴Laboratory for Solid State Physics, ETH Hönggerberg, CH-8093 Zürich, Switzerland

⁵Walther Meissner Institute, Bavarian Academy of Sciences, D-85748 Garching, Germany

The specific heat of the spin-chain compounds $\text{Ca}_{2+x}\text{Y}_{2-x}\text{Cu}_5\text{O}_{10}$ as a function of x ($0 \leq x \leq 1.2$) was measured in magnetic fields up to 9 Tesla.

Recently, the new system $\text{Ca}_{2+x}\text{Y}_{2-x}\text{Cu}_5\text{O}_{10}$ has been synthesized which consists only of linear chains and allows a variable doping level ranging from $x = 0$ to $x = 2$ (formal copper valences from +2 to +2.4) [1]. This wide range of hole doping makes these compounds particularly interesting for a detailed study of doping-induced dimensional crossover between 3D and 1D. In fact, the undoped compound exhibits long-range AF order with $T_N = 29$ K [2]; however, as holes are doped into the chains, the magnetic susceptibility and the specific heat data indicate a change from 3D long-range order to 1D chain behavior [3]. Therefore, these compound series are an excellent model for linking experimental and theoretical studies of spin and charge dynamics in doped low-dimensional copper oxides. The aim of the present study is to characterize the magnetic state of $\text{Ca}_{2+x}\text{Y}_{2-x}\text{Cu}_5\text{O}_{10}$ as a function of x by specific heat measurements.

The ceramic samples of $\text{Ca}_{2+x}\text{Y}_{2-x}\text{Cu}_5\text{O}_{10}$ ($0 \leq x \leq 1.5$) were prepared at high oxygen pressure (> 200 bar) as described in [1]. The specific heat was measured by the relaxation technique using a conventional PPMS (Quantum Design) in magnetic fields up to 9 Tesla. The magnetic state of the samples with $x = 0$ and $x = 1.5$ was also probed by μSR .

As expected, the highly doped composition $\text{Ca}_{3.5}\text{Y}_{0.5}\text{Cu}_5\text{O}_{10}$ shows no long-range magnetic order. Instead, the $x = 1.5$ data are indicative of a 1D Heisenberg chain behavior (Fig. 1). The specific heat results are in agreement with the magnetization measurements. Absence of a static magnetic order down to 4 K for this composition is confirmed by the μSR experiments.

In agreement with previous results [2], the undoped $\text{Ca}_2\text{Y}_2\text{Cu}_5\text{O}_{10}$ compound experiences an AF ordering at $T_N = 29$ K. The Cu ions form an orthorhombic sublattice within the orthorhombic $Fmmm$ structure. The magnetic peaks could be indexed within this chemical

unit cell with $\mathbf{k} = [0,0,1]$. The magnetic moments lie along the b direction of the unit cell, i.e. perpendicular to the chain direction [100]. Since the low temperature ordered moment (0.95 ± 0.03) μ_B is close to the free ion value for Cu^{2+} , spin fluctuations are expected to be negligible. However, Fig. 1 demonstrates that the magnetic specific heat does not vanish above T_N and, moreover, reveals the same temperature dependence as highly doped compositions. Essentially, the anisotropic character of the magnetic excitations in $\text{Ca}_2\text{Y}_2\text{Cu}_5\text{O}_{10}$ is probably responsible for the magnetic field-induced broadening of the AF (Fig. 2). Systematic investigation of the thermodynamic properties of the $\text{Ca}_{2+x}\text{Y}_{2-x}\text{Cu}_5\text{O}_{10}$ compounds as a function of doping is in progress.

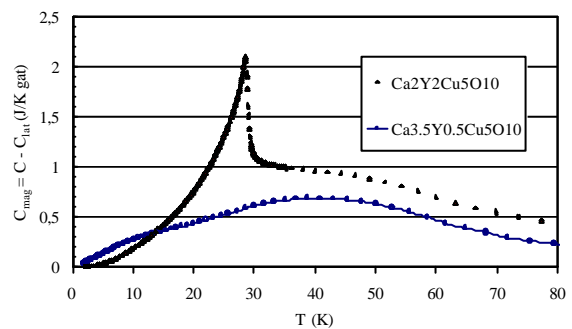


Fig. 1: The magnetic contribution to the specific heat $C_{\text{mag}} = C_{\text{measured}} - C_{\text{lattice}}$ of $\text{Ca}_{2+x}\text{Y}_{2-x}\text{Cu}_5\text{O}_{10}$ for $x = 0$ and 1.5.

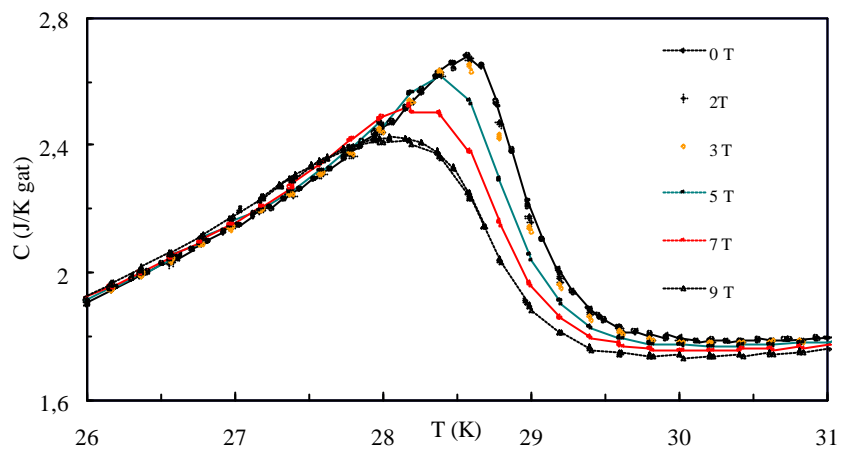


Fig. 2: The specific heat of $\text{Ca}_2\text{Y}_2\text{Cu}_5\text{O}_{10}$ as a function of magnetic field in the region of the AF transition.

References:

- [1] A. Hayashi et al., Phys. Rev. Lett. **58**, 2678 (1998)
- [2] H.F. Fong et al., Phys. Rev. B **59**, 365 (1999)
- [3] M.D. Chabot et al., Phys. Rev. Lett. **86**, 163 (2001)

1.9 Frustrated phase separation in the overdoped regime of '123' high- T_c superconductors

A. Mirmelstein^{1,2}, V. Bobrovskii², N. Golosova², A. Podlesnyak³, A. Furrer³

¹Technical University of Munich, Physics Department E21, D-85748 Garching, Germany

²Institute for Metal Physics, Russian Academy of Sciences, 620219 Ekaterinburg GSP-170, Russia

³Laboratory for Neutron Scattering, ETH Zurich & PSI, CH-5232 Villigen PSI, Switzerland

The systematic analysis of the concentration dependence of the crystal-field (CF) parameters for both Ho- and Er-based "123" high- T_c compounds shows that the local charge inhomogeneity in the CuO_2 planes of high- T_c cuprates is a characteristic feature of the doping process, which depends neither on the way of introducing doping nor on the doping level.

For some time, superconductivity in the cuprates has been believed to occur in a homogeneous system. However, the experimental evidence for spatial charge and spin inhomogeneities and lattice effects has been accumulated over the last years. The experiments show that the distribution of doped charges in the CuO_2 planes is very inhomogeneous in the underdoped regime and becomes more homogeneous when going above the optimal doping. Theoretical models emerging in response to these data emphasize the strong involvement of lattice degrees of freedom in mediating superconductivity in cuprates as well as a direct relation between the pseudogap phenomenon and an intrinsic electron inhomogeneity of the metallic phase [1]. Thus the experimental study of the spatial distribution of the doping-induced charges in the CuO_2 planes is of crucial interest.

The crystal-field (CF) interaction measured by the inelastic neutron scattering (INS) technique allows direct observation of the cluster formation upon doping of high- T_c cuprates with charge carriers [2]. This phenomenon (which may be called "frustrated phase separation") reflects a remarkable difference between the average carrier concentration and the local charge density in the CuO_2 planes near the doping centers. In this work [3] we demonstrate that the frustrated phase separation exists also in the overdoped regime of the "123" cuprates.

The INS experiments performed on the triple axis spectrometer DruelaL at SINQ (PSI, Switzerland) revealed the CF spectra of the overdoped $\text{R}_{1-y}\text{Ca}_y\text{Ba}_2\text{Cu}_3\text{O}_7$ ($\text{R}=\text{Ho}, \text{Er}$; $0 < y < 0.25$) to consist of two spectral components associated with the optimally doped and the overdoped domains (Fig. 1). Increase of the Ca concentration does not affect the local charge density of domains, but changes the spectral weight of the components. Similar "two-phase" picture was

established earlier for the underdoped region of the phase diagram.

We have demonstrated that the CF parameters as a function of the in-plane hole concentration follow the same dependence for both Er- and Ho-based 123-compounds, below and above optimal doping and independently of the way to introduce doping (by variation of the oxygen stoichiometry or by the partial Ca substitutions for rare-earths). The established systematic behavior of the CF parameters proves the charge origin of the superposition effect. Therefore, it exists a smooth crossover between the under- and overdoped parts of the phase diagram. It seems, that the results obtained are compatible with the scenario suggested recently in Ref. 1.

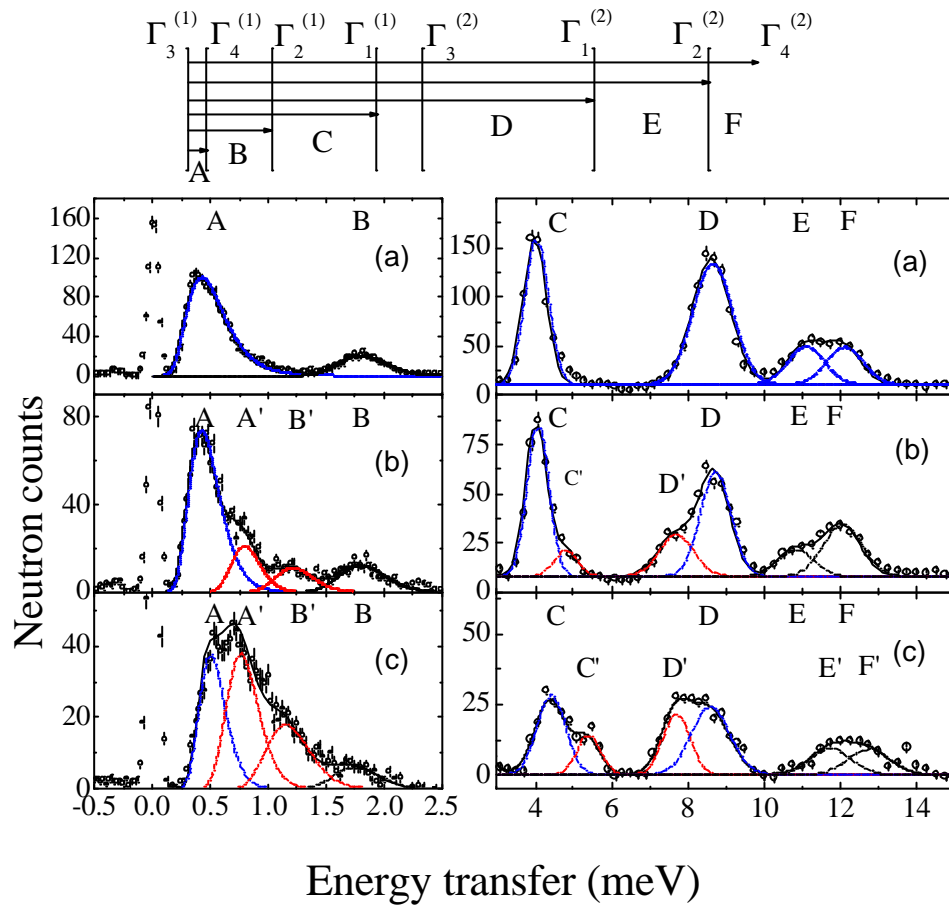


Fig. 1: Energy spectra of neutrons scattered from $\text{Ho}_{1-y}\text{Ca}_y\text{Ba}_2\text{Cu}_3\text{O}_7$ at $T = 1.5$ K for $y = 0, 0.1, 0.25$ (in panels (a), (b), (c), respectively). Left: high-resolution scans of the lowest CF transition at $Q = 0.85 \text{ \AA}^{-1}$, $E_f = 3.5$ meV. Right: scans at $Q = 1.8 \text{ \AA}^{-1}$, $E_f = 7$ meV. The top of the figure shows the low-energy CF splitting of $\text{Ho}_1\text{Ba}_2\text{Cu}_3\text{O}_7$. The observed transitions are indicated by arrows.

References

- [1] Yu. Ovchinnikov, S.A. Wolf, and V. Kresin, Phys. Rev. B **63**, 064524 (2001)
- [2] J. Mesot et al., Phys. Rev. Lett. **70**, 865 (2001)
- [3] A. Mirmelstein et al., J. Superconductivity: Incorporating Novel Magnetism **15**, 367 (2002)

1.10 X-ray and magnetization studies on FeCoV/Ti multilayers

M. Senthil Kumar¹, Shah Valloppilly², Christian Schanzer², Peter Böni², M. Horisberger³

¹Department of Physics, Indian Institute of Technology Bombay, Mumbai 400 076, India

²Physik Department E21, Technische Universität München

³Laboratory for Neutron Scattering, ETHZ & PSI, CH-5232 Villigen PSI, Switzerland

A series of FeCoV/Ti multilayers have been investigated by x-ray reflectivity, high angle x-ray diffraction and magnetization measurements in order to understand how the microstructural and morphological parameters influence the magnetic behavior of the multilayers. Interface roughness increases with the total thickness and the existence of lateral roughness correlation is observed from the x-ray diffuse scattering background. A strong magnetic coupling is observed between the ferromagnetic layers that depends on the Ti spacer layer thickness. For thicker Ti spacer layers a gradual magnetization reversal is observed.

Spin-dependent scattering of neutrons is being utilized as the working principle of the polarizer and analyzer in a neutron scattering experiments and this concept can be realized in FeCoV/Ti multilayers since the scattering length for polarized neutrons is:

$$b_{\pm} = b_{coh} \pm b_m$$

where the total scattering length has a nuclear and a polarization dependent magnetic part. Therefore, very large contrast between the $|+\rangle$ and $|-\rangle$ eigen states of the neutrons can be achieved by selectively choosing the non-magnetic material (e.g. TiN_x) and the angle of total reflection can be increased by increasing the number of layers [1]. However, the orientation of magnetic moments in the multilayers with respect to the neutron magnetic moment is an important factor that determines the efficiency of the polarizer, especially in the remanent state. Misorientation of the layer magnetic moment and the neutron moment can cause significant spin-flip scattering. In multilayers, sharp and flat interfaces are exceptional and in practice, they can be topographically and chemically rough due to morphology in the growth process and the interdiffusion. Such interfaces may influence the magnetic interlayer coupling and can affect magnetic properties like coercivity, anisotropy etc [2]. We have investigated the interface of FeCoV/Ti multilayers by specular x-ray reflectivity and off-specular scans. We have also studied the magnetization reversal as a function of varying the spacer layer thickness.

[FeCoV(100 Å)/Ti (x Å)/ FeCoV(30 Å)/Ti (x Å)]₂₀ (x = 30, 50, 80, 100, 120 and 150 Å) multilayers were sputter deposited by dc magnetron sputtering at PSI, Switzerland. High angle x-ray diffraction reveals that the films are textured and polycrystalline, and are grown in the orientation of highest in-plane atomic packing density, as deduced from [110] and [002] reflections for FeCoV and Ti

respectively. The analysis of the peak width using the Scherrer equation shows that the grain size is of the same order as the layer thickness. Specular reflectivity as a function of momentum transfer perpendicular to the film plane (q_z) show the Bragg peaks due to the periodically repeated FeCoV and Ti layers. The fast decay of the specular intensity with q_z is due to the roughness developing progressively during the film growth. The reflectivity curve simulated using appropriate film thickness, x-ray scattering factors, volume density of the materials and the roughness are compared with the experimental data and a typical example is shown in Fig.1.

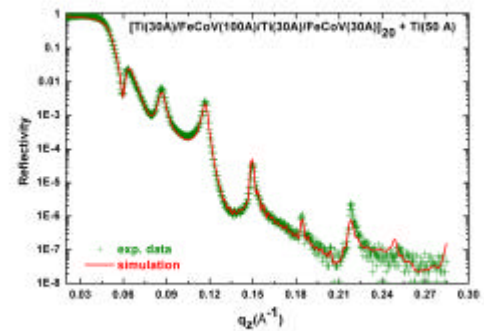


Fig.1 Specular x-ray reflectivity of Ti = 30 Å multilayer sample. The roughness is modeled to $0.1\sqrt{t}$ (t is in units of nm).

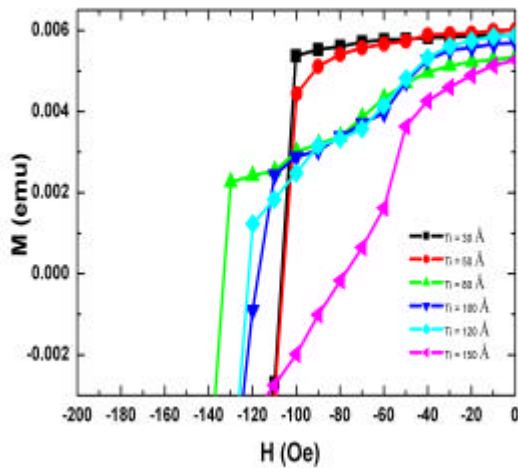


Fig.2. Switching of soft and hard layer magnetizations in FeCoV/Ti multilayers

From the specular reflectivity analysis it is observed that the roughness scales with \sqrt{t} , where t is the thickness of the film in nanometer. Since the specular reflectivity cannot distinguish the roughness from interdiffusion, we carried out off-specular reflectivity measurements by using rocking scans of the sample. A broad diffuse background and a sharp specular peak are visible in the diffuse scan. Since the width of the diffuse profile is inversely related to the effective in-plane roughness correlation length, it indicates the existence of vertically correlated roughness apart from the possible interdiffusion.

There exists an in-plane anisotropy in these multilayers of magnetoelastic origin arising from the in-plane stress distribution caused by the preparation conditions [3]. In fig.2, is shown the second quadrant of the hysteresis loop, where the magnetization reversals of the thin (soft) and thick (hard) FeCoV layers are found to be strongly dependent on the Ti spacer layer thickness. For thin Ti layers, the hard and soft layers switch almost at the same reverse field, whereas at higher Ti spacer thickness, the soft layers switch earlier compared to the hard layers. However, we observe that the switching fields are different irrespective of the same soft layer thickness and also the magnetization reversal becomes less sharp compared to their bilayer counterparts [4]. When the Ti spacer thickness is small, the exchange can be mediated through RKKY type mechanism or mediated through pinholes. At higher Ti spacer thickness, the coupling is mainly due to the Néel type (Orange-peel) coupling originating from the dipolar fields created by the rough

interfaces. The topographical roughness and 'magnetic roughness' are very important parameters in the performance of the neutron polarizer supermirrors and presently, we are investigating the origin of this 'magnetic roughness' by polarized neutron reflectivity experiments.

- [1] P. Böni, *Physica B* **234 – 236**, 1038 (1997)
- [2] Chung-Hee Chang and Mark H. Kryder, *J. Appl. Phys.* **75** 6864 (1994)
- [3] D. Clemens, A. Vananti, C. Terrier, P. Böni, B. Schnyder, S. Tixier and M. Horisberger, *Physica B* **234 – 236**, 500 (1997)
- [4] M.Senthil Kumar and P. Böni, *J. App. Phys.* **91**, 3750 (2002)

1.11 Preparation and Characterization of FeCoV/Ti Multilayers: a Comparison

C. Schanzer¹, S. Valloppilly¹, B. Russ¹, P. Böni¹, C. Breunig², A. Urban²

¹Physik Department E21 der Technischen Universität München

²Forschungsreaktor München II der Technischen Universität München

The physical properties of materials as a thin layer can be rather different from their bulk counterparts. Especially the magnetism of thin layers shows interesting behaviour. The aim of our investigations is to study the dependence of the magnetic properties on microstructural parameters like interdiffusion and interface roughness. In order to address such questions, metallic multilayers were prepared consisting of ferromagnetic layers separated by non-magnetic layers. The multilayers were grown by DC magnetron sputtering. The structural properties were characterized by specular and off-specular X-ray reflectometry. Furthermore we performed magnetization measurements to investigate the magnetic properties. There were clear differences from known similar systems [1], most likely originated from different growth conditions.

We investigated multilayers consisting of the alloy $\text{Fe}_{50}\text{Co}_{48}\text{V}_2$ as the magnetic layer and titanium as the non-magnetic layer. Such samples with different layer thicknesses were available from the Paul-Scherrer-Institut (PSI). Some of those results are discussed in [2]. Furthermore, we prepared similar samples using the sputter unit at Forschungsreaktor München II (FRM-II). Here we equipped an existing target head with two DC magnetron targets (viz. $\text{Fe}_{50}\text{Co}_{48}\text{V}_2$ and Ti) as shown in fig. 1. A first series of samples was deposited at a pressure of 1.6 μbar . A deposition rate of $\approx 28 \text{ \AA/s}$ at the power of 0.8 kW for the FeCoV target and a rate of $\approx 16 \text{ \AA/s}$ at the power of 0.7 kW for the Ti target was obtained. The accuracy of the layer thickness was estimated to be 1% of the nominal thickness.

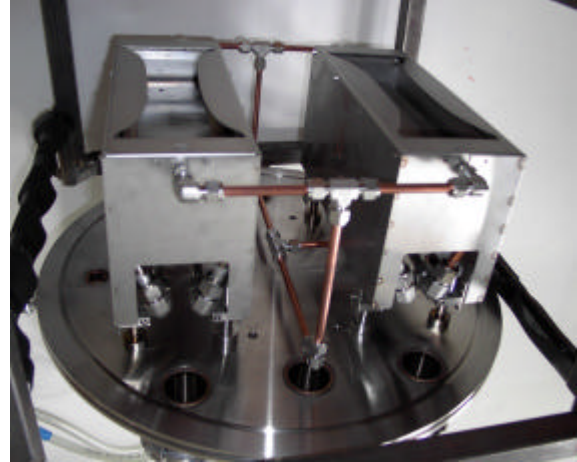


Fig. 1: Target head for the FRM-II sputter unit equipped with two DC magnetron targets: FeCoV and Ti

Specular and off-specular X-ray reflectometry were performed to characterize the structural properties of the multilayers. The measurements were carried out using a Siemens D5000 diffractometer. Originally, the unit was a dedicated powder diffractometer. After upgrading with a sample table equipped with tilting facility, a high precision knife-edge collimator, an automatic absorber and a monochromator, the instrument was enabled to perform high quality reflectometry measurements. The knife-edge collimator is especially beneficial for the off-specular reflectometry since, to a good approximation, the angular resolution is independent of the angle of incidence. A comparison of samples sputtered at FRM-II and PSI is shown in Fig. 2. The specular reflectivity showed more intense Bragg peaks for the FRM-II sample, which were also prominent at higher q_z . As a qualitative result one can deduce that the interface roughness of the FRM-II sample is much smaller than that of the PSI sample. This was also supported by the off-specular reflectometry results where the diffuse profile background for FRM-II sample is found to be much less than that for the PSI sample.

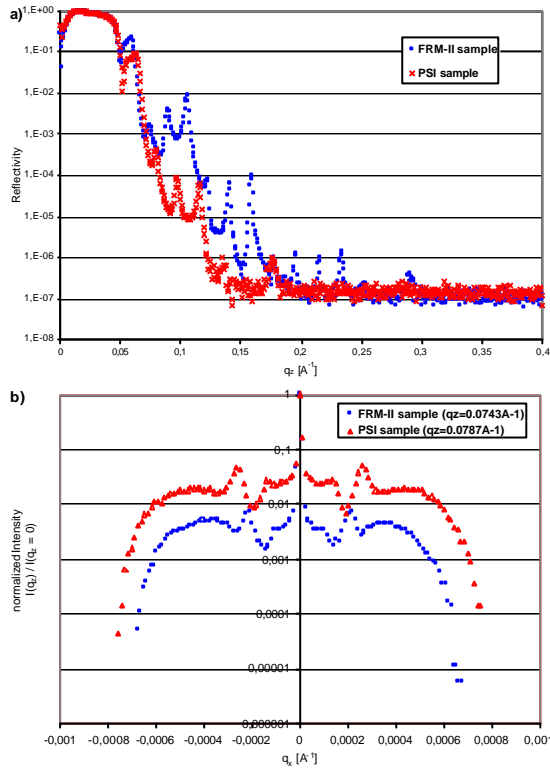


Fig. 2: X-ray measurements of multilayers: [Ti (100 Å) / FeCoV (100 Å) / Ti (100 Å) / FeCoV (30 Å)]₂₀ + Ti (50 Å), a) specular reflectivity b) diffuse scattering (rocking scan)

Magnetization measurements were performed using a Quantum Design PPMS. A comparison, like in the x-ray data, between the two types of samples showed a large difference in the magnetic properties although the thicknesses of the layers were identical. Basically, one would expect a dependence of the coercive field of the FeCoV layers to be proportional to the layer thickness in a certain thickness region [1]. This has been observed also for the FRM-II samples. But here, the coercivity was quite large compared to that of the PSI counterparts. This difference and some other magnetic properties like interlayer coupling have to be understood further in conjunction with the structural differences of the layers as seen from the x-ray studies.

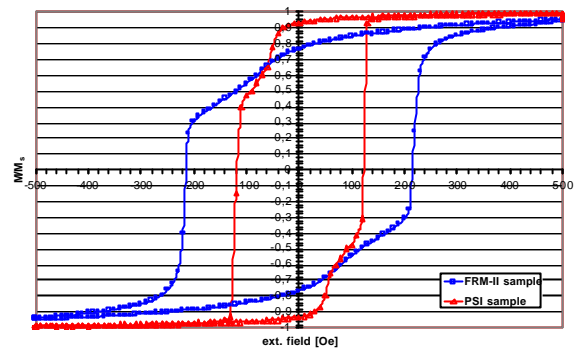


Fig. 3: Magnetization measurements of multilayers: [Ti (100 Å) / FeCoV (100 Å) / Ti (100 Å) / FeCoV (30 Å)]₂₀ + Ti (50 Å)

References

- [1] M.Senthil Kumar, P. Böni, J. App. Phys. **91**, 3750 (2002)
- [2] S. Valloppilly, this annual report

1.12 Critical spin dynamics in CsMnBr₃

C. Reich¹, P. Böni¹ and B. Roessli²

¹Technische Universität München, Physik-Department E21

²Laboratory for Neutron Scattering, ETH Zürich & Paul-Scherrer-Institut, CH-5232 Villigen, Switzerland

Inelastic magnetic neutron scattering studies were performed on CsMnBr₃ in the critical regime above $T_N = 8.3$ K. We observe an upward renormalization of the spin-wave dispersion at the magnetic zone center ($1/3$ $1/3$ 1) with increasing temperature. The different dispersion branches were precisely distinguished by applying polarization analysis techniques.

CsMnBr₃ represents a good realization of a triangular Heisenberg antiferromagnet on a stacked hexagonal lattice. A strong magnetic exchange coupling J_c exists between the stacked hexagonal net planes, but in the plane itself only a relatively weak coupling J_{ab} is present. Additionally, an anisotropy due to long-ranged dipole-dipole interactions confines the spins into the hexagonal plane. Three-dimensional magnetic ordering breaks down in the critical temperature region above $T_N = 8.3$ K, but strong short-ranged magnetic correlations still persist along the c-axis because of the large value of J_c (see figure 1). Thus CsMnBr₃ shows quasi-one-dimensional antiferromagnetic behaviour for a wide critical region above T_N .

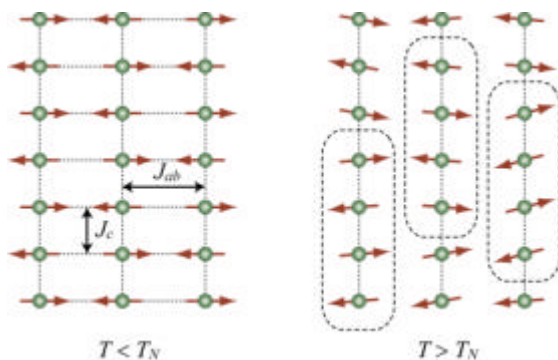


Fig. 1: Sketch of the spin chains along the c-axis. The dashed boxes represent one-dimensional AF-domains.

We investigated the spin wave dispersion spectra of CsMnBr₃ in the critical regime and especially the renormalization behaviour of the energy gap at the magnetic zone center ($1/3$ $1/3$ 1). CsMnBr₃ shows three dispersion branches in the ordered phase: Two branches of in-plane spin fluctuations (acoustic and optic) and one optic branch, corresponding to out-of-plane fluctuations (figure 2). The optical character of the latter is due to dipolar anisotropy, see Hummel et al. [1]. Previous critical scattering measurements [2] indicate a downward renormalization of the acoustic in-plane mode, but the behaviour of the two optical modes above T_N still remained unknown.

Our measurements were performed using the triple-axis-spectrometer TASP at the neutron spallation source SINQ, located at the Paul-Scherrer-Institute in Switzerland. In a first experiment, we clearly observed a linear renormalization upwards of at least one optical mode with rising temperature, see figure 2.

Since only one optical excitation peak was observed in the spectra of figure 2, we concluded that both optical branches may appear at very similar energies and merge together to one single scattering signal. Thus in a second experiment polarization analysis was applied with aim to resolve both components by means of polarized neutron scattering. The results confirmed that both modes linearly renormalize upwards with increasing temperature (figure 3).

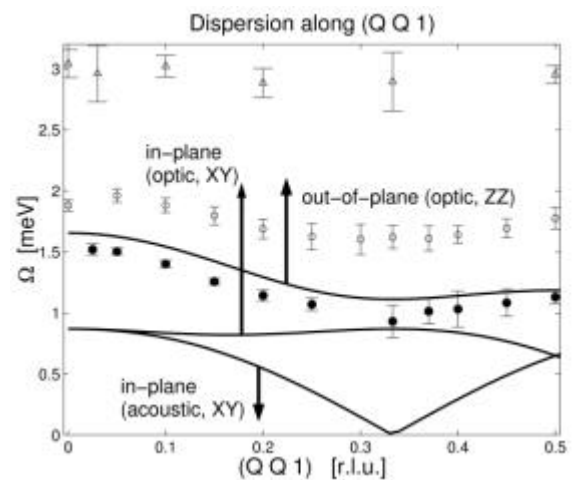


Fig. 2: Spin wave dispersion in the hexagonal plane. The lines represent the calculated dispersion branches in the ordered phase below T_N . The black points are values gained at $T = 9$ K, the circles correspond to $T = 17.5$ K and the triangles to $T = 40$ K. The arrows indicate the observed renormalization of the modes (see also figure 3).

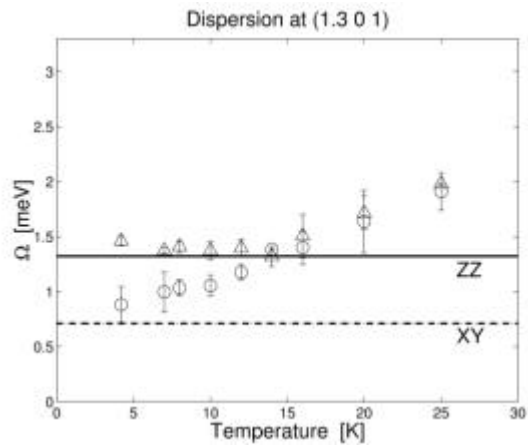


Fig. 3: Temperature dependence of the optical in-plane (XY, circles) and out-of-plane (ZZ, triangles) modes.

This very peculiar behaviour indicates that the interactions between the spin chains are *not* negligible. In fact, dipole effects seem to play a significant role by building up interchain-correlations. Especially the spin dynamics of the optical out-of-plane mode underlies strong competing influences by dipole and exchange forces.

References

- [1] Hummel et al., Phys. Rev. B 63, 094425 (2001)
- [2] Mason et. al., Phys. Rev. B 39, 586 (1989)

1.13 Polarized SANS studies from the weak itinerant helimagnet MnSi

R. Georgii¹, P. Böni², H. Eckerlebe³, S. Grigoriev⁴, N. Kardjilov²,
A. Okorokov⁴, K. Pranzas³, B. Roessli⁵ and W. Fischer⁵

¹Technische Universität München, Germany

²Technische Universität München, Physik-Department, E21, Germany

³FRG-1, GKSS, Geestacht, Germany

⁴PNPI, St. Petersburg, Russia

⁵PSI, Villigen, Switzerland

The intermetallic compound MnSi shows at $T_c = 28.5$ K a magnetic phase transition from the paramagnetic phase to an ordered phase with a long-period ferromagnetic spiral [1]. The antisymmetric exchange interaction, the so-called Dzyaloshinsky-Moria (DM) interaction, being responsible for this structure, arises from the lack of inversion symmetry in the cubic structure of MnSi. A unique feature of the DM interaction is that the spiral should be either right or left handed depending on the sign of the DM interaction. Polarized SANS is ideal for the investigation of chirality and the critical scattering in such a system. Furthermore in a SANS experiment, where the MnSi is orientated along its (111) direction, the magnetic peaks should be visible close the nuclear diffraction point, which is itself blocked by the beam stop. It also offers the advantage of better q -resolution compared to for example a three-axis spectrometer. Another interesting point is how the critical scattering around T_c develops from the ordered to the paramagnetic phase [2]. Here the critical indices can be determined.

Therefore we performed a polarised SANS experiment at the SANS-2 of the research reactor FRG-1 of the GKSS in Geestacht. The SANS-2 polarizes the neutrons after they have been monochromatised in a velocity selector with a multilayer supermirror such, that only one spin state can pass the mirror unperturbed. A RF spin flipper from PNPI, which has no material in the beam, can then flip this state for all neutrons without being sensitive to their velocity. Therefore the full wavelength spread of $\Delta\lambda/\lambda$ of $\approx 5\%$ at 5 \AA can be used for the experiment. The disk-shaped sample is mounted perpendicular to the beam in a cryomagnet and its temperature is being controlled by a Lake-shore controller. The position sensitive detector (55 cm x 55 cm sensitive area) can be moved from 1 m to 16 m from the sample offering a q -range of $10^{-3} \text{ \AA}^{-1} < q < 0.3 \text{ \AA}^{-1}$. For our experiment the magnetic peak is expected to be at 0.035 \AA^{-1} , thus the detector was positioned at a distance 1m behind the sample. The data were recorded for each spin state separately allowing for a polarisation sensitive evaluation. This is

ongoing, but some preliminary results are given here:

MnSi shows exactly the expected behaviour (see Figure 1) as described above. At temperatures slightly above the critical temperature a ring around the nuclear peak can be observed, which narrows when approaching T_c . Below the critical temperature two magnetic peaks form, which are sensitive to the incoming neutron polarisation. It should also be noted that the cross sections are huge. We get more than 500000 counts in 100 sec per magnetic peak! The next step will be to evaluate from the 2-dimensional intensity pattern the susceptibility and to determine the critical exponents for the phase transition.

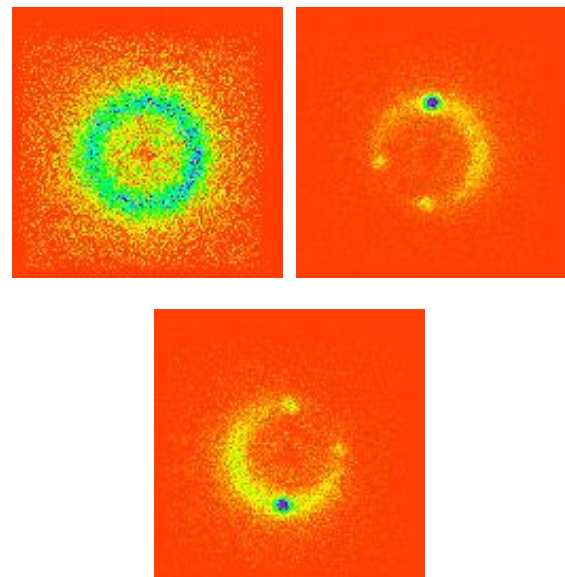


Fig.1: The transition from the disordered magnetic phase (left) to the spiral ordered phase (middle and right) in MnSi in the critical scattering regime around $T_c = 28.5$ K. The crystal was oriented along its (111) direction. The two pictures below T_c are shown for both polarisation states of the incoming neutrons.

References

- [1] G. Shirane et al., Physical Review B, **28**, 6251 (1983)
- [2] B. Roessli et al., Physical Review Letters **88**, 237204-1 (2002)

1.14 Design of an inelastic neutron spectrometer for catalytic applications at FRM-II

A. Jentys¹, J. A. Lercher¹, E. Steichele², W. Petry²

¹*Technische Universität München, Department of Chemistry*

²*Technische Universität München, Physics Department*

Background

Vibrational spectroscopy represents a versatile technique for material characterisation and the study of dynamics at the atomic scale. Besides the use of photons to excite vibrational and rotational transitions (e.g. in the IR- and Raman spectroscopy) the study of the interaction between neutrons and matter gains increasing importance. Inelastic neutron scattering (INS) excites transitions between vibrational levels and, thus, allows to study the motions of atoms and molecules. The advantage of INS over IR- and Raman spectroscopy results from (i) the absence of selection rules, (ii) the spectral range from 5 to 500 meV (40 to 400 cm⁻¹) can be observed, (iii) optically opaque samples are typically almost transparent for neutrons, (iv) the large incoherent cross-section of protons make INS very sensitive for hydrogen atoms, and (v) frequencies and intensities can be calculated with high accuracy, which supports the interpretation of the spectra obtained. Examples in the field of catalysis range from bulk samples such as Raney- metals, over highly dispersed oxide supported metal clusters, (micro-) porous metal oxides, metal sulfides and carbons. The use of (partially) deuterated molecules or the use of D instead of H should allow the identification of reactive species and the differentiation between the reactive and non-reactive intermediates.

Special Sample Environment

As most of the samples will consist of high surface area powders, specially designed reaction cells have to be developed, which should allow the complete removal of water and other contaminants such as hydrocarbons before the measurements. Aluminum, stainless steel and quartz can be used as materials for the in situ reaction cells.

The successful description of catalytic processes requires that the catalyst is characterized in direct contact with the reactant/product molecules under conditions closely related to those of the reactions with respect to solvent, pressure and temperature. Therefore, in most cases it will be necessary to intercept the reaction by rapid cooling (quenching), which has two advantages: (i) the widths of the bands in the INS spectra will be reduced and (ii) the reaction will be interrupted and, thus, the reaction kinetics can be

uncoupled from the time required to collect the spectra. This will allow to follow rapid kinetic reactions, because the time necessary to collect a single spectrum will be in the order of 60 minutes. The inherent disadvantage of this approach is that the reaction once stopped, cannot be restarted to observe a later time frame. Therefore, the development of a system, which allows collecting samples at given time interval and to store them for the later (asynchronous) analysis by neutron scattering has to be developed.

Design of a Catalysis Spectrometer at the FRM-II

The study of vibrational states needs to measure energy transfers of about 500 meV, what, at the FRM-II, is most advantageously done with hot neutrons from the Hot Source in front of beam tube SR-9. This beam tube has two channels (8 cm x 12 cm channel width), one of which (SR-9b) is already used for HEIDI, a hot neutron single crystal diffractometer. The second channel (SR-9a) can be used for the catalysis instrument, but the locality is confined by the neighbour instruments. INS needs energy determination of the neutrons before and after scattering, what is done normally either by Bragg reflexion from crystalline materials or by the Time-of-Flight (TOF) technique. Out of the manifold of possible spectrometer types we have studied the feasibility of a TOF spectrometer, of a crystal monochromator Be filter instrument and of a spectrometer with a PG graphite analyzer.

The Time-of Flight spectrometer design was a TOSCA- like instrument [1] with a fast chopper, a super mirror guide for hot neutrons ($m = 3.5$ or even $m = 4$) and a beryllium filter analyzer. The length of the guide to an external neutron laboratory was 30 – 40 m , the pulse-width about 100 μ s for an energy resolution of about 5 % for primary neutrons of 300 meV. Chopper rotors of a mass of 20 – 40 kg had to be rotated with typically 10 000 rpm. The relative energy resolution varied between 4% and 7 % for a primary neutron energy between 200 and 600 meV, the intensity of the instrument was comparable to a crystal monochromator and beryllium filter analyzer instrument of about the same resolution. Because of the high technological challenge and the resulting high costs the TOF-spectrometer was rejected.

As an alternative a crystal monochromator instrument in the experimental hall of the reactor building was studied. The distance from the hot source to the monochromator position at beam tube SR9-a is 8 m, allowing a maximum primary vertical divergence of about 1° and a horizontal divergence of about 0.5° . The maximum illuminated area of a monochromator can be about 22 cm x 12 cm, which can be focused down to about 7 cm x 4 cm at the sample. In such an „open“ configuration one gets a high intensity instrument with a poor energy resolution of about 6 % to 12 % for neutrons with an energy between 200 meV and 600 meV. A better energy resolution could be obtained by use of narrow Soller collimators in combination with large monochromator angles. High take-off angles are, however, not possible because of spatial limitations in the horizontal plane.

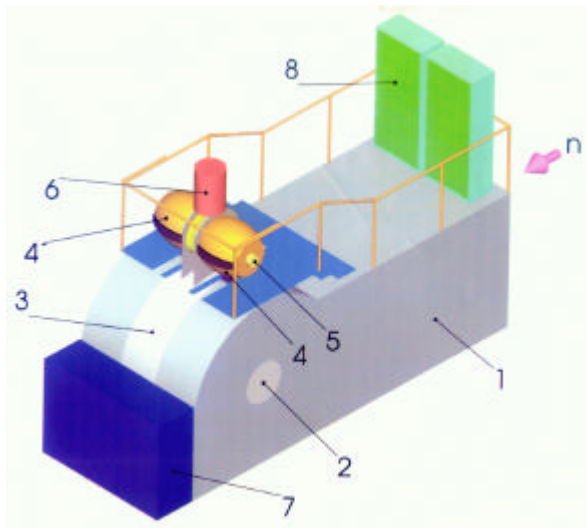


Fig. 1: Sketch of the catalytic application spectrometer

To overcome these limitations another design is proposed as shown in figure 1. The scattering plane at the monochromator is turned from the horizontal into the vertical plane. Neutrons from the beam tube are entering the shielding block (1) and are reflected by a monochromator crystal, which can be rotated around the horizontal axis (2). The monochromatic neutrons are reflected through a radial channel in the shielding block (3), which can rotate also around the horizontal axis (2) in a theta-two-theta coupling to the monochromator crystal. The instrument is thus operated with variable primary energy, which can be varied by rotation of the monochromator and the shielding block. The sample is fixed to the rotating shielding block (3) at the exit of the channel. Scattered neutrons are analyzed by pyrolytic graphite crystals, which are arranged in two rotational

ellipsoids (4) with a horizontal axis. Such an analyzer, typically 70 – 80 cm long with 40 – 50 cm diameter, was proposed in the „Millennium Programme“ at ILL by Ivanov [2] and its principle is shown in figure 2. The sample is located in one focus and the detector (5) in the other. Direct radiation without reflection at the graphite crystals is blocked by an absorber. Second order reflections from the graphite can be eliminated by a Be filter window at the entrance of the ellipsoids. The important advantage of such an analyzer is an unusually big acceptance angle of nearly 3 Steradian per ellipsoid. These analyzers are coupled to the rotating shielding block (3). With PG crystals of $\sim 3^\circ$ mosaic spread an energy resolution of $\sim 2\%$ for energy transfers of 100 meV can be obtained.

The last proposal is certainly the most attractive one as it is a high resolution and high intensity instrument, which fits well into the crowded surrounding. Nevertheless it is a challenge as that type of analyzer has not yet been realized before.

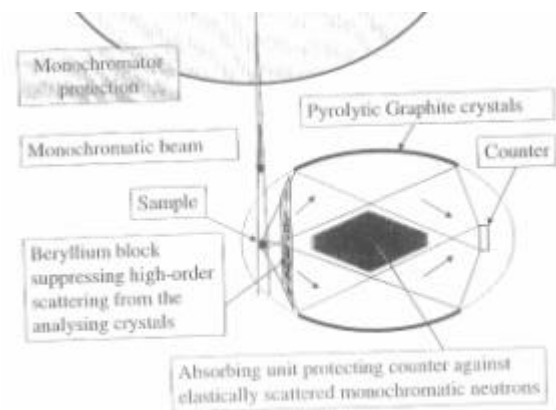


Fig. 2: Ellipsoidal energy analyzer of scattered neutrons [2]

References:

- [1] D. Colognesi et al., Appl. Phys. A 74 (Suppl.) S64 – S66 (2002)
- [2] A. Ivanov: „Beryllium Filter Spectrometer on IN1 in the Millennium Programme of ILL“ (2000)

1.15 MIRA -- Very cold neutrons for new methods

R. Georgii¹, N. Arend^{1,2}, T. Hils², P. Böni², H. Fußstetter¹, G. Langenstück¹

¹Technische Universität München

²Technische Universität München, Physik-Department, E21

A beam line for VCN has been built at the new neutron source FRM-II. Situated in the neutron guide hall at the end of a curved neutron guide looking to the cold source, MIRA will operate between 7.7 Å and 30 Å. The beam line is designed to develop, test and demonstrate new methods to use very cold neutrons therefore the instrument will be equipped with different instrument options.

The instrument consists of a neutron guide (1 cm x 12 cm) with a shutter in the neutron guide bunker. The monochromator mechanics is situated at the end of a 7 m long curved neutron guide (R = 84 m) inside the shielding. The differential flux will reach a maximum at the wavelength $\lambda = 8.5$ Å and will be around $4 \cdot 10^7$ neutrons/(Å cm²). A mica (Phlogopite) monochromator with $d_{200} = 9.9$ Å and a mosaicity of 0.9° will be used in the wavelength range from 7.7 Å, the cut-off of the curved neutron guide, up to 14 Å. A $\Delta \lambda/\lambda$ in the range of 2-8 % will be obtained, depending on the choice of the divergence of the beams before and after the monochromator. For wavelengths of 15 Å, 20 Å and 30 Å multilayer monochromators on glass or silicon substrates are foreseen. The multilayer monochromatises the neutrons with a $\Delta \lambda/\lambda$ of about 2 – 10 % depending on the bandwidth of the multilayer sequence. A low-band pass mirror in front of the monochromators can be brought into the beam for suppressing the long wavelength contributions (from the regime of total reflection), which would otherwise contaminate the beam after monochromatisation with a multilayer monochromator. The 4 monochromators can be individually rotated into the beam. The whole monochromator unit, with different tables for rotation and x-y-z translation, an aperture for the incoming neutrons and a monitor counter is surrounded by the shielding. It consists of 10 cm lead and 25 cm concrete $\rho = 4.7$ g/cm³ with a 10 mm neutron absorbing layer of B₄C (see figure 1).

During 2002 the design of the instrument was finished. The neutron guide with the shutter in the bunker was installed and is now ready for routine operation. The shielding was designed and manufactured at Swiss Neutronics. The shielding is now installed at its final position in the neutron guide hall. The mechanics and control electronics for the monochromator is waiting for the installation into the shielding. The mica monochromator is finished and was characterised with neutrons of 5 Å at PSI in

Switzerland. The data evaluation is proceeding.



Fig. 1: The shielding for the monochromator of MIRA

The very cold neutron reflectometer option of MIRA

One of the instrument options is a classical reflectometer in horizontal geometry (see figure 2). Such a reflectometer for very cold neutrons has the advantage over most existing reflectometers that the angles of reflection are larger and alignment errors near to the critical edge are less critical, yet the accessibility of the phase space is comparable to reflectometers with cold or thermal neutrons.

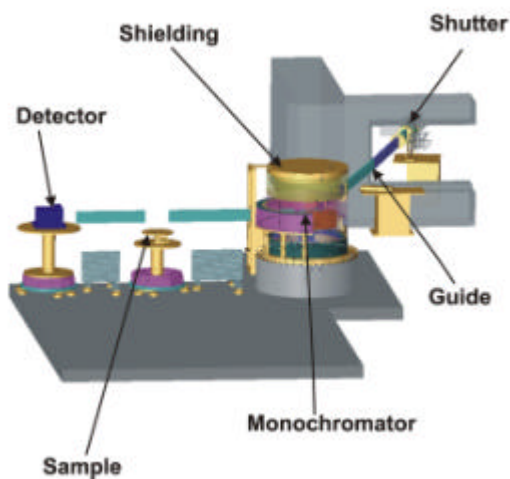


Fig. 2: MIRA in the reflectometer option with its neutron guide

After monochromatisation in the shielding the neutrons will enter a vacuum tube and hit a sample. Neutron mirrors above and below the beam for the transport of the vertical divergence from the monochromator to the sample are foreseen to be installed in this tube. In the beginning the instrument will mainly operate as a classical reflectometer, with a θ - 2θ scan for a vertical sample geometry. It will reach a q -transfer of $7.0 \cdot 10^{-4} \text{ \AA}^{-1} < q < 1.1 \text{ \AA}^{-1}$ within the wavelength range of the instrument. Apertures will be used to adapt the wavelength spread of the beam to the beam divergences from the different monochromators. The reflected radiation from the sample will be detected in the detector unit, which will be a ^3He -counter. Later the use of a 2-dimensional position sensitive detector is planned.

For using the reflectometer with polarised neutrons a multilayer polarisation filter shortly after the monochromator can be brought into the beam. After the sample there will be a supermirror-based analyser. There will be also spin-flippers before and after the sample. The idea is to perform specular and non-specular polarised neutron reflectometry in the classical way, i.e. measurement of the four moduli of the reflection matrix [1]. For this only 4 reflectivities need to be measured, namely R_{++} , R_{+-} , R_{-+} , and R_{--} , where the + and - refers to the polarisation of the beam before and after the sample.

In 2002 the design for the reflectometer option was finished and a performance analysis of the option was performed. First components, especially of the sample table have been ordered and are expected to be installed in summer 2003.

The Multiple SANS Option

Normal SANS machines are, due to the small angles being measured, relative long and need therefore long measurement times since the sample is seen from the detector only under a very small solid angle. Using a setup as shown in figure 3 two-dimensional small angle scattering with several partial-beams can be performed. For special cases (q -transfer) this might allow measuring with higher intensities and smaller machines as standard SANS or could be used as resolution enhancement option at a conventional SANS. In this project the main properties like resolution and intensity of a setup consisting of two periodical multihole-apertures (typical $\varnothing_{\text{hole}} 1 \text{ mm}$, $d = 2,5 \text{ mm}$) that lead to an incoherent superposition of a multitude of "little (ultra-high-resolution) SANS machines" are derived. The number of superpositions results from the product of illuminated aperture-holes. The basic idea therefore is to compensate the intensity loss due to the small apertures by incoherent addition of many partial solid angles. The working principle of such a device will be tested at MIRA and a comparison to conventional SANS is planned. In 2002 the basic design for this option was completed and 2 prototypes of the multihole-apertures were manufactured.

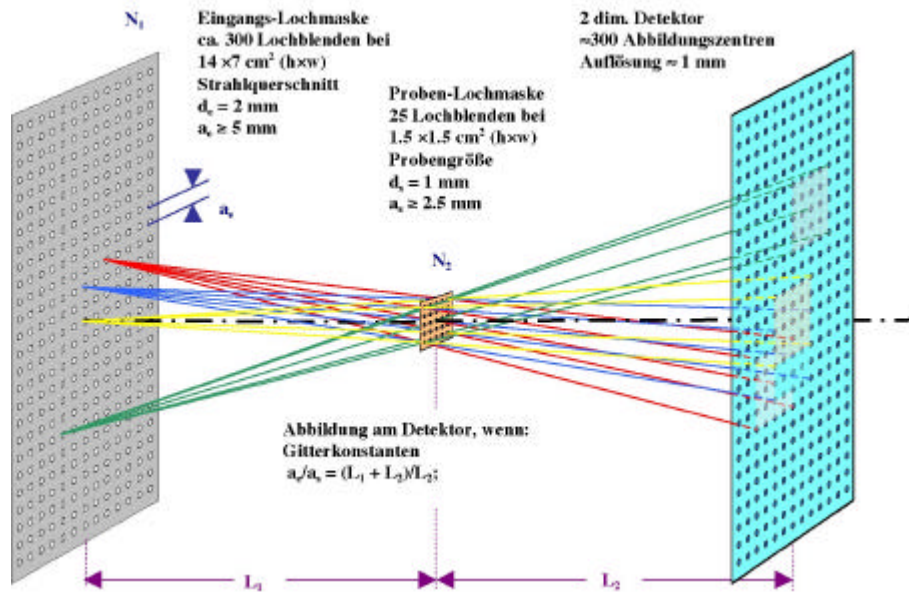


Fig. 3: The multi-SANS option

Multi level-MIEZE setup

This option of MIRA will be used for the investigation of longitudinal coherence properties of neutron beams. This can be achieved by using the multi level-MIEZE variant of the Neutron Resonance Spin Echo (NRSE) technique [2] with VCN.

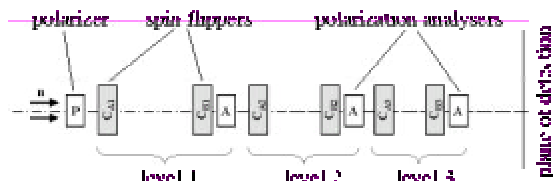


Fig. 4: Scheme of a multi level-MIEZE

The longitudinal coherence properties of the two neutron spin states can be studied by a very short temporal modulation of the polarisation of the neutron beam. Stacking of several MIEZE setups with a common detector position results in a signal, which is the product of the sinusoidal signals from all individual setups, see fig. 4. A time resolution of 10^{-7} is possible and the respective coherence length would be of the order of cm. It should be mentioned that the multi level-MIEZE principle has not been verified so far and shall be verified with this setup of MIRA.

Crucial parts of the instrument are the spin flippers, which will be constructed as bootstrap coils [3]. They must be suitable for the wavelength range of VCN. Since the neutron beam has to penetrate the coils, interaction (scattering, absorption) with the coil windings is a serious problem, especially in the cold

neutron range. Therefore material test measurements to find new adequate material combinations have been performed at the SANS machines at PSI.

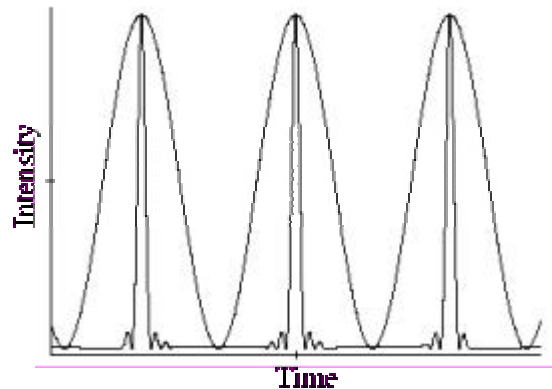


Fig. 5: Signal of a 4-level multi MIEZE setup

First evaluation of the data shows that the commonly used material for bootstrap flipper coils (Al_2O_3 coated Al band) will most presumably cause problems due to relatively high absorption and scattering features from the isolation layer.

To optimise the design concerning heat production, magnetic field homogeneity, etc, the coils are being simulated using finite element methods. Furthermore efforts on ray-trace simulations using McStas are planned.

[1] G.P. Felcher, Physica B, **198**, 1595 (1981)
 [2] Scattering and Inverse Scattering in Pure and Applied Science, edited by Roy Pike, Pierre Sabatier. pp. 1264-1286, San Diego, CA, Academic Press (2002)
 [3] R. Gähler and R. Golub, J. Physique, 49:1195 (1988).

1.16 Testing the shielding of the monochromator of Mira by Monte Carlo Method

Nico Wieschalla¹, Florian Grünauer¹, Robert Georgii^{1,2}

¹TU-München, Physics Department, E 21

²TU-München, ZWE FRM-II

Munich's new research neutron source FRM-2 will provide a variety of different neutron beams for many different applications. One of these applications will be 'Mira' - a station for experiments with cold neutrons.

At the entrance of this station the neutron beam will have a Maxwell energy distribution of about 40K. The neutron flux will be

$2.5 \cdot 10^8 \text{ sec}^{-1} \text{ cm}^{-2}$ at this position. For most experiments it is necessary to have a monochromatic beam. The wanted energy will be selected from the 'white' incoming beam by Bragg reflection in a phlogopit crystal. A Li-6 Beamcatcher will absorb neutrons, which pass this crystal.

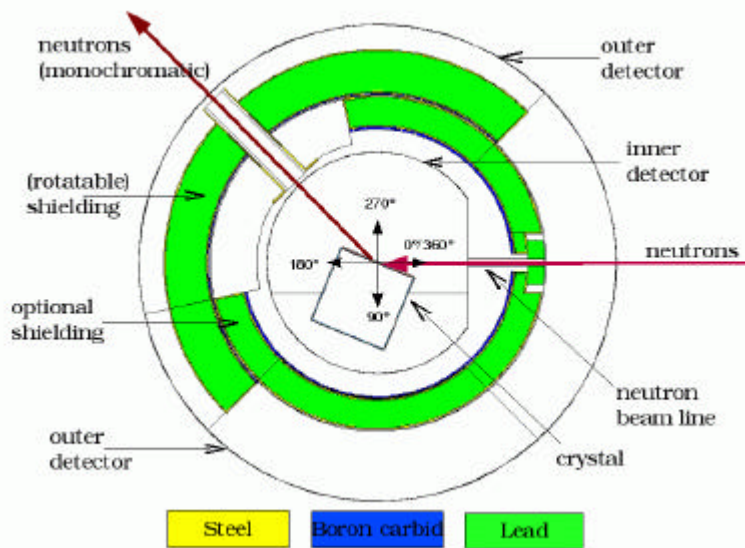


Fig 1: horizontal cut on beam level

In addition a large amount of neutrons will be scattered or absorbed (causing secondary radiation) in structure material of the experiment. The resulting unwanted radiation must be attenuated by a shielding, in order to meet radiation protection purposes and to reduce background radiation for other experiments.

The efficiency of this shielding was estimated by Monte Carlo Method, considering neutrons and generated gamma radiation. The geometry of the shielding is shown in fig. 1. It consists of two layers. The inner one is made of boron carbide. Neutrons are captured in boron by a (n,α)-reaction. This reaction is accompanied by 0.48 MeV gamma radiation. This energy is rather low compared to gamma radiation from neutron capturing in other materials like iron, aluminum or hydrogen; attenuation of the produced gamma radiation is therefore much easier. Nevertheless it is necessary to have a gamma shielding as second layer. In our case we use lead for this purpose, because of its high atomic number. This layer will be 10 cm thick and it will be surrounded by a steel liner (wall thickness: 0.6cm). At FRM-2 the dose level outside shieldings should not exceed 3μSv/h.

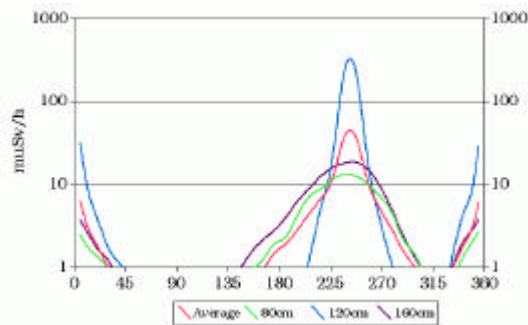


Fig 2: dose rate at the outer detector for different heights. The beam level is on 120 cm.

The simulated horizontal dose distribution outside the shielding at different heights is

shown in fig.2. The beam level is on 120 cm. For this simulation an angle of 120° between beam entrance and exit was assumed. Of course the highest dose values are reached at the beam entrance and the beam exit.

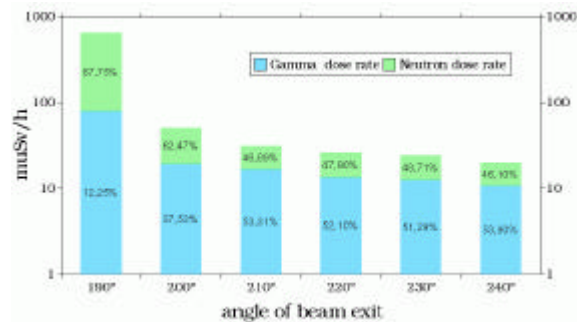


Fig 3: maximum dose rate for different angles of the beam exit

However the values at this locations are a conservative estimation:

- In reality there is an additional shielding surrounding the incoming beam, which was omitted in the Monte Carlo modell.
- The wideness of the beam after the Bragg reflection was assumed to be bigger than it can be expected in reality. Therefore more neutrons hit the steel liner that surrounds the exit channel. The resulting gamma production by neutron capturing in iron is increased by this effect.

Even in this last case, the dose peak can be limited by covering the steel structure of the beam exit by boron carbide layer (thickness 0.5cm)

Another problem appears when the beam exit is at 190° . A direct view from the source to the exit is possible due to the divergence of the beam. Now the neutron flux in the exit is much higher and the gamma production too, due to increased neutron capture in iron. Therefore it is not advisable to work at this angle neither for monochromating the neutron beam nor for the dose rate (see fig. 3).

Also this shielding was compared with another one: The boron carbide of the first layer of the shielding was replaced by Li-6. This neutron absorber produces no gammas by neutron capture, but the dose rate at the outer detector was exactly the same compared to boron carbide. This behaviour shows, that the influence of the outer steel liner of the shielding is dominant for the dose rate outside the shielding. Therefore it is not necessary to use Li-6 (much more expensive compared to boron carbide) for neutron capturing inside the shielding.

Another interesting point was the estimation of the neutron flux dependance on the thickness of the crystal. Figure 4 shows the neutron flux at the inner detector (fig. 1) for different thickness and without the crystal.

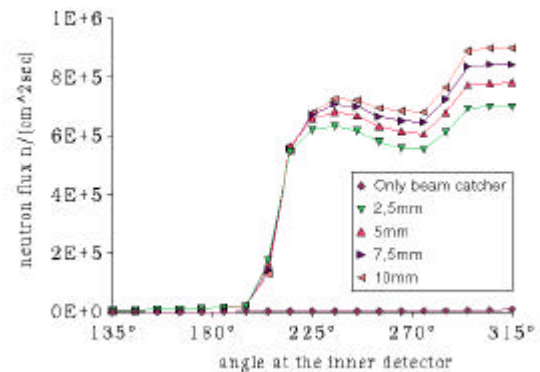


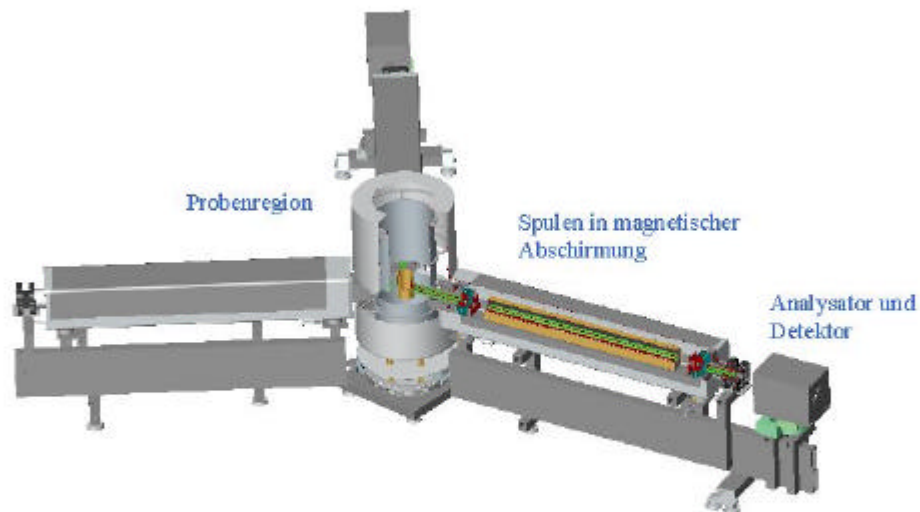
Fig 4: Neutron flux at the inner detector for different thickness of the crystal

Most neutrons were scattered by a crystal of a thickness of 10 mm. However the difference to the other investigated thicknesses are rather low: The thickness of the crystal can be optimized without regarding radiation protection purposes.

At least we can say, that the built shielding is a good protection against the radiation.

1.17 RESEDA Spectrometer: Jahresbericht 1.1.-31.12.02

M. Bleuel



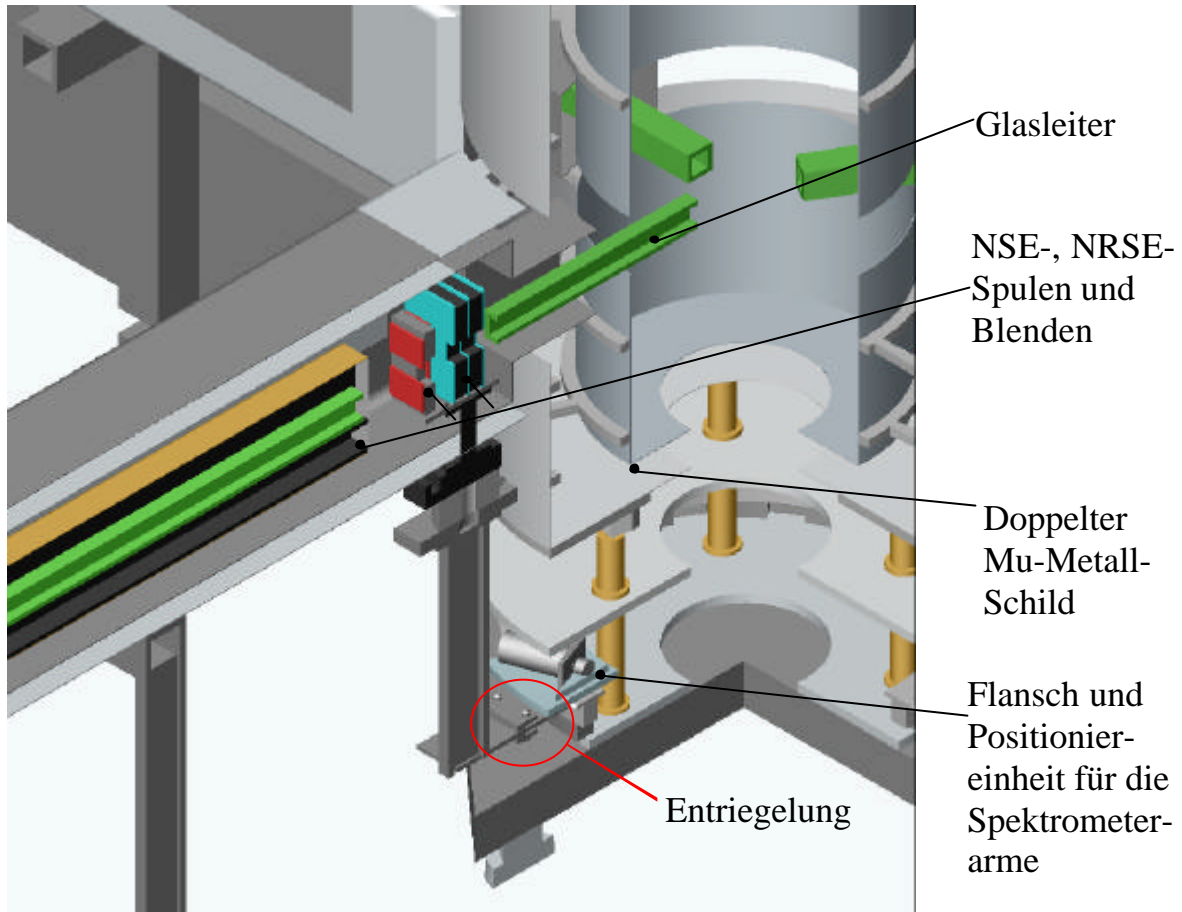
project team: TU München E21
project leader: Dr. R. Gähler,
instrument responsible: M. Bleuel

Activities in 2002:

- Continuous cabling of the instrument (Motors, air cushions, air sensors, water, DC- and HF-supply for the Bootstrapcoils)
- Additional detector for MIEZE is in development
- Further tests with the C-box for the resonance-HF-circuit leading to an improved resonance-HF-circuit with a ceramic ring ferrit
- Continuous programming on the instrument-control-program (component_test_panels, automated adjustment of the coils and the spectrometer, test of parameters before execution)
- True up of the NSE-Z-Coils in the spectrometer
- Winding of additional B₀-Coils and test for the best
- Further development on the multiplexer-platine together with the Elektronik-Labor
- Up-building of the guide field for the N-guide together with Christian Schanzer (4m are at the final position)
- Further tests of the Mu Metallshielding at the final position, model calculations of the shielding factor, first tests of the automated demagnetising switching mechanism
- Three-dimensional modeling of RESEDA and surrounding installations with the construction program solid works
- Conception of the „Selektorburg“ and „Meßkabine“
- Detailed simulations of the neutron beam with the Program Mcstas-1.6
- Removal of damage done to the spectrometer, as much as possible
- Sergey Prokudaylo left the RESEDA-team

Actual project state (12.02):

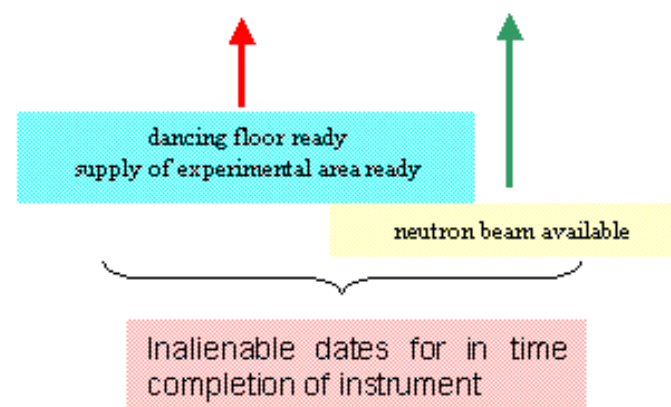
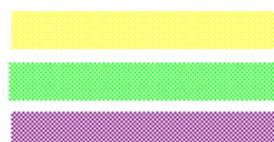
The estimated start of the FRM2 will not be before middle of 2003. Because of this delay of at least 2 years compared to the early time table, all RESEDA activities are stretched. It is important to keep the know how and not to break up the team.



Reseda Spectrometer: Time table

time table Reseda spectrometer	1999			2000				2001		
	4-6	7-9	10-12	1-3	4-6	7-9	10-12	1-3	4-6	7-9
Flipper coils										
base construction										
Magnetic shield										
Positioning devices										
Magnetic fields										
Selector										
Polarizers										
electronics and control										

design
fabrication
assembly/test



1.18 MUPAD Spectrometer: Annual Report 1.1.-31.12.02

M.Schulz, M. Janoschek

project team: TU München E21

project leader: Dr. R. Gähler,

instrument responsible: M.Schulz, M. Janoschek

Project Description:

MUPAD is a Spectrometer made for 3-D polarization-analysis with polarized neutrons, e.g. for measuring magnetic lattices of matter or magnetic excitations in matter. It uses two specially designed flipper coils with nearly no outer stray fields to turn the spin of neutrons in arbitrary directions in front of the measured sample and two after it for analyzation. Our goal is that the final setup of the instrument will make less than 1° turn error with all four coils together.

Activities in 2002

- First of all Sergey Prokudaylo performed some simulations of the coils in order to know whether the design for the coils should implement active or passive guides of the stray fields. It turned out that passive guides constructed out of mu-metal would be the best solution.
- The design for the first prototype of coils were made. The coils were build and measured. The measurement told us, that the coils were not meeting our guidelines. We decided to build more compact coils, which were winded with lot of tension. Additionally we enhanced our coils by using secondary outer mu-metall-screens out of thin foil, and by using a lot of time on demagnetization of all the mu-metal-parts of our design.
- With that design we could prove that our coils would match our given guidelines. Here are the field integrals in each direction in front and behind our coils and the from experimentally data calculated turn errors for 1 Angstrom neutrons (Measurements made with coil current of 1.8A corresponding to $B=18\text{Gs}$ inner field which is a turn of 180° for 1 Angstrom neutrons). Our results showed that the sum of outer field integral is smaller than $1/500$ of inner field integral!!!

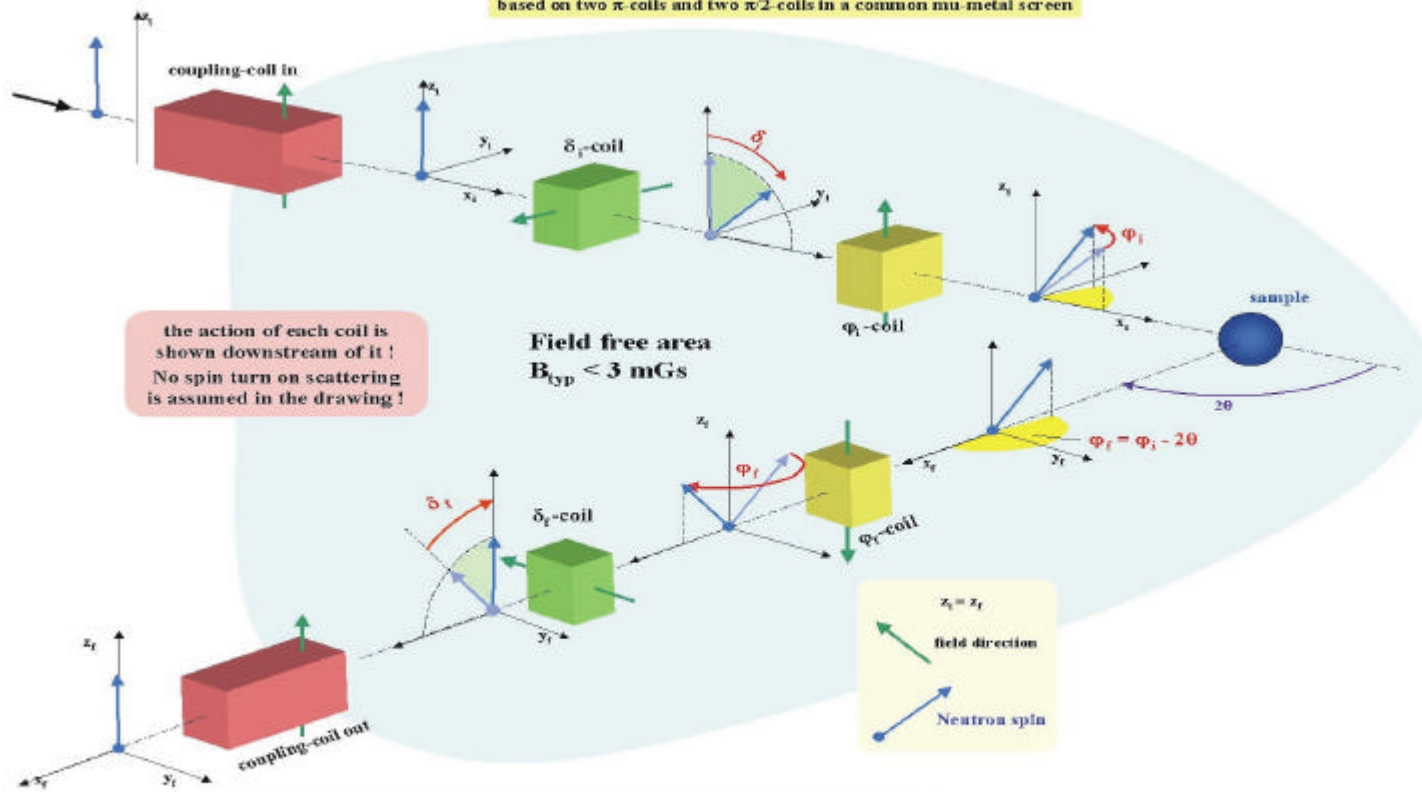
Direction	x	y	z	Direction	x	y	z
approx. Field-Integral [mGs cm]	47,9	-84,995	12,43	approx. Field-Integral [mGs cm]	-101,655	86,445	90,805
turn error [°]	0,063	-0,113	0,016	turn error [°]	-0,135	0,115	0,120

- Also our measurements and experience with demagnetization showed us some ways for further improvement of our design. The outer secondary screens will be made thicker. Also we came up with a new idea for using the connections of the coil to enhanced the field. We think that we can improve our results again by factor two which means that that the sum of outer field integral will be smaller than $1/500$ of inner field integral.

Outlook for 2003

In the next year we will hopefully build and test our new designed of coils. We are looking forward to integrate them in the instrument.

Principle of Mupad, 3-coil version
 based on two π -coils and two $\pi/2$ -coils in a common mu-metal screen



the action of each coil is shown downstream of it!
 No spin turn on scattering is assumed in the drawing!

Field free area
 $B_{0sp} < 3 \text{ mGs}$

$x_r = x_t$
 field direction
 Neutron spin

Assume spin turns on scattering:
 by φ_s in the scattering plane \Rightarrow set φ_r -coil to $\varphi_r = -\varphi_s - \varphi_s + 2\theta$
 by δ_s with respect to z-axis \Rightarrow set δ_r -coil to $\delta_r = -\delta_s - \delta_s$

1.19 Multiple Small Angle Neutron Scattering

T. Hils, R. Gähler

Technical University of Munich, Physics Department E21

Measuring density correlations in the μm range is a domain of light scattering, however it often fails due to low contrast or opacity of the sample. Research on polymers, colloid systems, cements, microporous media, are examples of a rising field, where μm correlations play a crucial role. Small angle X-ray and neutron scattering (SAXS and SANS), on the other hand, commonly measures lateral correlation lengths in the 0.01 to 0.1 μm range. To measure μm correlations with neutrons, various specific instruments have been designed, and the technique is commonly known as USANS (ultra small angle neutron scattering)¹. However these methods are sensitive to scattering only in one dimension and suffer from intrinsic small angle scattering due to structure material in the beam.

Here we propose MSANS (Multi hole SANS), a new USANS option for a standard long baseline SANS instrument on pulsed or steady state neutron sources. It uses the common SANS infrastructure except for the detector, which requires enhanced spatial resolution. The system is sketched in Fig1.

In a first attempt the main properties like resolution and intensity of a setup consisting of two periodical multihole apertures that lead to an incoherent superposition of a multitude of "little (ultra high resolution) SANS-machines" is to be derived.

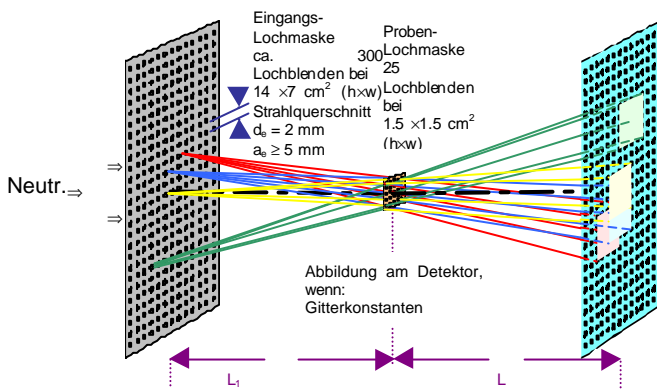


Fig. 1: For MSANS, the entrance- and sample apertures of a common SANS instrument may be replaced by multi-hole apertures. With proper lattice constants of these apertures, superposition of individual patterns at the detector can be achieved. The q-resolution is determined by the size of individual holes, the q-range is determined by the distance between holes.

¹ Instead of the lateral correlation length, often the q-resolution is used, which is in the order of 10^{-3} to 10^{-5} \AA^{-1} for USANS.

It is based on multi-hole apertures at the entrance (M_e) of the collimator and near the sample (M_s) with lattice constants a_e and a_s and hole diameters d_e and d_s respectively. With the choice

$$G_{e,s} = \frac{2p}{a_{e,s}}; \quad G_e \cdot L_1 = (G_s - G_e)L_2; \quad G_d = G_s - G_e$$

an intensity pattern of well separated peaks with lattice constant a_d in the detector plane is observed ($a_d = 2\pi/G_d$). The factor 2π is added for convenience. The equations holds separately for x and z-direction, i.e. the lattice constants in both dimensions can be chosen according to the requirements. The validity of the above equations may be directly seen from Fig. 2.

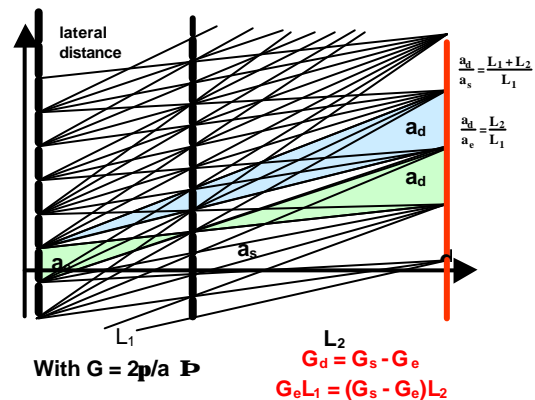


Fig.2: Condition for the lattice constants a_e and a_s and distances L_1 and L_2 for 'focussing' in the detector plane d.

Intensity and q-resolution:

The n-flux Φ_s at the sample can be estimated as follows:

$$\Phi_s = \frac{d^2 \Phi_0}{d\lambda d\Omega} \Delta\lambda \Omega_s T_s T_e$$

where the first factor is the double differential flux of the entrance guide (assumed as isotropic), $\Delta\lambda$ the mean wavelength band transmitted by the selector, Ω_s the solid angle of the entrance aperture seen from the sample aperture and $T_{e,s}$ are the transmission factors of both apertures $T_{e,s} = d_{e,s}^2 / 4a_{e,s}^2$. Ω_s is assumed to be smaller than the beam solid angle in the n-guide. For optimum spatial resolution at the detector the hole diameters $d_{e,s}$ and lattice constants $a_{e,s}$ should be related by

$$\frac{d_s}{d_e} = \frac{a_s}{a_e} = \frac{L_2}{L_1 + L_2}$$

which follows directly from Fig. 2. In this case the peak shape in the detector plane can be derived from the convolution of two round apertures of equal size. The peak shape can

be approximated by a triangular function of width

$$d_d \cong \frac{L_2}{L_1} d_e; \text{ (FWHM)}$$

and both transmission factors T_s and T_e will be the same (T). The relation $a_e/2d_e$ (or $a_s/2d_s$) determine T, and also the dynamic range, i.e. the max. q-value divided by the q-resolution, without overlap between neighboring peaks. Short range correlations in the sample may lead to significant overlap, however typical SANS intensities drop very rapidly with increasing q, and overlap will not be fatal in many cases. Sets of apertures with different relations $a_{e,s}/\varnothing_{e,s}$ can be used to adapt the pattern to the demand. In MSANS, resolution is decoupled from intensity, as long as T is kept constant. The increase in q-resolution in MSANS is typically one order of magnitude, compared to SANS at equal intensity. The gain originates from the reduction in q-range in MSANS and the increase of the input guide cross section and its divergence.

Diffraction from the aperture holes of typically 1mm are not yet crucial, as the beam correlation length is only in the μm range.

In 2002 a basic test-design for this option was completed and 2 prototypes of the multihole-apertures were manufactured.

2 NEUTRON RADIOGRAPHY AND TOMOGRAPHY

2.1 The design and construction of the neutron tomography facility ANTARES

B. Schillinger^{a,b}, E. Calzada^a, F. Grünauer^b

a) Technische Universität München, FRM-II, 85747 Garching, Germany

b) Technische Universität München, Physik Department E21, 85747 Garching, Germany

The neutron tomography facility ANTARES will have an unprecedented combination of high flux and high beam collimation with two selectable beam-adjusted collimators. The space for the installation was assigned very late during the planning of the new reactor FRM-II. This led to several harsh constraints due to surrounding experiments, e.g. the site is not accessible by crane. We describe the engineering solutions as well as the current progress in the construction.

The facility

In the early planning stage of the reactor, the tomography facility was foreseen at a neutron guide leading out of the reactor hall to an external building.

When it became clear that the beam geometry of a neutron guide was unsuited for tomography, a classical flight tube design had to be fitted into the remaining space in the reactor hall. The tomography facility at FRM II shares the beam port (with two channels) with the UCN source and is surrounded by a spin-echo spectrometer and the platforms of the positron source at the inclined beam tube above its beams tube (Fig.1a). The UCN source will insert a nozzle through the second channel of the drum shutter in the biological shielding, so an additional secondary shutter outside the reactor wall is required.

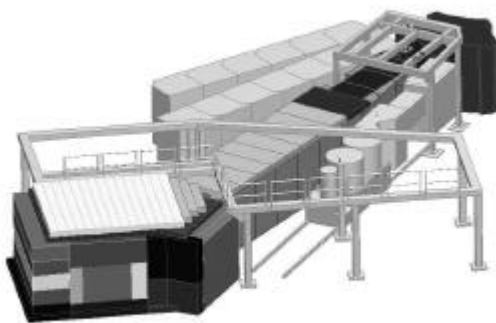


Fig. 1.: Tomography facility surrounded by other experiments

Shutter and collimator

The beam geometry resembles a classical pinhole camera imaging the square source area onto the sample area. A special beam-adjusted collimator with a cross section with varying shape follows exactly the contours of the pin-hole imaging of the source area. This collimator also limits the penumbra region of

the beam. The first part of this collimator is integrated into the drum shutter in the biological shielding, the second part consists of two separate channels above each other inside the vertical secondary shutter (Fig.2). With these two collimators, the beam can be adjusted for high resolution ($L/D=800$, 3×10^7 n/cm²s) or high flux ($L/D=400$, 1.2×10^8 n/cm²s). The secondary shutter is driven by a regulated hydraulic positioning system with a pressure storage and fail-safe mechanism that shuts the beam off even in case of power failure.

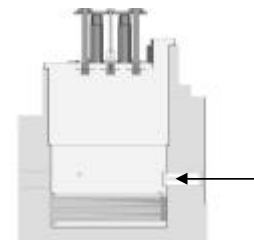


Fig. 2: Cross section of the vertical beam shutter

Flight tube and shielding

The collimator feeds a divergent 12m long flight tube. It consists of six sections made of aluminum with square cross section (Fig.3). Each section can be removed in order to install instruments, for example a velocity selector. The tube size and geometry are adapted to the beam generated by the collimator, therefore the penumbra region of the beam does not touch the beam tube wall, avoiding excessive gamma generation in the aluminum walls.



Fig. 3: The flight tube.

The flight tube is shielded by L-shaped walls and a roof made of heavy concrete-filled steel containers (Fig. 4a). As the access by crane is blocked by the positron source platform, the wall elements have to be positioned by air cushions, the roof components will be positioned onto the walls in the small accessible space between the platforms and will be rolled on ball bearings into their final position (Fig. 4b).

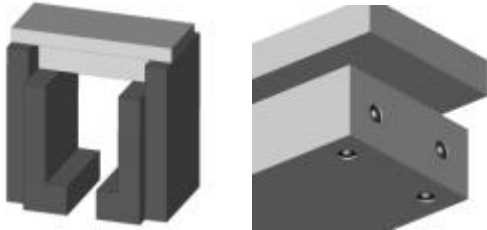


Fig. 4a,b: The flight tube shielding.

The neutron beam enters the measurement cabin through a square hole of 400 mm x 400 mm, the penumbra being absorbed by the wall. The walls consist of several segments with a thickness of 800 mm and less than 10 t weight which will be stacked vertically in the crane accessible area. The walls will then be positioned by air cushions.

As there is no space for a conventional door to swing open, a whole 20 t wall section will be moved on rails parallel to the UCN experiment (Fig.5).

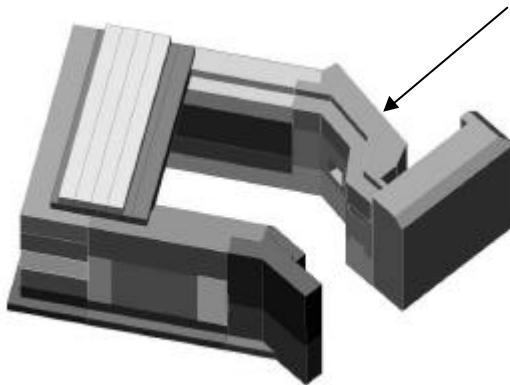


Fig. 5. Measurement cabin

Manipulator and beam size limiter

The motor driven sample manipulator (Fig.6) allows for samples of up to 500 kg and 1 m diameter to be rotated and translated in height and width across the neutron beam.



FIG. 6: SAMPLE MANIPULATOR

The maximum beam cross section is 400 mm x 400 mm. It can be reduced by a variable beam size limiter (Fig.7), installed at the end of the flight tube outside the cabin. It consists of a aluminum frame with four sliding plates covered with BorAl layers. A fast pneumatic beam shutter with B₄C, situated at the beginning of the flight tube, captures the thermal flux in intermissions between measurements (e.g. for data transfer time) to keep the activation of the sample as low as possible.



Fig. 7: Variable beam size limiter

THE COMPLETE LAYOUT

The complete layout of the facility is explained in Fig.8.

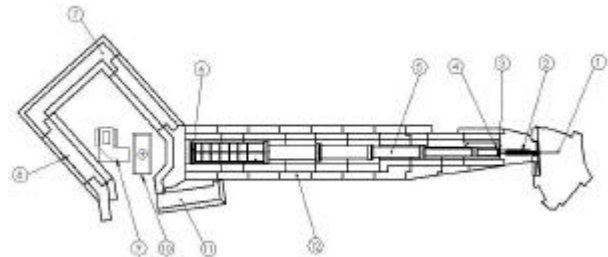


Fig. 8: Complete layout of the facility

- Collimator inside of the biological shielding
- External vertical beam shutter
- Iris diaphragm
- Pneumatic shutter
- Flight tube
- Variable beam size limiter
- Measurement cabin
- Wall and beam stop
- Detector and camera system
- Sample manipulator
- Sliding door
- Flight tube shielding

Status in January 2003

In January 2003, the status was as follows:

The primary collimator has been installed in the drum shutter, the secondary shutter inserts are near completion (Fig.9).

The sample manipulator and control are completed, cabling and programming are in progress (Fig.10).

The beam size limiter is almost completed, waiting for the Boral plates to be mounted (Fig.11).

All shielding walls except for the secondary shutter are completed and are being transported to an assembly hall to be filled with heavy concrete in the fully assembled state (Fig. 12,13,14).

The camera system (2048 x 2048 pixels) for the detector has been delivered and awaits first tests.

The hydraulic control system is being delivered in parts for assembly with the secondary shutter.

The mechanical mounting of the complete facility will be finished by March 2003, with electrical installations to be completed.



Fig. 9: The collimators



Fig. 10: The sample manipulator



Fig. 11: The frame of the beam size limiter



Fig. 12: Part of the flight tube shielding and entrance to the measurement cabin



Fig. 13: The beam entrance of the measurement cabin



Fig. 14: A side wall of the measurement cabin made from stacked segments

References

- [1] B. Schillinger: Estimation and Measurement of L/D on a Cold and Thermal Neutron Guide. World Conf. Neutron Radiography, Osaka 1999, in: Nondestr. Test. Eval., Vol. 16, pp.141-150
- [2] B. Schillinger, E. Calzada, F. Grünauer, E. Steichele: The design of the neutron radiography and tomography facility at the new research reactor FRM-II at Technical University Munich, 4th International Topical Meeting on Neutron Radiography, Pennsylvania 2001, acc. pub Journal of Radiation and Isotopes, 2002.
- [3] F. Grünauer, B. Schillinger: Optimization of the Beam Geometry and Radiation Shieldings for the Neutron Tomography Facility at the New Neutron Source in Munich. 4th International Topical Meeting on Neutron Radiography, Pennsylvania 2001, acc. pub Journal of Radiation and Isotopes, 2002.
- [4] E. Calzada, F. Grünauer, B. Schillinger, "Engineering solutions for the new radiography and tomography facility at FRM-II", World Conf. Neutron Radiography, Rome 2002

2.2 Steps toward a dynamic neutron radiography of a combustion engine

J. Brunner^a, G. Frei^b, E. Lehmann^b, B. Schillinger^a

a) Technical University of Munich, Physics Department E21, 85747 Garching, Germany

b) Paul Scherrer Institut, 5232 Villigen, Switzerland

The Dynamic NR is a new established technique, which is applied very successful for non destructive testing for time dependent phenomena with a similar resolution and a similar contrast as in conventional NR. Of special interest is the investigation of the injection process in a running combustion engine under real conditions.

For obtaining a 16 bit conventional radiography images one has to integrate scintillator light on the CCD chip typically for some seconds. Of course the sample thickness, the sample material as well as the neutron flux of the source determines the exact time. Additionally the readout time, depending on the dynamic range and the pixelnumber of the CCD puts a lower limit to the highest reachable framerate. The observation of objects in the millisecond time scale is impossible with standard methods. A possible solution for repetitive processes can be stroboscopic imaging. That means a synchronization of the detector (the CCD) with the repetitive process and an integration of 1000 images taken at the same millisecond timewindow of the cycle. That way a virtual opening time of some seconds can be realized as long as the noise is constant within time (i.e. negligible readout noise) and not determining the system.

With this method a combustion engine towed by a electric motor was observed in the first experiments testing the method with a selfconstructed detector. The reached spatial resolution was 1mm.

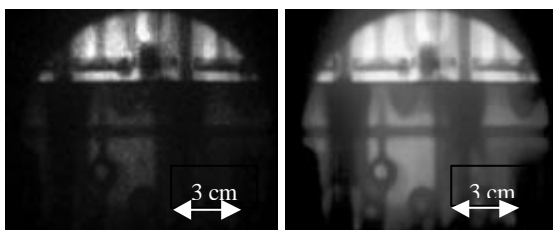


Fig. 1: A single frame (left) contains only 10 graylevels and 500 summed NR-images contain 3000, image after processing (right), $t=4ms$.

This year it was possible to perform dynamic neutron investigations at PSI with an excellent new detector system and at ILL at a very high flux test beam line with a detector built by a group of the University of Heidelberg.

At the NEUTRA facility a dynamic neutron radiography experiment of a running model aircraft engine was performed. The detector consisted of a CCD camera using a multi

channel plate as image intensifier coupled on the CCD-chip with fiberoptics.

With this equipment and the thermal neutron beam of 10^7 n/cm²s an extremely high detection sensitivity was possible hardly reached by any other system. As neutron to light converter a Li⁶F/ZnAg scintillator of a millimeter thickness was used. The reached spatial resolution was 0.15 mm.

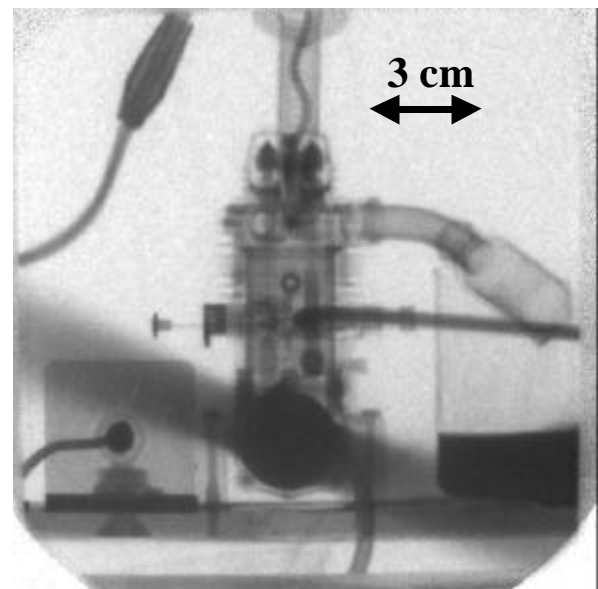


Fig. 2: 4000 summed frames of the neutron radiography movie of a running model aircraft engine (1 PS), one frame = 0.25 ms, running at 4800rpm

At ILL NR-measurements on an air brush nozzle with a very high flux of 10^9 n/cm²s were performed. In the false color image Fig. 3 the red cloud of injection liquid is clearly visible. Boron water and a Gadolinium emulsion were tested as a contrast liquid. Fig. 3 was obtained without synchronizing with the detector.

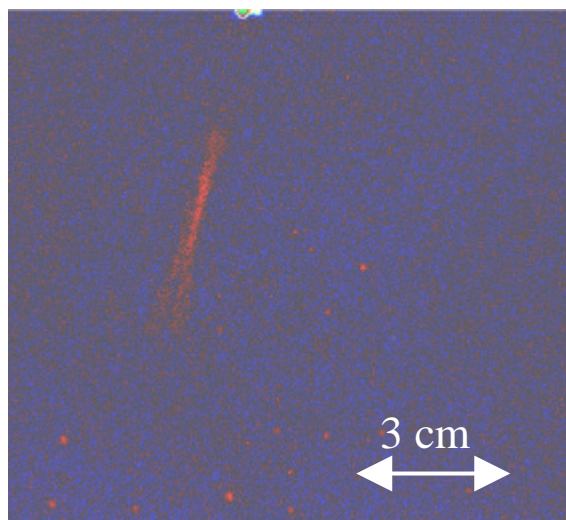


Fig. 3: A false color NR-image of boron water injection of an air brush nozzle, $t=20\text{ms}$, on the top of the image is the nozzle, the injection is the red strip. The spatial resolution is 0.5 mm.

References

- [1] B. Schillinger, "Neue Entwicklungen zu Radiographie and Tomographie mit thermischen Neutronen", Doktorarbeit an der Technischen Universität München
- [2] M. Balasko, "Neutron radiography visualization of internal processes in refrigerators", *Physica B: Condensed Matter*, Volumes 234-236, 2 June 1997, Pages 1033-1034

2.3 Phase contrast radiography using thermal neutrons

N. Kardjilov¹, E. Lehmann², E. Steichele¹, P. Vontobel²

¹ Fakultät für Physik E21, Technische Universität München, D-85747 Garching, Germany

² Paul Scherrer Institute, CH-5232 Villigen, Switzerland.

An alternative method to the standard radiography is the phase contrast imaging, where the intensity distribution in the radiography picture is proportional to the phase variations induced by the transmission of a coherent radiation through a medium. To achieve a phase contrast in radiography images usually a high spatial and chromatic beam coherence is required. It can be shown that a neutron phase contrast imaging can be performed without monochromatisation of the beam.

In case of high transversal spatial coherence all rays emanating from a point source, defined e.g. by a small pinhole, are associated with a single set of spherical waves that have the same phase on any given wavefront. As shown in [1] the variations of the thickness and the neutron refractive index n of the sample cause a change in the shape of a neutron wavefront on passing through the sample. The angular deviation of the normal to the wavefront, $\Delta\mathbf{a}$, can be expressed as:

$$\Delta\mathbf{a} \approx \frac{1}{k} |\nabla_{x,y} \mathbf{j}(x, y, z)| = |\nabla_{x,y} \int [n(x, y, z) - 1] dz|. \quad (1)$$

where the optical axis is parallel to z and \mathbf{j} is the phase change for a ray path through an object relative to vacuum. This means that the deformation of the wavefront after the transmission depends on the gradient of the refractive index n in a plane perpendicular to the direction of the wave propagation, \vec{k} .

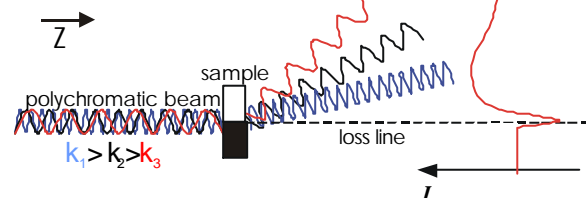


Fig. 1 Schematic illustration of the energy-dependent deflection of a polychromatic beam from a sample area with a strong variation of the refractive index.

To show that rapid variations in refractive index can lead to strong phase-contrast effect even with polychromatic radiation, the formal representation shown in Fig. 1 can be used [1]. The intensity variations due to the gradient of the refractive index in the sample area can be characterized by a very sharp minimum in the propagation direction (loss line) followed by a broad maximum beside it, Fig. 1. Such high values of the refractive index gradient exist mainly on the sample edges. Therefore the phase contrast imaging provides a high edge-enhancement in the resultant images.

The experiments were performed at the thermal neutron radiography setup NEUTRA.

To produce a high spatial coherence a pinhole with a size of 0.5 mm in a Gd foil (thickness of 0.1 mm) was used. It was placed at a large distance of 7 m from the sample. The sample to detector distance was fixed to 1 m. The exposure time at the used thermal neutron beam was 90 min per image.

Steel capillaries with diameters between 0.3 mm and 0.9 mm were investigated with phase contrast and conventional radiography. The obtained profiles through the capillaries are shown in Fig. 2.

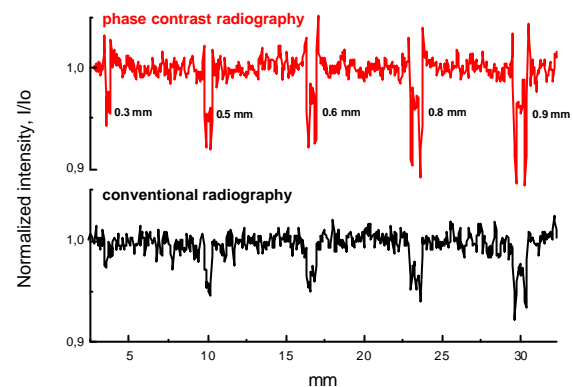


Fig. 2 Intensity profiles of steel capillaries obtained by phase contrast and conventional radiography.

The edge-enhancement on the needle borders in the case of phase contrast radiography follows the behaviour shown in Fig. 1 – a consequence of minimum and maximum in the intensity at rapid variations of the refractive index. In the case of conventional thermal radiography such an edge enhancement is missing.

An example of phase-contrast imaging with thermal neutrons of a small toothed wheel is shown in Fig. 3.

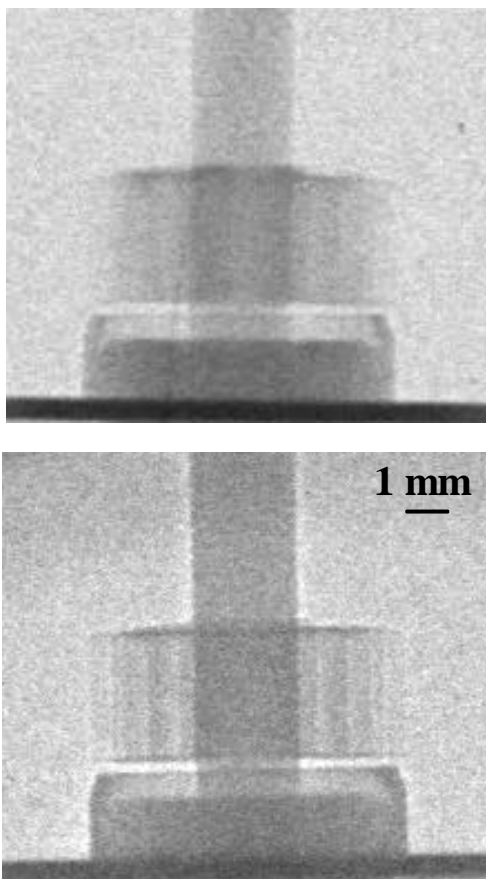


Fig 3 Conventional thermal radiography of a toothed wheel (top) and phase-contrast radiography (bottom).

The improved contrast in case of phase-contrast radiography is obvious. The observed edge-enhancement is due to a very sharp change of the intensity on the borders.

2.4 Neutron Topography at TOPSI

N. Kardjilov¹, S. Baechler^{2,3}, M. Dierick⁴, B. Masschaele⁴, J. Stahn³

¹ Fakultät für Physik E21, Technische Universität München, D-85747 Garching, Germany

² Physics Department, University of Fribourg, CH-1700 Fribourg, Switzerland

³ Paul Scherrer Institute, CH-5232 Villigen, Switzerland

⁴ Vakgroep Subatomaire en Stralingsfysica, University of Gent, B-9000 Gent, Belgium

The topography technique allows the imaging of crystalline materials using the whole beam diffracted by the individual crystallites. In comparison with the conventional micro beam techniques where only a small region of the sample is irradiated, in the topography experiments a large beam of the order of square centimeters is used.

To prevent overlapping of the rays diffracted from different areas of the sample, which will cause a loss of spatial information, soller collimators in vertical and horizontal directions were placed between the sample and the detector. In that case each of the rectangular cells defined by the collimators lamellae will provide a diffracted radiation only from a well-defined sample region onto the corresponding detector element. The advantage of the topography technique is the exploitation of the scattering information as complete as possible in reasonable time. The detector system was optimized for detecting low signals with a resolution not higher than determined by the soller collimators and the sample to detector distance. The used position sensitive detector was based on a conventional CCD radiography system. The visible light emitted from the ⁶LiF/ZnS(Ag) scintillator was imaged with an optical lens onto a Peltier-cooled CCD camera through a mirror at a 45° angle. The collimator/detector arrangement was aligned on the θ arm of the two axis diffractometer TOPSI at SINQ, (Fig. 1).

orientated single crystal is presented in Fig. 2 a. In a small angular interval of $\Delta\omega = \pm 0.2^\circ$ around the maximum intensity of $\omega = 42.7^\circ$ the whole sample volume gives a contribution to the Bragg reflection intensity. Opposite to that case a topography investigation of a crystal with a mosaic structure is presented in Fig. 2 b. To obtain a maximal intensity of the diffracted beam the crystal was tilted at $\varphi = -1.8^\circ$. Clearly two complimentary reflecting regions can be recognized on the images at $\omega = 43.0^\circ$ and $\omega = 43.5^\circ$. The transition between them is smooth as it can be seen from the diffraction spectrum. An example of an abrupt transition between two crystallites (domains) disorientated by $\Delta\omega \sim 1^\circ$ is shown in Fig. 2 c. The areas corresponding to the two domains can be located easily on the topography images taken at $\omega = 42.8^\circ$ and $\omega = 43.7^\circ$. The agreement between the topography images and the diffraction spectra is excellent.

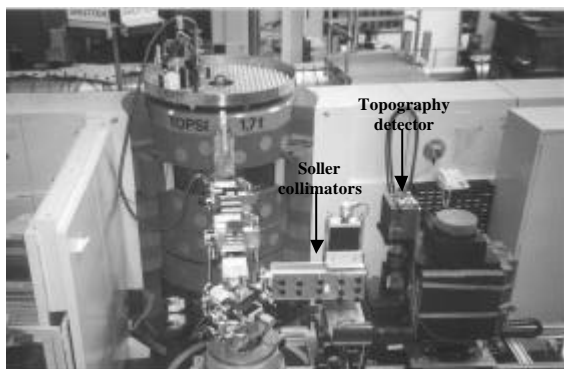


Figure 1: A view on the two axis neutron diffractometer TOPSI at SINQ, arranged for topography measurements.

The results from a topography investigation of Heusler crystals Cu_2MnAl with $d_{111}=3.53 \text{ \AA}$ intended for neutron monochromators are shown in Fig. 2. The measured diffraction spectra are shown together with the topography images. An example of a well-

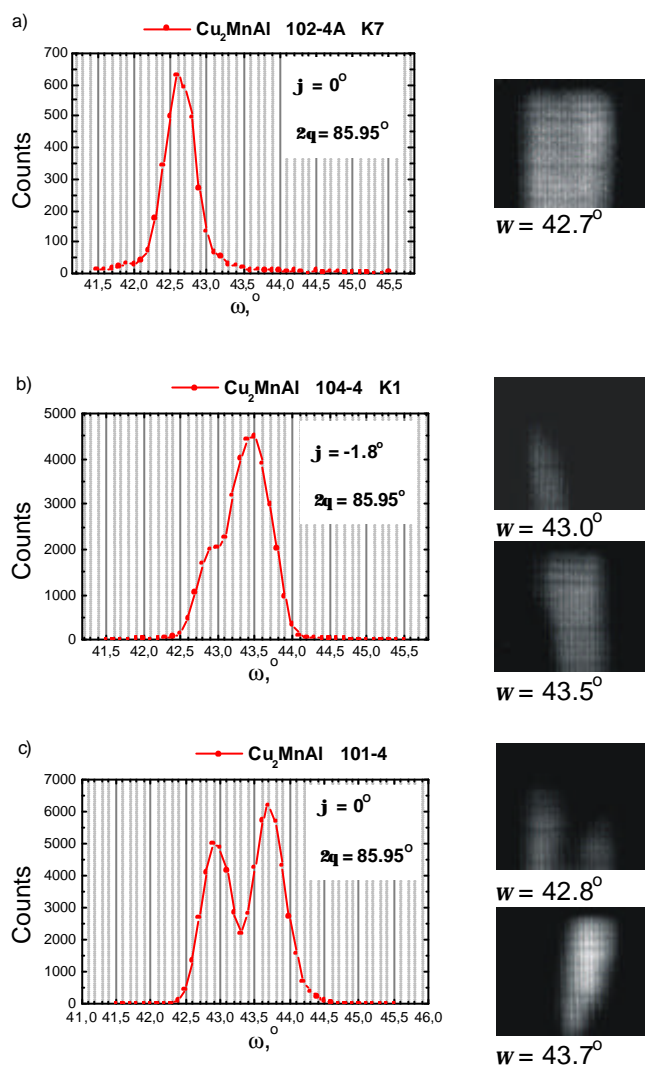


Figure 2: A topography investigation of Heusler crystals (right) together with the diffraction spectra (left)

2.5 Influence of gaps in shieldings against neutron radiation

F. Grünauer

Technische Universität München, Physik-Department E21

In most neutron experiments it is neither desirable nor possible to construct radiation shieldings in one piece. There would arise problems with the assembly, the accessibility, and flexibility. Therefore a modular construction has to be preferred. The single modules cannot be shaped to a precision that there will be no gaps between the elements. Gaps of up to some millimeters may occur inside the final shielding construction.

For the new neutron radiography station at Munich's new neutron source (FRM-II), we have the requirement that parts of the shielding can be moved on top of the lateral walls. Gaps between these parts and the walls are needful therefore. It is necessary to estimate the leakage of radiation through these gaps. The estimation was done by Monte Carlo Method. The neutrons are emitted from an area source on one side of the shielding. The dose on the opposite side of the shielding is calculated with a spatial resolution of 2mm. The shielding is infinite long and high. The gaps are repeated with a period of 50cm. The shielding material is heavy concrete (density: 3.5g/cm^3) with colemanite, hematite, and steel resin as additives.

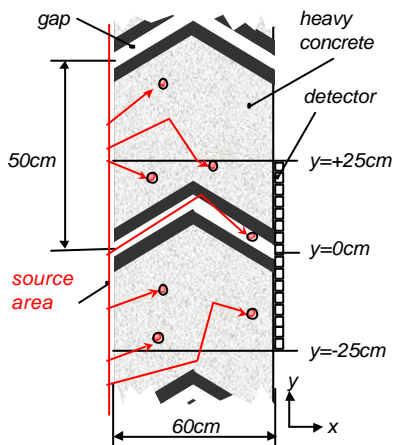


Fig. 1: Monte Carlo Model for the estimation of neutron radiation transport through gaps

Three different shapes of gaps were examined (Fig. 2):

- Curved
- Angular: one bend with an angle of 120°
- Labyrinth: two 90° bends, 20cm offset

For all shapes a gap width of 1cm was assumed. The shielding elements are coated by a steel liner of 1cm thickness along the gap.

For comparison two additional 'ideal' configurations were calculated (Fig. 2):

- Monolithic: homogeneous, no gaps
- Simple brick: coated by 1cm steel, no gaps

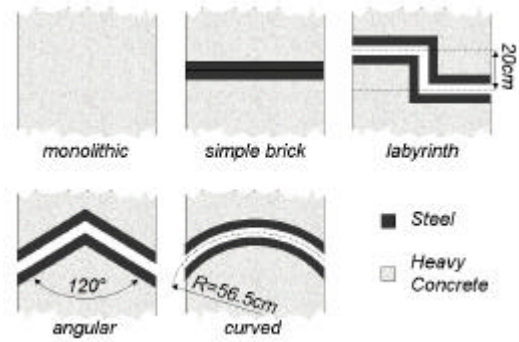


Fig. 2: Gap configurations in radiation shieldings: A: monolithic, B: simple brick, C: labyrinth (two 90° bends), D: angular (one 120° bend), E: curved gap

Factors of increase of the neutron dose outside the different shielding types compared to the monolithic shielding are shown in Fig. 3 for an isotropic source. The 'average' values show the average dose increase in the total detector area, and the peak values the increase at the gap mouth.

The curved structure shows the lowest and the labyrinth shows the highest dose peak at the gap mouth. However, the dose integral in the entire detector area is in all cases 20% above the integral dose without gap. The shielding power does not so much depend on the type of gaps.

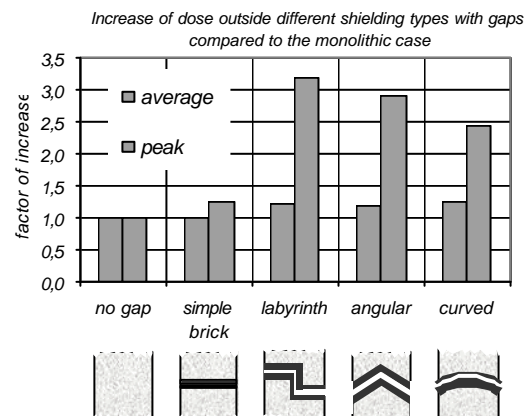


Fig. 3: Factors of neutron dose increase outside the different shielding types compared to the monolithic shielding for an isotropic source.

The situation changes completely for a parallel beam (neutrons enter the shielding perpendicular). The dose outside of the

different gap systems for a parallel beam is shown in Fig. 4.

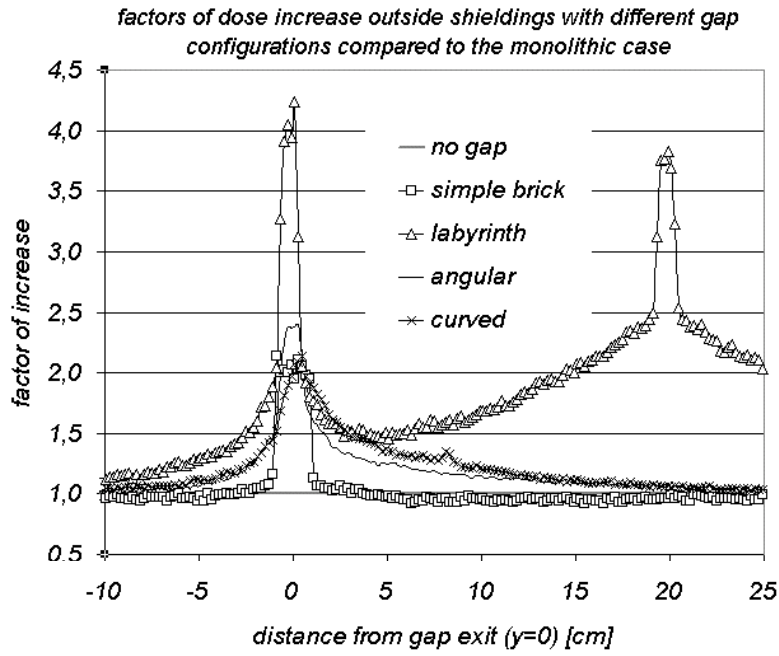


Fig. 4: spatial neutron dose distribution outside of shieldings with different gap configurations for a parallel beam (gap width=1cm)

The labyrinth with two 90° bends increases the dose considerably more than all other gap systems (78% in the total detector area). Two distinct dose peaks appear at the positions of the gap parts, that are parallel to the beam. The bad shielding quality of the labyrinth for a parallel beam is obvious: The transmission through both parallel parts of the gap (gap entrance and gap exit) is enormous.

All other gaps show even better results than for the isotropic beam.

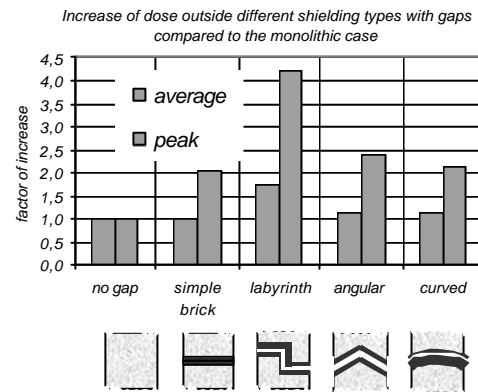


Fig. 5: Factors of neutron dose increase outside the different shielding types compared to the monolithic shielding for a parallel source. The average values show the average dose increase in the total detector area, and the peak values the increase at the gap mouth.

2.6 Estimation of the imaging quality of Munich's new neutron radiography station

F. Grünauer

Technische Universität München, Physik-Department E21

The imaging properties of the new neutron radiography and tomography station at Munich's new neutron source FRM-II were estimated and optimized by simulation of the whole facility by Monte Carlo method.

Homogeneity of open beam image

An important question is the influence of the structure of the cold source and its surrounding (Fig 1.) with regard to homogeneous illumination of our detector.

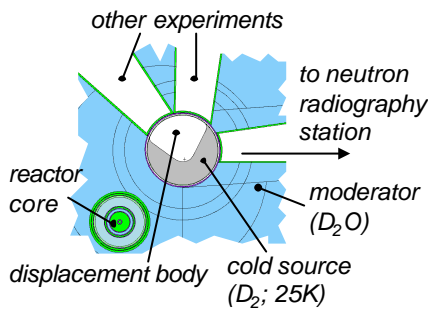


Fig. 1: horizontal cut through the cold source and its surrounding inside the moderator vessel

The cold source itself is not homogeneous. A displacement body without deuterium is included inside the cold source. This is to optimize flux and spectrum, especially for the other two beam tubes, that are connected to the cold source. In addition, the other beam tubes are arranged in an asymmetric way. The result is a flux depression on one side of the cold source, due to missing backscattering from the volumes of the tubes. These influences are estimated by calculation of open beam images in the detector plane for different theoretical arrangements inside the moderator vessel using our 4.3 cm aperture:

- a cold source without displacement body and without other beam tubes. The volumes of the tubes are replaced by heavy water
- cold source with displacement body but no other beam tubes
- the real arrangement.

Neutron flux profiles in the energy range below 1eV in our detector plane are displayed in Fig. 2 for different theoretical arrangements in the moderator vessel. Without displacement body a bias in the flux profile occurs, because both sides of the entrance of our beam tube are populated by neutrons that crossed different thicknesses of moderator. The situation is reversed with included displacement body: the

total flux increases. The resulting bias is nearly compensated by including the beam tubes for the other experiments. Inhomogeneities are rather low for neutrons in the interesting energy range below 1eV, whereas inhomogeneities in higher energy ranges occur.

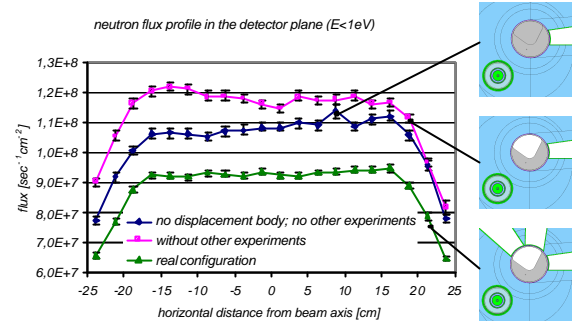


Fig. 2: Neutron flux profiles ($E < 1\text{eV}$) in the detector plane for different theoretical arrangements in the moderator vessel.

Point spread function

One of the most important imaging properties for a neutron radiography station is the point spread function. The point spread function defines the image of a point in the object on the detector plane. It is influenced by several factors: beam geometry, transmission through the collimator material, scattering inside structure material, scattering inside the object, etc. Of course for the last point no predictions can be made as long as the object is not known. The resulting point spread function (PSF) from all other factors was estimated for an object plane at a distance of 50cm before the detector. The results for our two different apertures are displayed in Fig.3.

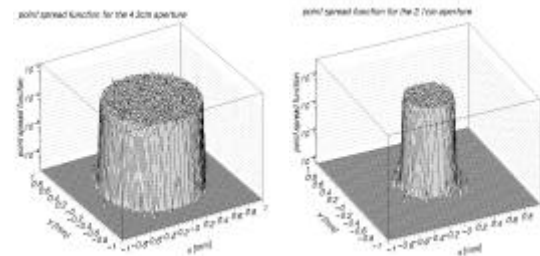


Fig. 3: Point spread functions for an object plane at a distance of 50cm before the detector plane for the 4.3 cm aperture (left-hand side) and for the 2.1 cm aperture (right-hand side)

Both PSFs have the shape of a pill-box, that can theoretically be expected for the case of a homogeneous and isotropic source, that is observed through a round aperture in 'black'

material. That means our beam geometry, especially our 'beam adjusted' collimator is very close to the ideal configuration. The PSFs can be used for image deconvolution in the future.

3 SAMPLE ENVIRONMENTS

3.1 Minimization of the background radiation of a sample environment

Nico Wieschalla¹, Florian Grünauer¹, Jürgen Peters²

¹TU München, Physics Department E21

²TU München, ZWE FRM-II

At the new neutron source FRM-2 many tools for neutron scattering experiments are provided. One of them will be a sample environment for experiments at low temperatures and high magnetic fields. One important question during construction of this tool was the amount of background radiation from structure material. This radiation was estimated by Monte Carlo simulations for different configurations of the tool.

Because of mechanical reasons most of the structure material of the tool is steel. Thermal neutron capturing in iron causes a considerable flux of generated high energetic gammas, which is unwanted because of a big dose outside the experiment. In order to avoid this additional radiation, all iron structures have to be covered by a neutron absorber layer. Thickness and choosing of the material of this layer was optimized by Monte Carlo Method. A three dimensional cut through the Monte Carlo model and a horizontal cut is shown in fig.1. In the Monte Carlo simulations the neutrons started on an area of 1cm x 1cm located outside the tool (fig.1 0°). The energy

distribution is a Maxwell spectrum of 40K or 300K (this tool will be used for cold neutrons as well as for thermal neutrons). The assumed source yield was 10^9 sec^{-1} and the maximum angle between the direction of a neutron and the beam axis is 4° .

Because the super conducting coils cause a high secondary radiation, it is essential to find the best shielding positions and materials to reduce the neutron flux in the coil bodies. For this reason we cover surfaces, which are closest to the neutron beam (shielding 1 in fig.1) with different materials of 1mm thickness.

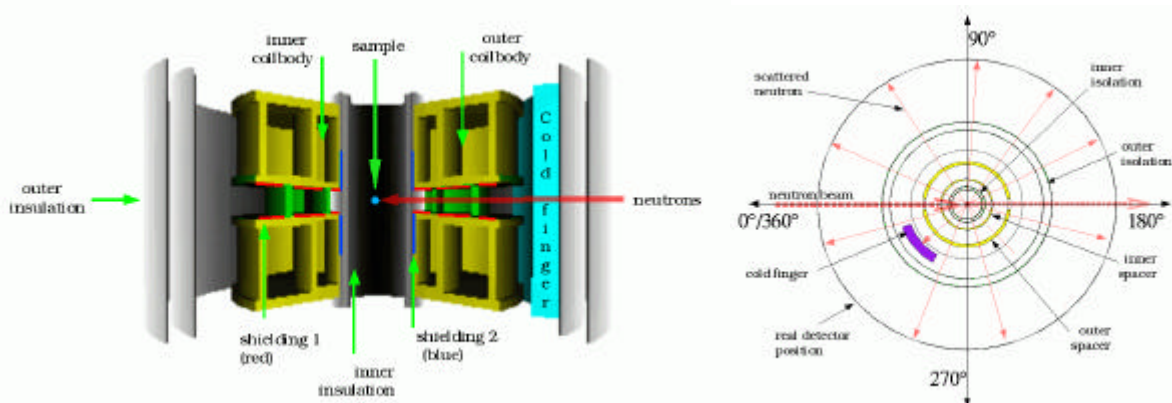


Fig. 1: three dimensional cut through the Monte Carlo model (left hand side) and horizontal cut on beam level (right hand side)

The covering of this surface reduces the neutron flux in the outer coil by two orders of magnitudes. By adding the shielding 2 (fig. 1) the neutron flux in the inner coil is reduced by the same factor. In spite of the different macroscopic cross sections of the shielding materials, the neutron flux in the coils is always noted to be approximately the same. The reason is amazingly simple. The biggest part of the neutrons inside the coils comes through the spacer rings, which are necessary because the coils will attract with a force of 100kN and only a small part comes through the shielding. Unfortunately, it is not possible to bring some shielding material between the coils and these spacers due to the very high forces. The resulting leakage is not avoidable.

In contrast to the neutron flux inside the coil bodies, the noise to signal ratio (scattered neutrons from structure material compared to unscattered neutrons) at the sample position in the center of the tool, depends on the shielding material. In this case gadolinium is the best choice ($5 \cdot 10^{-7}:1$) followed by cadmium ($10^{-5}:1$) and lithium ($2 \cdot 10^{-5}:1$).

But if we have a look at the gamma dose at the real experimental detector outside the tool, gadolinium is the worst of all. It is even worse than no shielding (see fig. 2). One might guess lithium must be the best choice in this case, because it doesn't produce secondary gamma radiation by neutron capturing. But it is comparable to cadmium. The reason is the not negligible gamma production by neutron

capturing in the steel structure of the coil body. As shown above, the neutron flux inside the coil body is dominated by leakage neutrons from the spacer rings, that is independent from the shielding material.

However the lowest gamma background can be reached by a cadmium layer.

Cadmium has the following advantages compared to the other materials:

- lowest gamma dose at detector position
- low noise to signal ratio at sample position
- easy to mount (but toxic)
- low costs
- available in appropriate thickness
- because of the high cross section, a thin layer is sufficient (0.2mm). This important because thicker layers could disturb the magnetic field.

Other simulations showed also that other additional shieldings at other positions don't decrease background radiation much more.

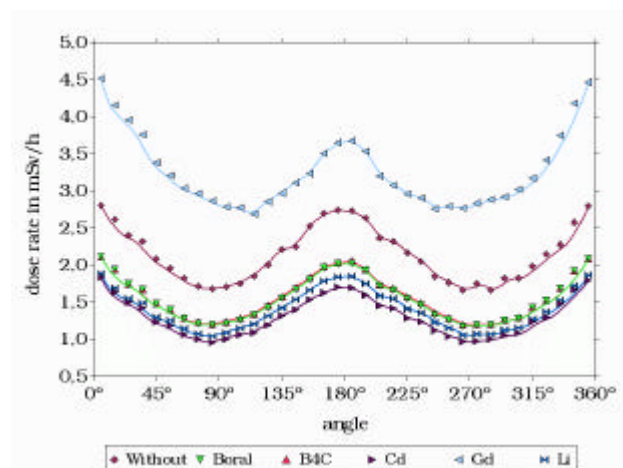


Fig 2: gamma dose rate at the detector position outside the tool for different layers of absorber materials (1mm thickness)

4 POSITRON PHYSICS

4.1 Experimental facilities at the intense positron source at FRM II

C. Hugenschmidt¹, G. Kögel², R. Repper¹, K. Schreckenbach¹,
P. Sperr², B. Straßer¹, W. Triftshäuser²

¹ Physik Department E 21, FRM-II, Technische Universität München, D-85747 Garching

² Institut für Nukleare Festkörperphysik, Universität der Bundeswehr München, D-85577 Neubiberg

The Positron Source at FRM II

At the new Munich research reactor FRM-II an in-pile positron source based on neutron capture is installed. After thermal neutron capture in cadmium the absorption of the released high-energy γ -radiation in platinum generates positrons by pair production [1].

The positron source is placed in the tip of the declined beam tube SR11 at FRM-II. The design of the source is schematically shown in figure 1. Inside the tip of the beam tube a cap of cadmium ($\varnothing = 11$ cm, $l = 9.5$ cm) is encapsulated in aluminium. Besides the function as γ source after neutron capture, cadmium is a perfect shielding for thermal neutrons. Consequently, it also protects inner source components from neutron activation. The inner part of the source consists of a honeycomb structure at the tip and rings of platinum acting as converter and positron moderator. Electrical acceleration lenses and magnetic coils are used for beam formation.

The source is placed at a position where the calculated unperturbed thermal neutron flux amounts to $2 \cdot 10^{14} \text{ n} \cdot \text{cm}^{-2} \cdot \text{s}^{-1}$. Taking into account the neutron capture rate, the absorbing mass, the geometry, the moderation efficiency, and a recent test run at an external neutron beam at the ILL high flux reactor in Grenoble [2], an intensity of the order of 10^{10}

slow positrons per second in the primary beam is expected.

Experimental Facilities at the Positron Source

The beam line guides the positrons to an experimental platform where it will be connected via a beam switch to three experiments: A **pulsed low energy positron beam system (PLEPS)** [3], a scanning positron microscope [4] and a facility for **positron annihilation induced Auger electron spectroscopy (PAES)** [5].

The PLEPS and the positron microscope were constructed and built at the university of the Bundeswehr in Munich (figs. 2 and 3). At present, both facilities are under operation with ²²Na positron sources with beam intensities up to 10^3 positrons per second. In order to get depth dependent information from the surface to the bulk of the material, the positron energy can be varied from a few 100 eV up to 18 keV. The lateral resolution is about 3 mm at PLEPS and less than 10 μm at the microscope.

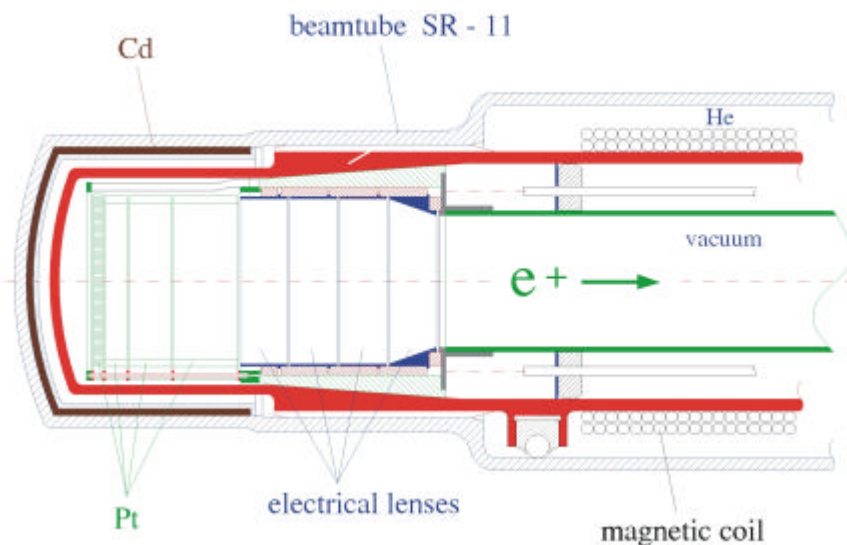


Fig. 1: Cross-sectional view of the in-pile positron source at FRM-II.

The PAES facility was built at E21 at TUM and is designed for extremely sensitive studies in surface science [5]. The Auger process is usually initiated by photo- or impact ionization of core electrons by irradiation with X-rays or keV-electrons. An alternative technique to induce core shell ionization is the annihilation of core electrons with slow positrons. Due to the low positron energy of some 10 eV, no background of secondary electrons is produced in the higher energy range of released Auger electrons. Besides this advantage, PAES is an exceptionally surface sensitive technique since most of the implanted positrons annihilate with electrons of the topmost atomic layer. In first experiments on polycrystalline copper the spectrometer was tested and optimized with a low intense positron beam at TUM.

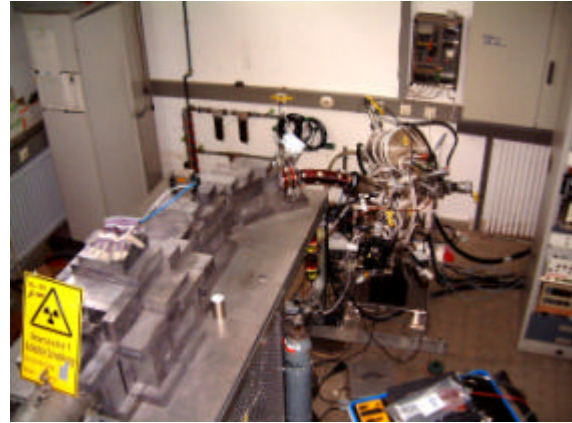


Fig. 4: Facility for positron annihilation induced Auger electron spectroscopy (PAES) at E 21, TUM.

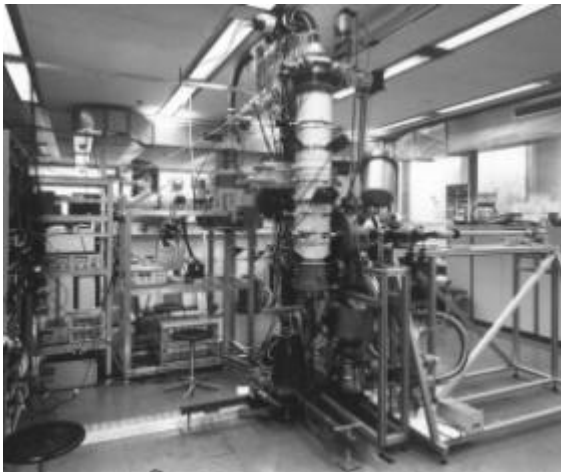


Fig 2: Pulsed low energy positron beam system (PLEPS) under operation at the university of the Bundeswehr in Munich.

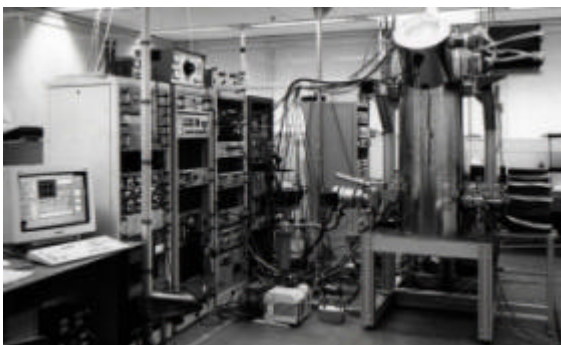


Fig. 3: The scanning positron microscope under operation at the university of the Bundeswehr in Munich.

References

1. C. Hugenschmidt, G. Kögel, R. Repper, K. Schreckenbach, P. Sperr, B. Straßer, and W. Triftshäuser; *Appl. Phys. A* 74, S295 (2002)
2. C. Hugenschmidt, G. Kögel, R. Repper, K. Schreckenbach, P. Sperr, and W. Triftshäuser; *Nucl. Instr. Meth. B* 198, 220 (2002)
3. A. David, G. Kögel, P. Sperr, and W. Triftshäuser; *Phys. Rev. Lett.* 87, 067402 (2001)
4. W. Bauer-Kugelmann, P. Sperr, G. Kögel, and W. Triftshäuser; *Mat. Sci. For.* 363-365, 529 (2001)
5. B. Straßer, C. Hugenschmidt, and K. Schreckenbach; *Mat. Sci. For.* 363-365, 686 (2001)

4.2 Investigation of the Annealed Copper Surface by Positron Annihilation Induced Auger Electron Spectroscopy

B. Straßer, C. Hugenschmidt and K. Schreckenbach

*Fakultät für Physik E21, Technische Universität München,
D-85748 Garching, Germany*

Auger electron spectroscopy (AES) is a well established technique in surfaces physics. The Auger process is usually initiated by photo- or impact ionization of core electrons due to irradiation with X-rays or keV-electrons. The recorded spectra show a high background of secondary electrons which are released by the X-rays or the primary electron beam. An alternative technique to induce core shell ionization is the annihilation of core electrons with slow positrons. Due to their low energy of some 10 eV, no background of secondary electrons is produced in the higher energy range of released Auger electrons [1]. Besides this advantage, positron annihilation induced Auger electron spectroscopy (PAES) is an extremely surface sensitive technique since most of the implanted positrons annihilate with electrons of the topmost atomic layer [2].

Experimental Setup

A PAES facility comprises a slow positron beam and an analysis unit, which detects Auger electrons, that are emitted from the sample surface.

The positron beam consists of a 4 mCi ^{22}Na source and an annealed 1 μm tungsten moderation foil, in which the primary positrons are slowed down to thermal energy in transmission geometry (figure 1). Subsequent electric lenses accelerate the moderated positrons up to the desired energy (30 eV) into beam direction. A longitudinal magnetic field of 2 mT guides the positrons along a curved beamline to the entrance of the analysis chamber, where a μ -metal structure is installed to extract the positron beam out of magnetic field. After that, the beam is electrically focused onto the sample, where an intensity of $1.1 \cdot 10^4$ positrons per second is achieved [3].

Electrons released from the sample are detected by an electrostatic hemispherical energy analyzer. In addition, the analysis chamber is equipped with a heatable sample holder, an argon sputter source, an electron gun for conventional AES and a mass spectrometer for rest gas analysis. Moreover, a tungsten shielded NaI-detector is directed onto the sample at the center of the analysis chamber (figure 2) in order to detect the annihilation radiation. A negative bias of -10 V

was applied at the sample in order to focus the positron beam onto the sample surface. Consequently, the kinetic energy of the positrons that enter the specimen amounts to 40 eV. Due to the negative potential of the sample, the emitted electrons are accelerated onto the grounded entrance of the energy analyzer.

Measurements and Results

EAES (electron induced Auger electron spectroscopy) and PAES measurements were performed for an Ar^+ -sputtered and annealed polycrystalline copper sample. An EAES spectrum for the as-received sample was recorded as well.

At the beginning, the as-received copper foil was analyzed by EAES (lower curve in figure 3). Besides the Auger peaks according to copper, the adsorbates sulfur, chlorine and carbon can clearly be identified. After Ar^+ -sputtering and the annealing procedure, the pronounced peaks of the surface contamination vanish. The peaks according to the Auger transitions $\text{Cu M}_{2,3}\text{VV}$ and $\text{Cu M}_1\text{VV}$ become more significant.

The PAES spectrum is shown in figure 4. The background due to secondary electrons ends at 40 eV according to the kinetic energy of the implanted positrons (blue line). Hence, the $\text{Cu M}_{2,3}\text{VV}$ transition (60 eV) can clearly be observed at the Ar^+ -sputtered and annealed copper sample. The background at higher energy depends on annihilation radiation induced photo and Compton electrons and on beam independent noise of the energy analyzer. Due to the low intensity of the positron beam, the recording time of the PAES spectrum was 20 days.

It is planned to install this PAES facility at the intense positron source at the Munich research reactor FRM-II [4]. Taking into account the expected intensity of 10^9 slow positrons per second, the measuring time should decrease by at least four orders of magnitude.

References

1. A. Weiss, R. Mayer, M. Jibaly, C. Lei, D. Mehl, K. G. Lynn, Phys. Rev. Lett. 61 (1988) 2245
2. D. Mehl, A.R. Köymen, K.O. Jensen, F. Gotwald, A. Weiss, Phys. Rev. B, 41 (1990) 799
3. B. Straßer, C. Hugenschmidt, and K. Schreckenbach; Mat. Sci. For. 363-365 (2001) 686
4. C. Hugenschmidt, G. Kögel, R. Repper, K. Schreckenbach, P. Sperr, B. Straßer, and W. Triftshäuser; Mat. Sci. For. 363-365 (2001) 425

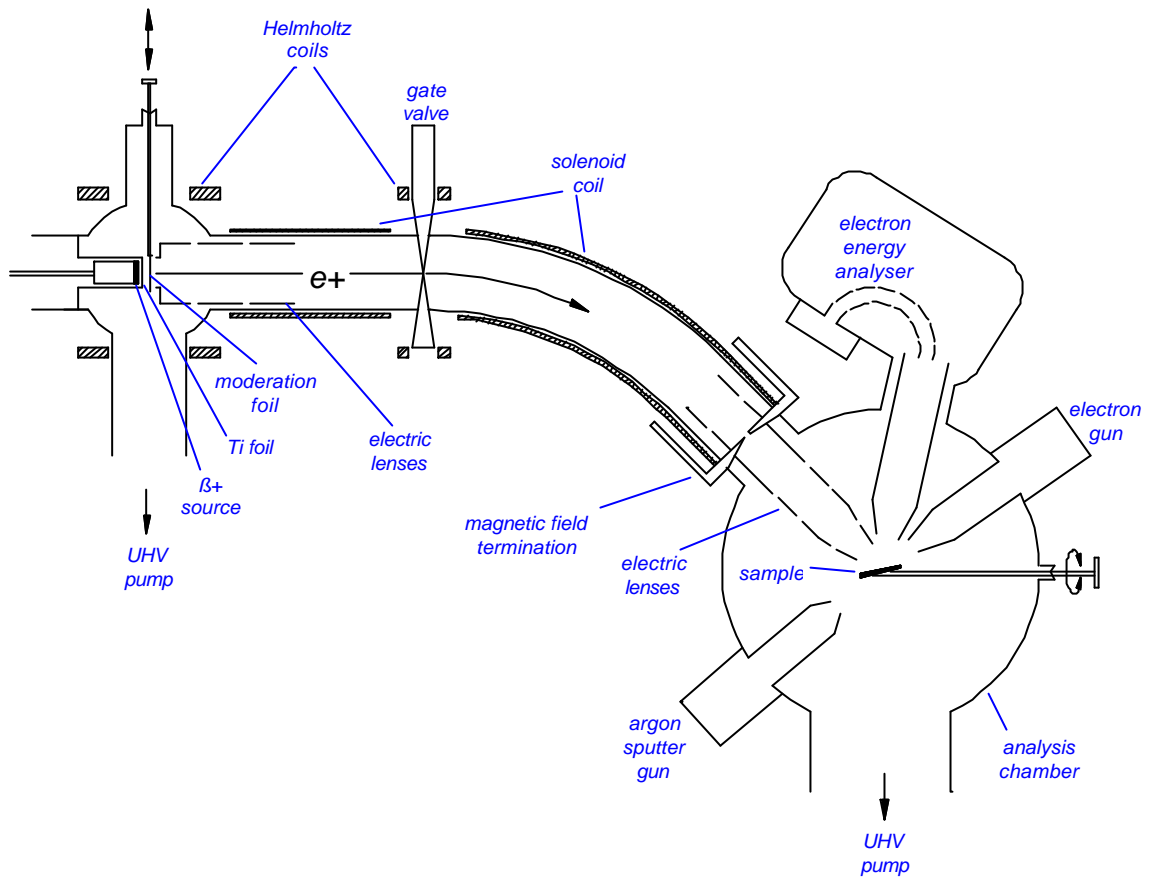


Fig. 1: Experimental set-up of the positron beam and the PAES analysis chamber (schematically). The Photography of the entire experimental set-up is shown in report 4.1 "Experimental facilities at the intense positron source at FRM-II", fig. 4.



Fig. 2: View into the analysis chamber. The incoming positrons are focused by electric lenses (top left) onto the sample in the center of the analysis chamber. Top: entrance of the electron energy analyzer. Top right: tungsten shielded NaI-detector.

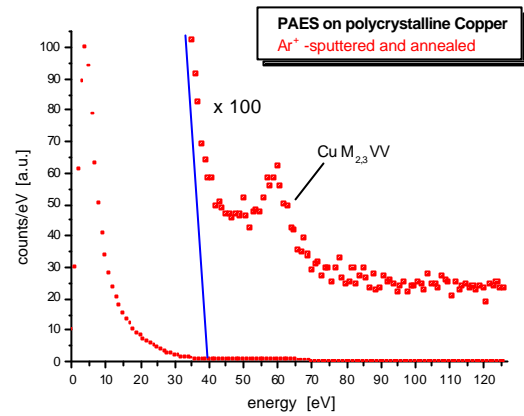


Fig. 4: PAES at Ar^+ -sputtered and annealed copper: The secondary electron spectrum ends at 40 eV according to the kinetic energy of the implanted positrons (blue line). The Auger-electron peak of the $Cu M_{2,3}VV$ transition is significantly detectable.

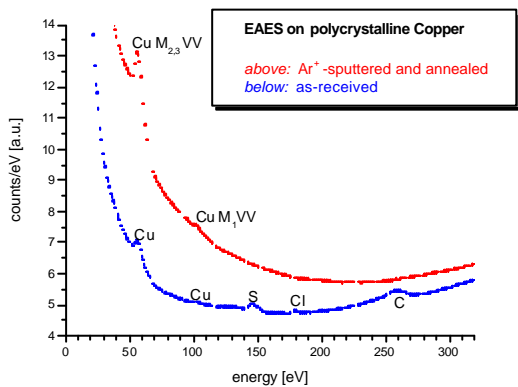


Fig. 3: EAES at polycrystalline copper (primary electron energy: 1 keV; measuring time: 10 minutes at each case). The pronounced peaks of the surface contamination vanish after Ar^+ -sputtering and annealing.

4.3 High Resolution Gamma Spectrometer for Doppler Broadening Measurements of the 511 keV Positron Annihilation Line

C. Hugenschmidt, M. Rykaczewski and K. Schreckenbach

*Fakultät für Physik E21, Technische Universität München,
D-85748 Garching, Germany*

In solid state physics positron annihilation is used as a high sensitive and non-destructive technique for the investigation of the microstructure and the momentum distribution of electrons. In these experiments, positrons are implanted into the sample material where they thermalize in a few picoseconds. After diffusion (typical diffusion length 0.1 μm), the positron together with an electron annihilates into two 511 keV quanta, which are emitted at an angle of 180° in the center-of-mass-system. In the laboratory system one measures a Doppler shift of the annihilation radiation due to the momentum of the annihilating electron – the momentum of the thermalized positron is negligible.

Experimental

A new spectrometer was constructed with two facing germanium detectors for the measurement of the annihilation radiation with high energy resolution. In between, a positron source (^{22}Na , 3.0 MBq) is sandwiched between two identical samples in order to use almost the whole solid angle of the emitted positrons (figure 1). The 180° -geometry of the germanium detectors allows the coincident detection of both annihilation photons, i.e. in these events the whole annihilation gamma energy of 1022 keV is deposited in the Ge-detectors. This 2D-Doppler broadening technique leads to a better energy resolution and much lower background.

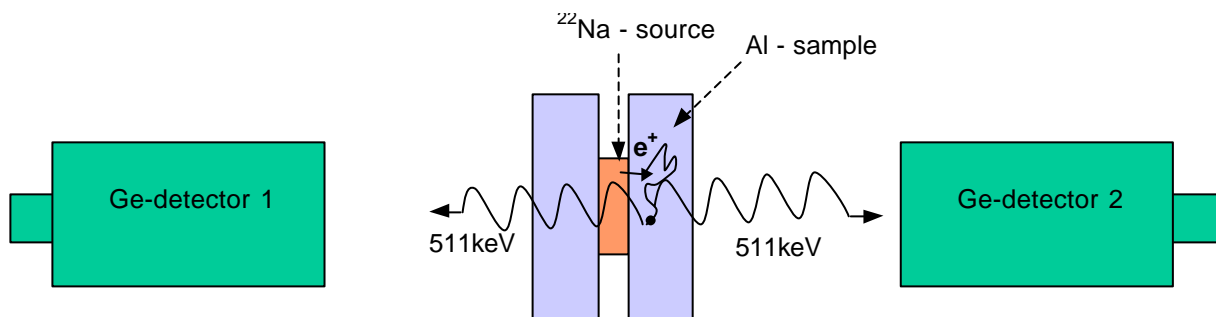


Fig. 1: Experimental set-up

Measurements and Results

The contour plot (fig. 2, left) and the 3D-intensity profile (fig. 2, right) show the result of the first test run with the new spectrometer. The peak intensity is located at the annihilation energy $E = m_e c^2 = 511 \text{ keV}$. The dark blue lines at $E_1 = 511 \text{ keV}$ and at $E_2 = 511 \text{ keV}$ respectively are due to events where one detector detects the whole energy of one annihilation photon and the other records the energy of Compton scattered gammas mainly of the 1275 keV deexcitation of ^{22}Ne . The diagonal from top left to the down right at

$$\begin{aligned} E &= E_1 + E_2 \\ &= (511 \text{ keV} - \Delta E)_1 + (511 \text{ keV} + \Delta E)_2 \\ &= 1022 \text{ keV} \end{aligned}$$

corresponds to the whole annihilation energy and contains the information of the Doppler shift ΔE . The resulting broadening is clearly observable in the contour plot in figure 2.

Figure 3 shows the conventionally recorded spectrum of one Ge-detector in single mode operation (red). The energy resolution of one Ge-detector at 511 keV is $\text{FWHM} = 1.2 \text{ keV}$ which is broadened to $\text{FWHM} = 2.42 \text{ keV}$ due to the Doppler effect. For comparison, the data cut diagonally from down left to the top right through the 511 keV peak of the contour plot recorded with the spectrometer in coincidence mode of both Ge-detectors is also plotted (blue). One can observe a significantly better energy resolution of $\text{FWHM} = 0.97 \text{ keV}$ and even more obviously the reduction of background events of several orders of magnitude.

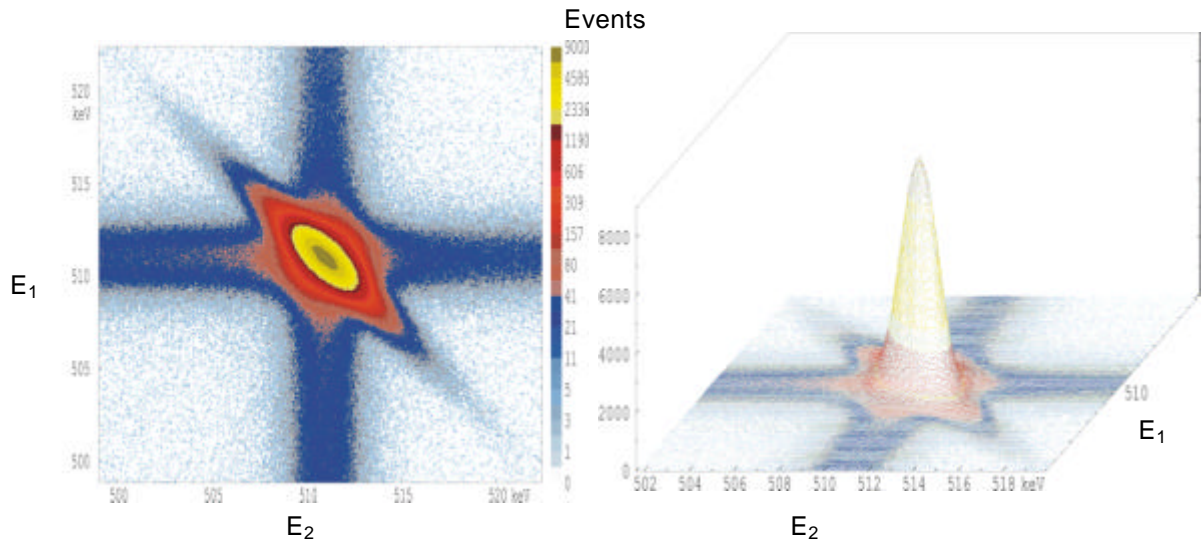


Fig. 2: Contour plot (left) and 3D-intensity profile (right) of the gamma energy (E_1, E_2) recorded with two Ge-detectors in coincidence. The peak intensity is located at the g energy $E = m_e c^2 = 511$ keV. The diagonal from top left to the down right at $E = E_1 + E_2 = (511 \text{ keV} - \Delta E)_1 + (511 \text{ keV} + \Delta E)_2 = 1022 \text{ keV}$ corresponds to the whole annihilation energy and contains the information of the Doppler shift ΔE .

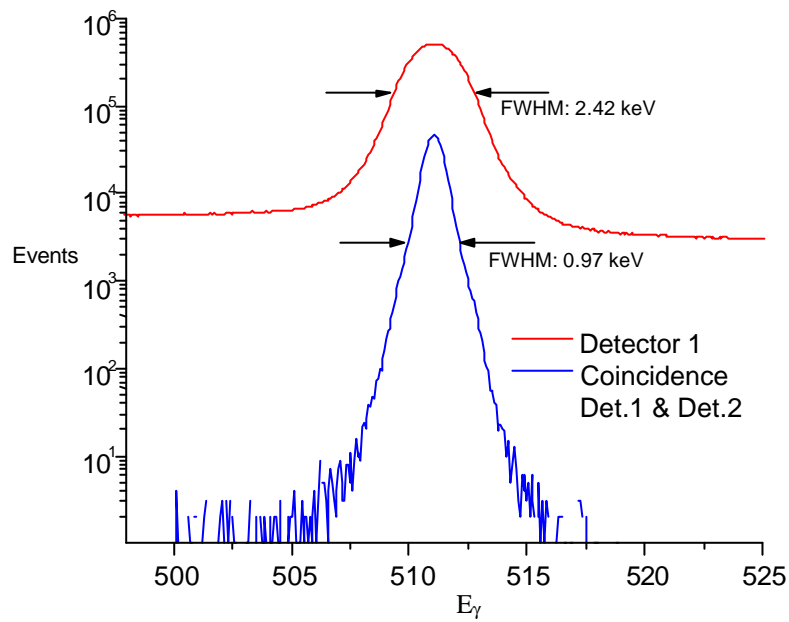


Fig. 3: Comparison between the spectrum in single mode (red) and coincidence mode of both detectors (blue)

4.4 Investigation of Laser Treated AlN and Silica by Positron Lifetime Measurements

C. Hugenschmidt¹, L. Liskay², W. Egger²

¹ Physik Department E 21, Technische Universität München, D-85747 Garching

² Institut für Nukleare Festkörperphysik, Universität der Bundeswehr München, D-85577 Neubiberg

Aluminumnitride has become a technical material of great interest that simultaneously comprises two important macroscopic properties: an uncommonly high thermal conductivity ($180 \text{ Wm}^{-1}\text{K}^{-1}$ at RT) and good electric insulation properties ($\rho > 10^{14} \text{ }\Omega\text{cm}$ at RT). For this reason, AlN is used in a wide range of technical applications such as high-temperature electronics, substrates and heat sinks for power electronics equipment as well as for pans for various molten-metal baths.

The sensitive positron annihilation technique is well suited to study defects and changes in matter on a microscopic scale. The presented measurements have profited particularly from the surface sensitivity of a low energy positron lifetime facility. In this work sintered AlN was irradiated with 532 nm laser pulses in order to study damage effects of the material due to optical induced changes or thermal load. In addition, amorphous SiO_2 was laser treated for comparison.

Experimental

Thin plates (0.6 mm thickness) of AlN and samples of amorphous SiO_2 (HERASIL2) were irradiated with intense laser light at the Walter Schottky Institute at the TUM. The wavelength of the Nd:YAG laser light was 532 nm according to a photon energy of 6.33 eV. The maximum energy per 8 ns pulse of 272 mJ leads to a total power of 34 MW, which permits localized heat- or photo-treatment of materials. The diameter of the laser beam at the sample surface was 7 mm with a Gaussian intensity profile. Consequently, the mean energy density amounted to 7 mJ/mm^2 per pulse. For the AlN samples the laser energy was varied between 10 mJ and 272 mJ and one specimen was exposed to ten laser pulses of maximum power according to a total energy of 2720 mJ. Two as-received samples of silica were studied as a reference and one silica sample was irradiated with one 272 mJ laser pulse.

The positron lifetime measurements were performed with the pulsed low energy positron beam system (PLEPS) at the university of the Bundeswehr in Munich [1]. This facility will be transferred to the intense positron source at FRM-II [2]. In order to get depth dependent information from the surface to the bulk, the

positron energy was varied from 1 keV up to 18 keV.

Results

The positron lifetime spectra of AlN were analyzed by fitting two lifetime components τ_1 and τ_2 (fig. 1). With increasing positron energy the lifetimes τ_1 and τ_2 decrease. Due to the small positron diffusion length, surface effects become negligible above a positron implantation energy of 3 keV. Hence, at 3 keV – corresponding to a penetration depth of about 60 nm – the bulk value of τ_1 of about 160 ps is reached. In the near surface region ($E_{\text{e}^+} < 3 \text{ keV}$) an increase of τ_1 and τ_2 is observed with increasing laser light intensity.

The data analysis for the recorded SiO_2 -spectra was performed with three lifetime components. The corresponding lifetime of para-positronium (p-Ps) was fixed at $\tau_1 = 125 \text{ ps}$. τ_2 with the intensity I_2 is attributed to the free positron annihilation in the sample and seems not to be affected by the laser irradiation (not shown). The long component with τ_3 describes the lifetime of ortho-positronium (o-Ps). The intensity I_3 corresponds to the o-Ps formation rate in matter. At the surface ($E_{\text{e}^+} = 1 \text{ keV}$) the value of τ_3 drops down from 1450 ps for the as-received material to 1200 ps after laser treatment. The intensity I_3 is also much lower for laser irradiated silica in particular at low positron energy.

Discussion and Conclusion

Due to the high molecular stability of N_2 which forms on and desorbs from the surface, most heated metal nitrides evaporate primarily by decomposition to their elements. Therefore, the thermal impact of a laser pulse leads to a sublimation of nitrogen molecules and to small grains of aluminum at the AlN surface. The increase of τ_1 and τ_2 with increasing laser energy is attributed to larger defects in AlN and in Al at the surface.

The prompt decrease of the o-Ps lifetime τ_3 and the corresponding intensity I_3 show that almost no o-Ps-formation occurs at the surface and the near surface region after laser treatment. It is known that silica contains OH⁻ groups and hence dangling bonds. For this

reason, the decrease of Ps formation may be attributed to a lower concentration of dangling bonds, i.e. less "free" electrons, which may be optically activated if silica is irradiated by intense laser light.

The present results show that the damaging in AlN and in fused silica due to laser irradiation is completely different. In AlN the thermal impact of the laser pulse creates positron trapping sites at the surface, whereas in silica less Ps-formation is observed due to less dangling bonds after laser irradiation.

Acknowledgement

The author likes to thank CeramTec and Heraeus which made the sample material available. The assignment of the laser facility and the technical help by Christoph Nebel of the Walter Schottky Institute at the TUM is gratefully acknowledged.

References

- [1] W. Bauer-Kugelmann, P. Sperr, G. Kögel, and W. Triftshäuser, *Mat. Sci. For.* 363-365 529 (2001)
- [2] C. Hugenschmidt, G. Kögel, R. Repper, K. Schreckenbach, P. Sperr, B. Straßer, and W. Triftshäuser; *Appl. Phys. A* 74 (2002) S295-S297

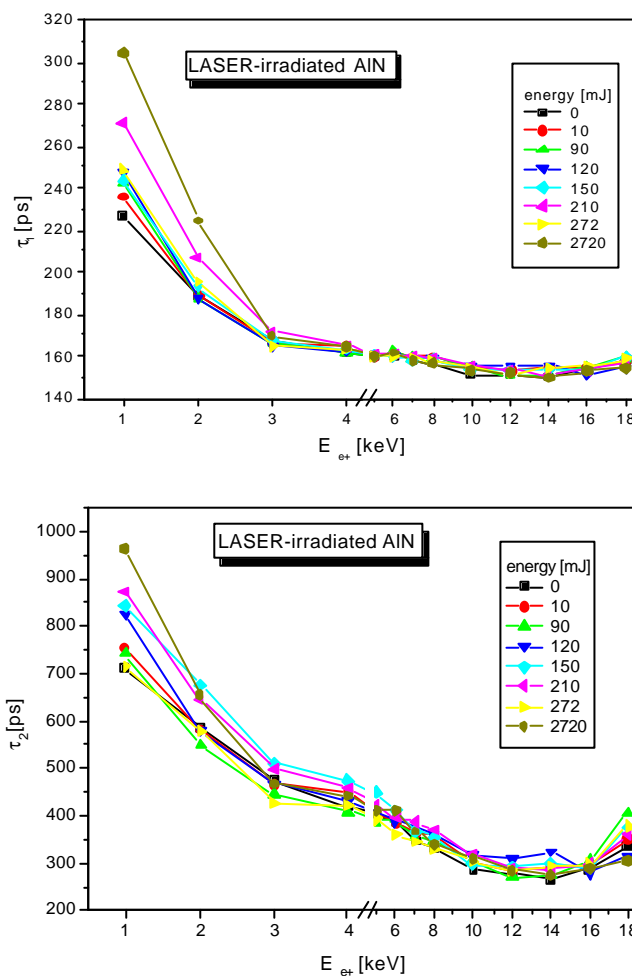


Fig. 1: As-received and laser treated AlN: The positron lifetimes t_1 and t_2 as a function of positron energy. The significant increase of the lifetimes below 3 keV – according to a positron penetration depth of 60 nm – is attributed to the creation of defects.

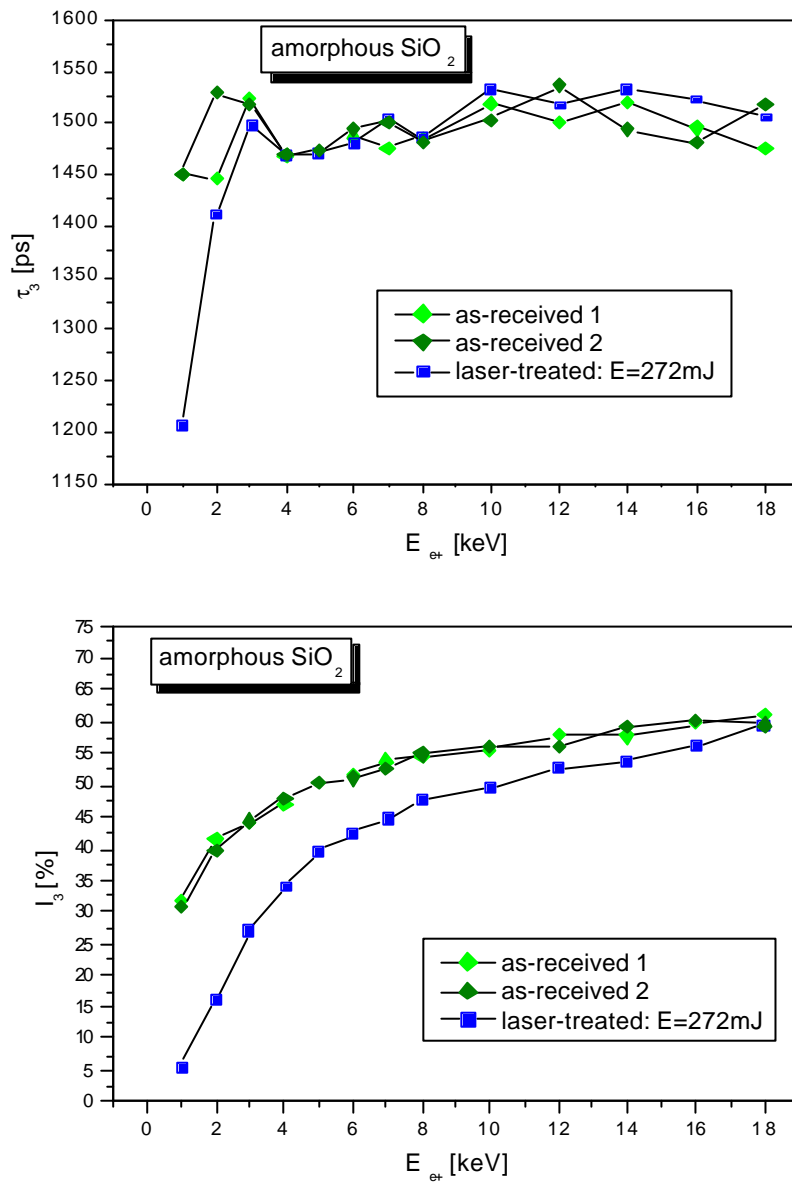


Fig. 2: As-received and laser treated amorphous SiO₂: τ₃ and the intensity I₃ describe the o-Ps lifetime and the o-Ps formation rate.

5 REACTOR PHYSICS

5.1 Nuclear Licensing of the FRM-II

Prof. Dr. K. Böning

Technische Universität München

The first draft of the Third Partial Nuclear License of the FRM-II, which includes the license to start up and operate the reactor, had been sent by the Nuclear Licensing Authority, the Bavarian State Ministry of State Development and Environment (StMLU), to the Federal Ministry of Environment and Reactor Safety (BMU) already in August 2000. After numerous meetings of the representatives of the Technische Universität München (TUM) and its general contractor Framatome-ANP with the technical experts and advisors of the BMU, the Reactor Safety Commission (RSK) and the Commission on Radiation Protection (SSK), the BMU issued its Federal Supervisory Assessment to the StMLU in January 2002. This document listed some 65 questions or conditions – more and including additional topics than contained in the positive assessments of both RSK and SSK - which the BMU wanted to get further discussed in more detail. This represented very hard work for

both TUM and Framatome-ANP until we could deliver all the relevant documents to the StMLU and the StMLU could submit an updated draft of the Third Partial Nuclear Permit to the BMU in July 2002.

At the end of October 2002 the BMU sent an updated List of Questions which still contained some 10 items with a focus on Beyond Design Basis Accident scenarios. This again meant hard work for both TUM and Framatome-ANP until we could submit the last documents in mid January 2003. Having answered all these questions we are pretty confident now that the StMLU will receive a positive Federal Supervisory Assessment of the BMU in early 2003. The final, Third Partial Nuclear License of the StMLU would probably follow shortly later and the transport of the first fuel elements and the nuclear startup of the FRM-II could be initiated immediately after that.

5.2 Fuel Element with Reduced Enrichment for the FRM-II

Prof. Dr. K. Böning

Technische Universität München

The outstanding performance of the FRM-II to provide a high thermal neutron flux ($8 \times 10^{14} \text{ cm}^{-2}\text{s}^{-1}$ unperturbed) in a large usable volume at a relatively low reactor power (20 MW) is directly related to the design of a single, very compact fuel element in a large tank filled with heavy water moderator. This compact fuel element is cooled by light water and contains uranium-silicide (U_3Si_2) aluminum dispersion fuel with high enrichment (93 % U235) and with a relatively high uranium density (3.0 gU/cm^3 , graded).

After its election in 1998 the red-green Federal Government – following its nonproliferation philosophy - decided to investigate if the FRM-II could be converted to use low-enriched fuel (with 20 % U235 only). The Federal Ministry of Education and Research (BMBF) established an experts' committee which – after many sessions – presented a final report listing a number of alternatives in June 1999. The position of the TUM was always to maintain the reactor power and the compact dimensions of the fuel element – so that the FRM-II reactor facility would not need to be modified and built once again and that the penalties in reactor performance would be marginal; this means

that the enrichment of U235 could be reduced only so far as this could be fully compensated by an increase in the uranium density of new fuels (i.e. without making the fuel element larger). An agreement following this line has been negotiated between the Bavarian State Ministry of Science, Research and Arts (StMWFK) and the BMBF; this agreement was finalized in October 2001 but will be signed by the ministers only once the green light has been given by the Federal Government to start up and operate the FRM-II. This agreement says that the FRM-II will be permitted to operate with fuel elements using highly enriched uranium for about ten years, i.e. until an advanced fuel with a higher uranium density has been developed and tested so that a new fuel element with reduced enrichment can be designed, fabricated, tested and licensed.

The TUM has already established an international working team to develop such an advanced fuel and a modified fuel element for the FRM-II. This work will actually begin once the green light for the FRM-II has been obtained and the agreement has been signed and the necessary budget has been allocated.

6 ACTIVITIES 2002

6.1 Publications

1. P.A. Alekseev, E.Clementyev, P.Allenspach, Yu.Chumlyakov, V.N.Lazukov and I.P.Sadikov, "Soft mode and magnetic phase transition in PrNi", JETP Lett. 76, (2002) 110
2. P.A. Alekseev, J.-M.Mignot, K.S.Nemkovski, R.Kahn, N.Yu.Shitsevalova, R.I. Bewley, R.S.Eccleston, E.Clementyev, V.N.Lazukov, "Yb-Yb correlations and crystal field in the Kondo-insulator YbB_{12} ", Appl. Phys. A 74, (2002) s562-s564
3. P.A. Alekseev, J.-M.Mignot, A.Ochiai, E.V.Nefeodova, I.P.Sadikov, E.Clementyev, V.N.Lazukov, M.Braden and K.S.Nemkovski, "Collective magnetic excitations in mixed-valence $\text{Sm}_{0.83}\text{Y}_{0.17}\text{S}$ ", Phys. Rev. B 65, (2002) 153201
4. P.A. Alekseev, J.-M.Mignot, U.Staub, A.Ochiai, A.V.Golubkov, M.Braden, R.Bewley, E.V.Nefeodova, I.P.Sadikov, E.Clementyev, V.N.Lazukov, K.Nemkovski, "f-electron excitations in the neutron spectra of mixed-valence $\text{Sm}_{1-x}\text{Y}_x\text{S}$ ", Physica B 312-313, (2002) 333
5. S. Baechler, N. Kardjilov, M. Dierick, J. Jolie, G. Kuhne, E. Lehmann, T. Materna, "New features in cold neutron radiography and tomography Part I: thinner scintillators and a neutron velocity selector to improve the spatial resolution", Nuclear Instruments and Methods in Physics Research A 491 (2002) 481-491.
6. M. Bleuel, F. Demmel, R. Gähler, R. Golub, K. Habicht, T. Keller, S. Klimko, I. Köper, S. Longeville, and S. Prokudaylo, "Future Developments in Resonance Spin Echo", Springer-Verlag LNP 601 (2002), p. 176 ff.
7. P. Böni, "Experimental Methods: Neutron Scattering", in 'Magnetism', Lecture Notes of the 1st Summer School on Condensed Matter Research, Zuoz, Switzerland, August 10-17 2002, PSI-Proceedings 02-02, ISSN 1019-6447, 1-21 (2002).
8. P. Böni, E. Clementyev, Ch. Stadler, B. Roessli, G. Shirane, and S. A. Werner, "Fincher-Burke Excitations in Single-Q Chromium", Applied Physics A 74, S716 - S718 (2002).
9. P. Böni, B. Roessli, D. Görlitz, and J. Kötzler, "Damping of Spin Waves and Singularity of the Longitudinal Modes in the Dipolar Critical Regime of the Heisenberg-Ferromagnet EuS", Phys. Rev. B 65, 144434-(1-9) (2002).
10. K. Böning: „Use of Highly Enriched Uranium at the FRM-II“. Proceedings of the 6th International Topical Meeting on Research Reactor Fuel Management (ENS RRFM 2002), Ghent, Belgium, 17. – 20. 03. 2002, Seite 73 – 77.
11. K. Böning, A. Axmann, K. Schreckenbach, M. Köhler, H.-J. Didier: „Die neue Forschungs-Neutronenquelle FRM-II“. Jahrbuch der Atomwirtschaft 2002, Manuskript 17 Seiten
12. K. Böning: „Ausschluß einer Rekritikalität der abgebrannten Brennelemente und Konverterplatten des FRM-II im Endlager und Konzept einer möglichen Konditionierung“. Technische Universität München, Bericht OPA00290 vom 25. 01. 2002 (22 + 10 Seiten).
13. K. Böning: „Zur Endlagerung der abgebrannten Brennelemente und Konverterplatten des FRM-II: Radionuklide und Aktivitätsinventar“. Technische Universität München, Bericht OPA00292 vom 05. 03. 2002 (3 + 30 Seiten).
14. Braun, K. M. Briggs, and P. Böni, "Analytical Solution for Matthews'and Blakeslee's Critical Dislocation Formation Thickness of Expitaxially Grown Thin Films", Journal of Crystal Growth 241/1-2, 231-234 (2002).
15. E.Clementyev, P.A.Alekseev, P.Allenspach and V.N.Lazukov, "Soft-mode-driven magnetic ordering in the singlet ground-state system PrNi", Appl. Phys. A 74, (2002) s589-s591
16. R. Georgii, S. Plüschke, R. Diehl, G.G. Lichti, V. Schönfelder, W. Hermsen, J. Ryan and K. Bennett, "COMPTEL upper limits for the ^{56}Co γ -ray emission from SN1998bu", A&A 394, (2002), 517 - 523
17. N. Golosova, V. Bobrovskii, E. Mitberg, A. Podlesnyak, I. Zhakhin, A. Mirmelstein, "Superposition structure of crystal spectra in high- T_c superconductors: overdoped mode", JETP 94, (2002) 1013-1025

18. N. Golosova, A. Podlesnyak, E. Mitberg, V. Bobrovskii, A. Mirmelstein and A. Furrer, "The effect of Ca and Th substitution on the crystal-field spectrum in the high- T_c superconductor $\text{HoBa}_2\text{Cu}_3\text{O}_x$ ", *J. Phys.: Condens. Matter* **14**, (2002) 1923-1936
19. C. Hugenschmidt, G. Kögel, R. Repper, K. Schreckenbach, P. Sperr, B. Straßer, and W. Triftshäuser, "Monoenergetic Positron Beam at the Reactor Based Positron Source at FRM-II", *Nucl. Instr. Meth. B* **192**, 1-2 (2002) 97-101
20. C. Hugenschmidt, G. Kögel, R. Repper, K. Schreckenbach, P. Sperr, B. Straßer, and W. Triftshäuser, "Intense Positron Source at the Munich Research Reactor FRM-II", *Appl. Phys. A* **74** (2002) S295-S297
21. C. Hugenschmidt, K. Schreckenbach and B. Straßer, "Investigation of Positron Work Function and Moderation Efficiency of Ni, Ta, Pt and W (100)", *Appl. Surf. Sci.* **194**, 1-4 (2002) 283-286
22. C. Hugenschmidt, G. Kögel, R. Repper, K. Schreckenbach, P. Sperr, and W. Triftshäuser, "First Platinum Moderated Positron Beam Based on Neutron Capture", *Nucl. Instr. Meth. B* **198** (2002) 220-229
23. N. Kardjilov, S. Baechler, M. Bast=FCrk, M. Dierick, J. Jolie, E. Lehmann, T. Materna, B. Schillinger, P. Vontobel, "New features in cold neutron radiography and tomography Part I: Applied energy-selective neutron radiography and tomography", accepted for publication in *Nuclear Instruments and Methods in Physics Research A* (2002)
24. N. Kardjilov, E. Lehmann, P. Vontobel, "Representation of the image formation in applied neutron radiography in terms of a PSF superposition", *Appl. Phys. A* **74** [Suppl.], S228-S230 (2002).
25. M. Koppe, M. Bleuel, R. Gaehler, R. Golub, P. Hank, T. Keller, S. Longeville, U Rauch, J. Wuttke, "Prospects of resonance spin echo", *Physica B* **266**, (1999) 75
26. V.N.Lazukov, P.A.Alekseev, N.N.Tiden, Ch.Beck, E.Clementyev and I.P.Sadikov, "The Special Features of the Ground State in CeAl_3 ", *JETP Lett.* **76**, (2002) 295
27. A. Mirmelstein, V. Bobrovskii, N. Golosova, A. Podlesnyak, and A. Furrer, "Frustrated phase separation in the overdoped regime of "123" high- T_c superconductors", *Journal of Superconductivity: Incorporating Novel Magnetism* **15**, (2002) 367-371
28. A. Mirmelstein, A. Podlesnyak, V. Bobrovskii, N. Golosova, "Crystal-field spectrum of $\text{R}_{1-y}\text{Ca}_y\text{Ba}_2\text{Cu}_3\text{O}_x$ high- T_c superconductors in the overdoped regime", *Applied Physics A* **74**, [Suppl.] (2002) S1019-1021
29. P. Müller-Buschbaum, P. Böni, A. Meyer, J. Neuhaus, W. Petry, and E. Steichele, Editors of *Proceedings of the International Conference on Neutron Scattering 2001*, 9-13 September, Munich, Germany, *Applied Physics A* **75** (Springer, Berlin, 2002).
30. M. Nuding, K. Böning: „Bericht über das Brennstoff-Bestrahlungsexperiment am OSIRIS-Reaktor“. Technische Universität München, Bericht OPA00297 vom 15. 04. 2002 (49 Seiten).
31. Pirogov, A. Podlesnyak, Th. Strässle, A. Mirmelstein, A. Teplykh, D. Morozov, A. Yermakov, "Neutron diffraction investigation of the metamagnetic transition in ErCo_2 ", *Applied Physics A* **74**, [Suppl.] (2002) S598-600
32. Podlesnyak, A. Mirmelstein, N. Golosova, E. Mitberg, I. Leonidov, V. Kozhevnikov, I. Sashin, F. Altorfer, A. Furrer, "Magnetic properties and crystal-field excitations in the $\text{Ln}_x\text{Sr}_{1-x}\text{CoO}_3$ ($\text{Ln} = \text{La, Pr, Ho}$)", *Applied Physics A* **74**, [Suppl.] (2002) S1746-1748
33. Podlesnyak, Th. Strässle, A. Mirmelstein, A. Pirogov, R. Sadykov, "Magnetization and neutron scattering studies of the pressure effect on the magnetic transition in $\text{Er}_{0.57}\text{Y}_{0.43}\text{Co}_2$ ", *Eur. Phys. J. B* **29**, (2002) 547- 552
34. Podlesnyak, Th. Strässle, J. Schefer, A. Furrer, A. Mirmelstein, A. Pirogov, P. Markin, and N. Baranov, "Magnetic transition in $\text{Er}_{1-x}\text{Y}_x\text{Co}_2$ ($x = 0, 0.4$) single crystals probed by neutron scattering in magnetic fields", *Phys. Rev. B* **66**, (2002) 012409 (4 pages)
35. S. Prokudaylo, R. Gähler, T. Keller, M. Bleuel, M. Axtner, A. Selvachev, "Calculations on resonance spin-echo coils", *Appl Phys A* **74** (2002) [Suppl1], s317-s319
36. B. Roessli and P. Böni, "Polarized Neutron Scattering", in 'Scattering and Inverse Scattering in Pure and Applied Science', edited by E. R. Pike and P. Sabatier, S. 1242-1263, Academic Press 2002.

37. B. Roessli, P. Böni, W. Fischer, and Y. Endoh "Chiral Fluctuations in MnSi above the Curie Temperature", Phys. Rev. Lett. **88**, 237204 (2002).
38. M. Senthil Kumar and P. Böni, "Influence of Interstitial Nitrogen on the Structural and Magnetic Properties of FeCoV/TiN_x Multilayers", J. Appl. Phys. **91**, 3750 (2002).
39. M. F. Thomas, G. S. Case, J. Bland, A. D. F. Herring, W. G. Stirling, S. Tixier, P. Böni, R. C. C. Ward, M. R. Wells, and S. Langridge, "Studies on Rare-Earth/Iron and Actinide/Iron Multilayers", Hyperfine Interactions **141/142**, 471-476 (2002).

6.2 Conference, Workshop and Seminar Contributions

P. Böni

"Spindynamik in magnetischen Materialien: Ein Spielplatz für Neutronen", Kolloquium Universität Braunschweig, 29. Januar 2002.

P. Böni, B. Roessli, D. Görlitz, and J. Kötzler

"Spin waves and singularity of the longitudinal modes in the dipolar critical regime of ferromagnetic EuS", European Conference on ESS, Bonn, 16-17 May 2002.

P. Böni

"Chirale Anregungen in magnetischen Systemen", Workshop 'Magnetismus und Streumethoden', Forschungszentrum Jülich, 7. Juni 2002.

P. Böni

"Grundlagenphysik: Experimente am FRM-II", Treffen Bund der Freunde der TUM, TU-München, 19. Juli 2002.

P. Böni

"Experimental Methods: Neutron Scattering", Lecture, 1st Summer School on Condensed Matter Research, Zuoz, Switzerland, August 10-17 2002.

P. Böni

"Spindynamik in magnetischen Materialien – Ein Spielplatz für Neutronen", Tag der offenen Tür, Alumni-Forum, Technische Universität München, 23. November 2002.

K. Böning

„Der steinige Weg zum FRM-II“. Vortrag auf dem Festkolloquium der Münchner Physiker aus Anlaß der Emeritierung von Prof. Dr. Wolfgang Gläser, Physik-Department der Technischen Universität München, Garching, 18. 02. 2002

K. Böning

„Use of Highly Enriched Uranium at the FRM-II“. Vortrag auf dem 6th International Topical Meeting on Research Reactor Fuel Management (ENS RRFM 2002), Ghent, Belgium, 18. 03. 2002.

K. Böning

„Forschungsreaktor München 2 – Risiko oder Chance?“ Vortrag und Diskussion mit Dipl. Phys. C. Pistner (Gruppe IANUS an der Technischen Universität Darmstadt), veranstaltet von der Volkshochschule im Norden des Landkreises München, Bürgerhaus Garching, 16. 04. 2002.

J. Brunner, B. Schillinger

"Dynamic Neutron Radiography of a Combustion Engine", 7th World Conference on Neutron Radiography, Rome, 15-20 September 2002

E. Calzada, F. Grünauer, B. Schillinger,

"The Design of the tomography facility at the new research reactor FRM-II at TU München", European Conference on ESS, Bonn, 16-17 May 2002

E. Calzada, F. Grünauer, B. Schillinger

"Engineering solutions for the new radiography and tomography facility at FRM-II", 7th World Conference on Neutron Radiography, Rome, 15-20 September 2002

F. Grünauer, P. Böni

"Optimization of the composition of heavy concrete for neutron shielding purposes", European Conference on ESS, Bonn, 16-17 May 2002

F. Grünauer, B. Schillinger

"Shielding aspects for the neutron tomography facility at FRM-II", 7th World Conference on Neutron Radiography, Rome, 15-20 September 2002

C. Hugenschmidt

"Positron Generation and Extraction at FRM-II", EPOS-02, The 1st Annual ELBE Positron Source Meeting, Rossendorf, September 2002

C. Hugenschmidt

"Der neue Forschungsreaktor FRM-II und die intensive Positronenquelle", Seminar im Helholtz-Institut für Strahlen- und Kernphysik, Bonn, Dezember 2002

C. Hugenschmidt

"The In-Pile Positron Source at the Munich Research Reactor FRM-II", Jahrestagung Kerntechnik, Stuttgart, Mai 2002

C. Hugenschmidt

"The Positron Source Based on Neutron Capture", PPC-7, 7th International Workshop on Positron and Positronium Chemistry, Knoxville, USA, June 2002

C. Hugenschmidt

"Investigation of Laser Treated AlN by Positron Lifetime Measurements", PSSD-2002, The 3rd International Workshop on Positron Studies of Semiconductor Defects, Sendai, Japan, September 2002

C. Hugenschmidt, G. Kögel, K. Schreckenbach, P. Sperr, B. Straßer, and W. Triftshäuser;

"Intensive Positronenquelle am neuen Münchner Forschungsreaktor FRM-II", DNJ, Deutsche Neutronenstreutagung, Bonn 2002

C. Hugenschmidt, B. Straßer and K. Schreckenbach

"Investigation of the Annealed Copper Surface by Positron Annihilation Induced Auger Electron Spectroscopy", PPC-7, 7th International Workshop on Positron and Positronium Chemistry, Knoxville, USA, June 2002

E.H. Lehmann (Paul Scherrer Institut, CH), P. Vontobel (Paul Scherrer Institut, CH), B. Schillinger,

"Stand und Perspektiven der Tomographie mit Neutronen als Werkzeug der zerstörungsfreien Materialanalyse", Vortrag am Fraunhofer Institut für Produkttechnik und Automatisierung (IPA) in Stuttgart

N. Kardjilov, S. Baechler, M. Bastürk, M. Dierick

"Energy-selective neutron radiography and tomography with cold Neutrons", 7th World Conference on Neutron Radiography, Rome, 15-20 September 2002

N. Kardjilov, S. Baechler, E. Lehmann, G. Frei

"Applied energy-Selective neutron radiography and tomography with cold neutrons", 7th World Conference on Neutron Radiography, Rome, 15-20 September 2002

N. Kardjilov, F.C. de Beer, M.F. Middleton, B. Schillinger

"Corrections for scattered neutrons in quantitative neutron radiography", 7th World Conference on Neutron Radiography, Rome, 15-20 September 2002

B. Schillinger, M. Bleuel, P. Böni, E. Steichele, "Design and simulation of a neutron guide plus flight

tube for neutron radiography and tomography at the new research reactor FRM-II at Technical University Munich", 7th World Conference on Neutron Radiography, Rome, 15-20 September 2002

B. Schillinger

"Neutron computed tomography", invited lecture, Korean Atomic Energy Research Institute in Daejeon, Korea

B. Schillinger

"Neutron computed tomography as an industrial tool", invited lecture, Korean Atomic Energy Research Institute in Daejeon, Korea

B. Schillinger

"Neutronentomographie", Eingeladener Vortrag am Hahn-Meitner-Institut

B. Schillinger

"Die Neutronentomographie-Anlage am neuen Forschungsreaktor FRM-II", Eingeladener Vortrag am Hahn-Meitner-Institut

Shah Valloppilly

"Influence of interfaces on the magnetism of ultra thin films and multilayers: 3 case studies", Neutrons in research and industry seminar, Technische Universität München, October 28, 2002.

6.3 Lectures, Courses and Seminars

M. Bleuel:	Tutorial "Experimental Physics for Civil Engineers 1" Tutorial "Experimental Physics for Civil Engineers 2" Tutorial "Introduction to Solid State Physics I"
P. Böni:	Lectures "Experimental Physics for Civil Engineers 1" Lectures "Experimental Physics for Civil Engineers 2" Lectures "Introduction to Solid State Physics I" Seminar "Neutrons in Research and Industry"
K. Böning:	Lectures "Reaktorphysik I: Grundlagen" Seminar "Neutrons in Research and Industry"
J. Brunner:	Tutorial "Elektronikpraktikum"
R. Georgii:	Seminar "Neutrons in Research and Industry"
F. Grünauer:	Tutorial "Experimental Physics for Civil Engineers 1" Tutorial "Experimental Physics for Civil Engineers 2" Tutorial "Introduction to Solid State Physics I"
N. Kardjilov:	Tutorial "Elektronikpraktikum"
T. Keller:	Tutorial "Elektronikpraktikum"
B. Schillinger:	Tutorial "Elektronikpraktikum"
K. Schreckenbach:	Seminar "Neutrons in Research and Industry"

6.4 Committee Memberships

P. Böni

- Nutzausschuss deutsches Kontingent, Institut Laue Langevin, Grenoble
- Instrument Subcommittee, Institut Laue Langevin, Grenoble
- SINQ Scientific Committee
- Projektbegleitender Beirat FRM-II
- Instrumentierungsausschuss FRM-II
- Direktorium FRM-II
- TUM-Beirat für den FRM-II
- Coordinator of Work Package on Neutron Optics, Joint Research Projects in EU: FP6

K. Böning

- Chairman (President) of the International Group on Research Reactors IGORR.
- Member of the Technical Review Committee (TRC) of the Taiwan Research Reactor System Improvement and Utilization Promotion Project (TRR-II).
- Member of the Scientific Committee of the ENC (European Nuclear Conference) of the European Nuclear Society ENS, Track Leader (together with Alain Ballagny, CEA, France) for „Experimental, Research Reactors and Neutron Sources“ at the ENC 2002 Scientific Seminars.

B. Schillinger

- Vice President of the European Neutron Radiology Association (ENRA)
- Board Member of the International Society for Neutron Radiography (ISNR)

K. Schreckenbach

- Komitee für Neutronenforschung (KFN)
- Instrumentierungsausschuss FRM-II
- Direktorium FRM-II
- TUM-Beirat für den FRM-II
- Arbeitsgemeinschaft Forschungsreaktoren (AFR)

E. Steichele

- International Conference on Neutron Scattering ICNS 2001, Munich: Co-Editor Committee
- Instrumentierungsausschuss FRM-II

6.5 E21 Members

Name	Phone +49-89- 289-	Fax +49-89- 289-	Room	email
Arend Nikolas, Dipl. Phys.	-14723	-	PH 1, 2205	Nikolas.Arend@frm2.tum.de
Axtner Markus	-12125	-13776	RS, 140	maxtner@frm2.tu-muenchen.de
Bleuel Markus, Dipl. Phys.	-13777	-13776	RS, 124	mbleuel@frm2.tum.de
Böni Peter, Prof. Dr.	-14711	-14713	PH 1, 2215	peter.boeni@ frm2.tum.de
Böning Klaus, Prof. Dr.	-12150	-12191	FRM-II UBA 0325	kboening@frm2.tum.de
Braun Hans-Benjamin, Dr.	-12512	-14713	PH 1, 2367	bbraun@frm2.tum.de
Brunner Johannes, Dipl. Phys.	-12106	-13776	RS, 102	brunnerj@frm2.tum.de
Clementyev Evgeni, Dr.	-14722	-14713	PH 1, 2207	eclement@frm2.tum.de
Gläser Wolfgang, Prof. emerit.	-12476	-12474	PH 1, 2227	wglaeser@frm2.tum.de
Grünauer Florian, Dipl. Phys.	-12125	-13776	RS, 140	fgruenau@frm2.tum.de
Hils Thomas, Dr.	-14721	-	Flachbau, 17	thomas.hils@hils-consult.de
Kardjilov Nikolay, Dipl. Phys.	-12106	-13776	RS, 102	nikolay@frm2.tum.de
Kargl Verena, Dipl. Phys.	-12515	-	PH 1, 2373	vkargl@frm2.tum.de
Mirmelstein Alexey, Dr.	-14718	-14713	PH 1, 2207	alex.mirmelstein@frm2.tum.de
Plonka Christian, Dipl. Phys.	-12299 -12199	-13776	Flachbau, 13	cplonka@frm2.tum.de
Prokudaylo Sergey, Dipl. Phys.	-13777	-13776	RS, 124	sprokuda@frm2.tum.de
Reich Christian, Diploma Student	12515	-	PH I, 2373	creich@frm2.tum.de
Russ Barbara, Dipl. Ing.	-14717	-14713	PH 1, 2207	barbara.russ@frm2.tum.de
Schanzer Christian, Dipl. Phys.	-14725	-	PH 1, 2214	cschanze@frm2.tum.de
Schreckenbach Klaus, Prof. Dr.	-12183	-12191	RS	Klaus.Schreckenbach@ frm2.tum.de
Skorski Cornelia, Secretary	-14712	-14713	PH 1, 2217	cskorski@frm2.tum.de
Stadler Christoph, Diploma Student	-	-	-	-
Steichele Erich, Dr.	-12141	-12112	RS	esteich@frm2.tum.de
Straßer Benno, Dipl. Phys.	-12137	-12191	RS	bstrasse@frm2.tum.de
Daniel Tejic	-12656	-	FB PH. T. ABT, 1321	-
Valloppilly Shah, Dr.	-14723	-14713	PH 1, 2205	shah@frm2.tum.de
Wieschalla Nico, Diploma Student	-12111	-13776	RS 146b	nico@frm2.tum.de

PH: Physics Department

RS: Reactor Station

6.6 Associated Members at FRM-II

Name	Phone +49-89-289-	Room	email
Calzada Elbio, Dipl. Ing.	-14611	RS	ecalzada@frm2.tum.de
Georgii Robert, Dr.	-14986	RS	robert.georgii@frm2.tum.de
Hugenschmidt Christoph, Dr.	-14609	RS, 4	hugen@frm2.tum.de
Langenstück Guido, Dipl. Ing.	-14915	-	langenst@frm2.tum.de
Schillinger Burkhard, Dr.	-12185	RS	schilli@frm2.tum.de

PH: Physics Department

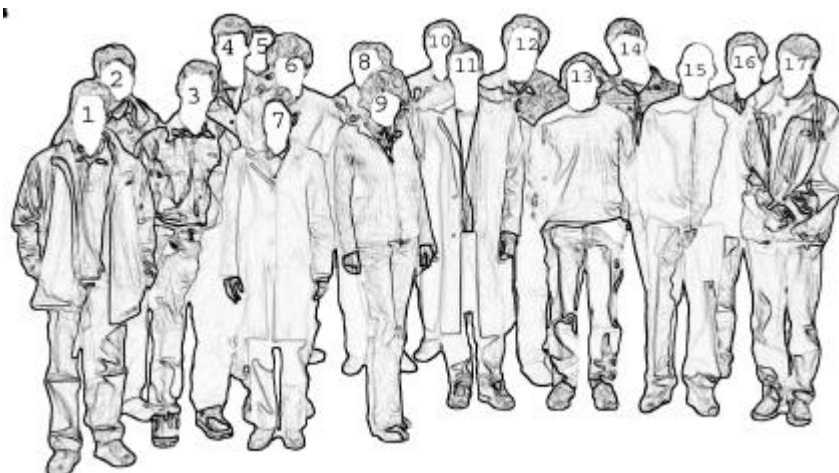
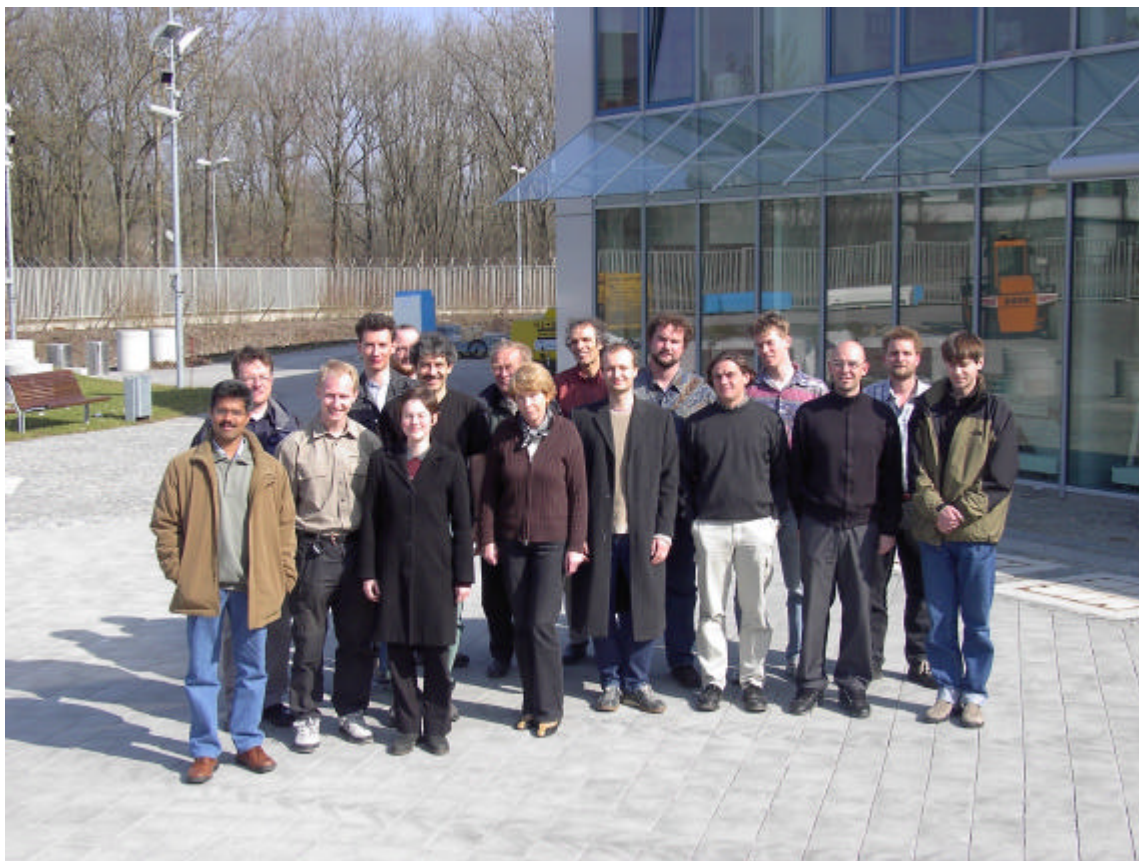
RS: Reactor Station

6.7 Guests

Name	Phone +49-89-289-	Room	email
Gähler Roland, Dr.	-12111	RS 146b	rgaehler@frm2.tum.de
Keller Thomas, Dr.	-12164	RS, 4	tkeller@frm2.tum.de

PH: Physics Department

RS: Reactor Station



1 – Shah Valloppilly

2 – Christoph Hugenschmidt

3 – Nico Wieschalla

4 – Benno Straßer

5 – Markus Bleuel

6 – Elbio Calzada

7 – Verena Kargl

8 – Wolfgang Gläser

9 – Barbara Russ

10 – Peter Böni

11 – Christian Reich

12 – Burkhard Schillinger

13 – Markus Axtner

14 – Klaus Lorenz

15 – Christian Schanzer

16 – Florian Grünauer

17 – Evgeni Clementyev

not on the picture:

Nikolas Arend

Klaus Böning

Johannes Brunner

Robert Georgii

Thomas Hils

Daniel Lamago

Guido Langenstück

Alexey Mirmelstein

Christian Plonka

Klaus Schreckenbach

Cornelia Skorski

Erich Steichele